NASA CONTRACTOR REPORT

NASA CR-603

A FEASIBILITY INVESTIGATION CONCERNING THE SIMULATION OF SONIC BOOM BY BALLISTIC MODELS

by J. G. Callaghan

Prepared by
DOUGLAS AIRCRAFT COMPANY, INC.
Long Beach, Calif.
for Langley Research Center

NATIONAL AERONAUTICS AND SPACE ADMINISTRATION • WASHINGTON, D. C. • OCTOBER 1966

NASA CR-603

A FEASIBILITY INVESTIGATION CONCERNING THE SIMULATION OF SONIC BOOM BY BALLISTIC MODELS

By J. G. Callaghan

Prepared under Contract No. NAS 1-5149 by
DOUGLAS AIRCRAFT COMPANY, INC.
Long Beach, Calif.

for Langley Research Center

NATIONAL AERONAUTICS AND SPACE ADMINISTRATION

For sale by the Clearinghouse for Federal Scientific and Technical Information
Springfield, Virginia 22151 – Price $2.50

Prepared under Contract No. NAS 1-5149 by
Douglas Aircraft Company, Inc. for
National Aeronautics and Space Administration
A FEASIBILITY INVESTIGATION CONCERNING THE SIMULATION OF SONIC BOOM BY BALLISTIC MODELS.
J. G. Callaghan. 24 June 1966.

The test program consisted of the determination of appropriate instrumentation to measure the pressure signature of small-scale, rapidly moving ballistic models and the definition of problems associated with launching winged ballistic models. Good quality pressure signatures were recorded using both commercially available and specially tailored transducers. Motion of delta wing ballistic models varied from a smooth type of flight to one of highly erratic oscillatory motion. Limited testing indicates that the real potential of this technique lies in the use of bodies of revolution, rather than winged bodies, particularly at higher Mach numbers.

A FEASIBILITY INVESTIGATION CONCERNING THE SIMULATION OF SONIC BOOM BY BALLISTIC MODELS

By J. G. Callaghan
Douglas Aircraft Company

SUMMARY

A series of tests has been conducted to determine the feasibility of using ballistic models to provide laboratory simulation of sonic boom. The test program consisted of two main parts: (1) the determination of appropriate instrumentation to measure the pressure signature of small-scale, rapidly moving ballistic models, and (2) the definition of problems associated with launching winged ballistic models.

In order to ensure the best possible reproduction of the pressure signature associated with the particular model in question, two approaches were used. The testing of commercially available pressure transducers was conducted, as well as the testing of transducers especially tailored to the particular requirement of the subject study.

The testing of winged ballistic models consisted of determining the type of flight path obtainable in a ballistic range at launch Mach numbers of about 3.0, and defining the fabrication problems associated with such models. Various sabot configurations were tested in combination with a simple delta-wing, parabolic-nose, cylindrical afterbody configuration with a vertical tail.

The results of these tests indicate the following conclusions:

1. Commercially available pressure transducers can provide, in a rapid fashion, good quality pressure signatures resulting from shock wave systems of ballistic models in flight. Measured maximum overpressures were generally higher than theoretically predicted levels. It is felt that this is primarily due to nonlinearity in transducer sensitivity.

2. Specially tailored transducers show promise of improvement in the quality of pressure signatures over those commercially available.

3. Motion of delta wing ballistic models varied from a smooth type of flight to one of highly erratic oscillatory motion. Consideration of model tolerances, sabot design, and light-gas gun tolerances revealed no significant parameters which would lead to the allowance of any degree of repeatability of model flight path. On those tests wherein model motion was of a nonoscillatory type, good shock wave pressure signatures were obtained.

4. Models launched into the ballistic range tank at reduced pressures exhibited a more acceptable type of motion.

5. Limited testing was conducted to explore the possibility of launching bodies of revolution at Mach numbers up to 5. Good quality pressure signatures were obtained.

INTRODUCTION

The nature of the sonic boom problem has been well documented (e.g., in References 1, 2, and 3). In an effort to better understand various phenomena associated with sonic boom, considerable experimental work has been conducted. Full-scale flight test measurements of sonic boom overpressure are, of course, desirable for any particular configuration. Practical considerations preclude this approach for many configurations, resulting in the need for a laboratory simulation of sonic boom. NASA has simulated sonic boom by sting-mounting small-scale models in supersonic wind tunnels and determining the resulting overpressures by means of plate and probe measurements. Reference 4 outlines this technique in detail. This reference also indicates that the existing theory (References 5 and 6) provides reasonably accurate estimates of sonic boom overpressure.

Certain problem areas presented themselves in the wind tunnel technique, however. For any fully developed shock wave system, the so-called far-field pressure signature exhibits the characteristic N-wave shape. Near-field effects cause a departure from this shape to one of several pressure peaks, as would be expected. However, the wind tunnel testing technique introduces further distortion into the pressure signature. The desirability of achieving far-field pressure signatures dictates, for the given physical confines of a wind tunnel, that the model and associated sting support be quite small in size. This consideration not only introduces model fabrication problems, but also introduces vibration of the model and support apparatus. As described in Reference 4, this results in a rounding off of the pressure signature, so that the true amplitude of the wave is not measured. Further, boundary layer build-up on the pressure probe results in measured pressure changes across shock waves which are less abrupt than the true pressure discontinuity across the shock wave. An additional viscous problem is encountered due to boundary layer growth on the model itself. This is particularly amplified as the model size becomes quite small.

The technique used in Reference 4 to adjust the test pressure signature was simply to extend the linear portion of the measured signature and to form a right triangle whose area is equal to the area under the measured signature. For convenience, a typical measured and adjusted pressure signature from the wind tunnel data of Reference 4 is presented in Figure 1.

The problems inherent in the wind tunnel technique led to the consideration of simulating sonic boom by small-scale models launched in a ballistic range. As the pressure signature would be obtained from a model in free flight, the problems of vibration of the model support system and pressure probe boundary layer buildup are eliminated. Further, because ballistic range facilities are considerably less limited in test section size as compared to wind tunnels, larger model sizes are permitted. The ballistic range technique was felt to offer sufficient potential advantage to warrant its detailed investigation. Reference 7 proposed a test program to investigate the degree of complexity of the problems associated with this technique and to determine their relationship to its feasibility. This proposed program was subsequently funded under NASA Contract NAS-1-5149. This report presents the results of the funded study.

The author wishes to acknowledge the valuable assistance of T. D. Beatty, J. A. Boyd, and R. N. Teng for their efforts toward the completion of this program.

SYMBOLS

B	resistive damping constant, used in transducer mechanical analog
$\bar{c}$	mean aerodynamic chord
C_D	drag coefficient
C_{D_E}	drag coefficient for equilibrium flight condition (lift = weight)
C_L	lift coefficient
C_{L_E}	lift coefficient for equilibrium flight condition
C_{L_α}	lift curve slope
C_M	pitching moment coefficient
F	membrane tension, dynes/cm
f_o	natural resonant frequency
k	stiffness constant for spring
M	Mach number
m	mass
ΔP	incremental pressure due to model flow field
S	wing area, ft^2
T	$\frac{2\pi}{\omega_n} t^*$
t	time, seconds
t^*	time constant, $\frac{\bar{c}}{2V}$
V	flight velocity, ft/sec
W	weight, lb
X	distance, ft
ΔX	distance from point on pressure signature to point where pressure signature curve crosses zero pressure reference axis
α	membrane radius, cm; angle of attack
β	$\sqrt{M^2 - 1}$

ζ	ratio of damped to undamped natural resonant frequency
ζ_P	phugoid damping ratio
μ	mass parameter, $\frac{2W/S}{g\rho\bar{c}}$; Mach angle
ρ	density, slugs/ft^3
σ	membrane surface density, grams/cm^2
ω_n	$\frac{C_{L_E}}{\sqrt{2}\,\mu}$

RESULTS AND DISCUSSION

The potential advantages of the ballistic sonic boom technique have been pointed out. The purpose of the current study was to determine whether this potential could be practically realized. Consideration of this technique brings to light two distinct problem areas: (1) suitable instrumentation to measure the shock wave pressure signature, and (2) the ability to launch ballistic models in a prescribed fashion.

The first problem results from the fact that for all practical purposes, a shock wave is infinitely thin (about 10^{-5} inches, according to Reference 8) and therefore presents a discontinuous pressure jump. The requirement is then that a physical measuring system must respond in essentially zero time to faithfully reproduce this pressure discontinuity.

The second problem area is due to the fact that the historical application of ballistic range testing techniques has been oriented toward stability derivative determination as discussed, for example, in References 9 and 10. The ballistic technique of simulating sonic boom is then a new concept which requires that the model be launched in a uniform, nonoscillating, nonrolling, flight path as compared to a desired oscillating trajectory in stability derivative determination.

The investigation of these problem areas was conducted in the Light-Gas Gun Ballistic Range at the Aerophysics Laboratory of the Douglas Aircraft Company.

Facility

The major components of the ballistic range facility are the pump tube, launch tube, blast receiver, and range tank. A schematic of these components is presented in Figure 2.

The highest performance light-gas gun that can be assembled with this equipment is a two-stage, deformable-piston-compressor type. The first stage consists of a 2.5-inch-diameter powder chamber and a 1.5-inch-diameter pump tube. The second stage can incorporate barrel diameters between 0.25

and 0.80 inch. For the sonic boom ballistic model testing, the models were launched through the 1.5-inch pump tube in a fashion similar to the piston of a two-stage light-gas gun. For testing at Mach numbers of 3 and below, the gun is not used as a light-gas gun. The model and sabot placed as indicated in Figure 2, at the end of the pump tube, are propelled by the combusted rifle powder gases similar to the process of any large military gun. For higher launch Mach numbers, a light-gas is used to propel the model.

An 8-foot-diameter blast receiver is used to prevent powder gases and sabot parts from entering the range tank. It contains seven baffle plates which have holes of varying diameter along the centerline of the flight path to allow the model to pass through and simultaneously stop the parts of deflected sabots. A relief valve which opens at 16 psia allows propellant gases to vent to the atmosphere.

A quick-operating valve separates the range tank and the blast receiver. The two tanks may thus be kept at different pressures. The blast receiver is generally operated at a pressure sufficient to strip the sabot and not appreciably impede the model. The range tank may be operated at any pressure from 10 atmospheres down to 3 mm Hg. The quick-operating valve opens in 10 milliseconds, and closes in 100 milliseconds.

The range tank is 10 feet in diameter and 100 feet long. It can be maintained at pressures up to 10 atmospheres or can be evacuated to 3 mm Hg in approximately 30 minutes. At present, three shadowgraph stations are available to record simultaneous horizontal and vertical shadowgraphs of the contour of the model and its angular orientation. A fiducial reference system allows the x, y, z position of the model to be determined from the shadowgraphs while a system of counters accurately measures the times at which the shadowgraphs are recorded. The shadowgraph stations may be positioned at any of 12 locations along the length of the range tank. Three flash x-ray stations are also available.

From the time-distance data thus obtained, values of velocity can be calculated. Flow characteristics as well as model integrity can be observed from the shadowgraphs and flash x-rays. At the end of the range tank the model enters a catcher and its flight is terminated.

Basically, each shadowgraph station includes the spark light sources, optics, and film plates necessary to obtain two simultaneous, mutually orthogonal shadowgraphs of the model with a known time relationship to other flight events, e.g., launch. The shadowgraphs not only provide information relating to the model space-time history, but also to its orientation and flow-field characteristics.

Detection of the model is normally accomplished by a lightscreen photocell device oriented in such a manner as to produce an electrical pulse when the model reaches the desired position in the shadowgraph field of view. After amplification and conditioning, this pulse is used to fire the spark-light sources.

The optical arrangement used is shown in Figure 3. From this figure it will be noted that the diverging and converging light beams associated with the main mirrors overlap part of the parallel beam. Depending on model location in the field of view, this sometimes results in a double image of the model. Actually, the larger image has better contrast in flow-field visualization. This phenomenon is the result of the longer length of travel of the light beam from the density disturbance to the film plane and consequent greater lateral displacement.

Data from the flash x-ray are recovered in the form of photographic records called radiographs. While these radiographs do not give any information concerning the model flow field, they nevertheless give a very clear picture of model orientation.

The pressure traces recorded from testing in the ballistic range were recorded on cathode ray oscilloscopes, generally having rise times on the order of 10 nanoseconds. The oscilloscope and timer arrangement, as well as the console from which the ballistic range is controlled is shown in Figure 4.

Transducer Development

The problem of developing a pressure transducer suitable to the measurement of rapidly varying transients can better be appreciated by considering a mechanical one-degree-of-freedom analog. This analog is composed of a mass-spring-damper system as described in Figure 5. This system is driven by a forcing function f(t) which is, for the current consideration, an N-wave. Ideally, this system should have a flat response at all frequencies from zero to infinity; i.e., the output would be identically reproduced regardless of the frequency of the input. This cannot, of course, be the case because no mechanical system can respond to a given input in zero time. Further, any mechanical system will have resonance at certain frequencies depending on the characteristics of that system. Investigation of the transient response of this mechanical analog (Reference 11) reveals that the natural resonant frequency is

$$f_o = \frac{1}{2\pi}\sqrt{\frac{k}{m}} \tag{1}$$

and that the ratio of the damped to undamped natural frequency is

$$\zeta = \frac{\pi f_o B}{k} = \frac{B}{2}\frac{1}{\sqrt{km}} \tag{2}$$

As previously discussed, a very high resonant frequency would be desired; Equation (1) indicates that for a given mass a higher stiffness is required; however, high stiffness gives a low value of the damping ratio which is undesirable. Flat response to very high resonant frequencies, which will be coupled with poor damping, permits short rise times to peak amplitude. This is because the leading wave of the N-wave is of very high frequency. On the other hand, the lower resonant frequency, which was seen to accompany good damping, will not permit the high frequency components of the leading wave to be clearly defined, i.e., longer rise time.

It is clear, then, that compromises must be made in pressure transducers as demonstrated by the above mechanical analog. An indication of the compromises to be made in the selection of a transducer for ballistic sonic boom testing is presented in Figure 6.

In order to ensure the broadest practicable range of transducer choice, two approaches were taken: first, to determine whether a transducer could be tailored to the specific requirement of the current study, and, second, to investigate applicability of commercially available pressure transducers.

The approach by custom tailoring was conducted by Ling-Temco-Vought Research Center. A capacitance (also referred to as condenser) type transducer, shown in Figure 7, was used for the basic configuration. This type of transducer acts as a parallel plate capacitor, consisting primarily of a diaphragm and a back plate, with either a solid or gas dielectric between the two plates. A change in the gap between the two plates resulting from a change in pressure on the diaphragm is output as change in voltage. This voltage change is then compared to the known sensitivity of the transducer, the voltage output per pressure level input.

The primary approach taken for this development was to improve the high frequency characteristics of the basic microphone. The various tailoring techniques are described in detail in Appendix A. These techniques consisted mainly of modifying the diaphragm to change resonance and damping characteristics.

Transducer characteristics were determined by recording the pressure trace from a 0.30 caliber rifle bullet fired in the ballistic range tank. (The manner in which the transducers were mounted is discussed in a subsequent section.) This afforded rapidity and economy for a wide variety of testing for both the tailored as well as the commercially available transducers. The rifle mounting installation, shown in Figure 8, was designed so that it could be raised to fire along the centerline of the tank and lowered out of the way when the larger guns are fired. A shadowgraph of a typical rifle bullet shot is shown in Figure 9; two images are present due to the nature of the optical system as previously discussed.

Each of the tailored transducers was tested in the Ling-Temco-Vought shock tube before testing in the ballistic range. The resulting pressure signature was recorded on a cathode ray oscilloscope. For testing in the ballistic range, to ensure that the full pressure signature is recorded on the oscilloscope, two transducers, placed in tandem, were used for each signature. In this way, the uprange transducer triggers the sweep on the scope which receives the signature from the downrange transducer. The transducer spacing will be a function of the speed of the passing projectile and the amount of delay desired in the signature before the start of the first pressure rise. A typical arrangement for achieving this result is shown in Figure 10.

Representative oscilloscope pressure traces, from both the shock tube and the ballistic range, are shown in Figures 11 and 12. A signature for a transducer with a somewhat slow rise time of about 4 microseconds and good damping is presented in Figure 11. Figure 12 presents a signature for a transducer with a high level of resonant frequency and associated good rise time, about 2 microseconds, but with noticeably poor damping.

The characteristics of these tailored transducers were then compared to those obtained from a range of commercially available models. Seven transducers had been previously eliminated as possible candidates as a result of the work of Reference 7. Four other available transducers were tested for the current study.

Results from a piezoelectric transducer with a high level of resonance are shown in Figure 13; however, no damping is present, resulting in considerable ringing at about 250,000 cps. A second type of piezoelectric transducer, designed primarily for high-pressure testing, was tested which indicated considerably better damping, but fairly low sensitivity with a resulting low signal-to-noise ratio. A representative signature is included in Figure 13.

An example of a capacitance type transducer with damping unsuited for the present investigation is shown in Figure 14. A pressure signature from a second commercially available capacitance transducer which had been previously tested with good success (reported in Reference 7) is also shown in Figure 14. This transducer was judged to be the most applicable transducer of those tested, both tailored and commercially available. It was considered to be the best compromise among damping, sensitivity, and rise time. It is also to be noted that time and availability were strong factors in this choice. Much of the work in the effort to tailor a transducer to this particular need seems quite promising. It seems reasonable to expect that increases in performance can be expected with further research.

The remaining tasks were then to:

1. Determine proper transducer mounting.

2. Isolate cause of transducer ringing.

3. Calibrate transducer.

4. Compare test and theoretical signature.

A series of mountings were tested for the transducer. In general, the transducers were flush-mounted as shown in Figure 15. This type of simple mounting box offered a rigid support for the transducer coupled with ease of mobility and accessibility. As the mountings were placed on the metal floor of the range tank (see Figure 10), a rubber base was attached to the mounting box to ensure that no sound was picked up through the floor. However, use of an aluminum base in place of the rubber base showed no observable difference in the pressure signature. Further, an acrylic plastic reflecting plate was tested in place of the aluminum reflecting plate, and no differences in signature were observed. In general, the transducers were threaded directly into the metal reflecting plate, so that there was a metal-to-metal contact. To determine whether any vibration was reaching the transducer through the reflecting plate, various types of insulating seats between the transducer and reflecting plate were tested. Again, there seemed to be no effect on the pressure signature except in the case of a rather soft insulating seat. For this configuration, a rubber seat surrounding the transducer resulted in noticeably higher oscillation in the pressure signature as can be seen by comparing Figures 14 and 16. One further important consideration was observed concerning the mountings: the fit between transducer and reflecting plate must be one of close tolerance. One configuration was tested wherein a gap of about 0.10 inch existed between the transducer and the side of the reflecting plate, the transducer having been mounted from below the plate rather than threaded into it. As can be seen in Figure 17, this cavity acted as a small resonance chamber permitting considerably more noise to be picked up by the transudcer. The uprange end of the mounting box was sealed and subsequent testing indicated that there were no effects of any wave reflections inside the box.

Testing was conducted to determine whether the heavily damped ringing observed in the pressure signature was caused by the system electronics or by mechanical resonance in the transducer diaphragm. This was done in the following manner: the diaphragm was removed from the transducer and a square wave signal was input directly into the microphone cathode follower. This was done for several frequencies of square wave (Figure 18). It can be seen that no ringing is present at any frequency, indicating the problem is a mechanical resonance associated with the diaphragm rather than an electronic resonance. The distortion from the square wave form at the higher frequencies is due to the fact that the duration of the wave is a significant fraction of the rise time of the transducer.

Attempts were made using filters to remove this oscillation which is at about 80,000 cycles per second. Typical of the results is the signature shown in Figure 19, wherein a 50-kc filter was used. Clearly, the filter worked, but the signature is rounded off to the point of being unacceptable.

The transducers chosen for use in the current program were calibrated by means of a pistonphone. This device inputs into the transducer a sine wave which has a very accurately known sound pressure level. A sample calibration is shown in Figure 20. There is a wide variation in sensitivity from one transducer to another; further, the sensitivity will vary for a given transducer depending on the amplifier used. For these reasons, care must be exercised in conducting a new calibration each time any changes are made in the pressure measuring equipment.

The frequency response characteristics for the transducers were also determined. A representative response curve is shown in Figure 21. It is seen that the response is flat to about 25,000 cps and falls off rapidly after 80,000 cps. Knowing these frequency response characteristics, it is of considerable interest to construct a Fourier synthesis for an N-wave input. An N-wave with a 160-microsecond period (6250 cps fundamental frequency) was assumed. This meant that the first 13 harmonics (i.e., 13 times the fundamental harmonic, or about 80,000 cps) could be used for the Fourier synthesis. Beyond these frequencies, the various harmonic contributions were taken to vary according to the roll-off shown in Figure 21. The harmonics were arbitrarily cut off at a frequency of about 180,000 cps or the 29th harmonic. This synthesis is shown in Figure 22. It can be seen that the ringing is essentially damped out after three oscillations, which is quite similar to the characteristics observed in the test signature presented in Figure 14.

Representative .30-caliber pressure signatures from several transducers were compared to those predicted using the theory presented in Reference 5.

The normal area distribution (Mach 1 area rule cut) for the rifle bullet was determined by measurement and the assumed wake scaled from a shadowgraph. The Mach area cut for the test cases was then determined from area rule considerations. Both area distributions are presented in Figure 23. The distributions are shown as smooth since there is no provision in the computing procedure for handling abrupt discontinuities in area. In reality, the rifle bullet has a crimping ring which, in conjunction with the rifling marks scribed on the bullet, creates a weak compression field which does not coalesce with the leading and trailing shock waves. Close examination of shadowgraphs reveals the presence of this wave.

The resulting test and theoretical correlations are presented in Figure 24. If the linear portions of the measured pressure signatures are extrapolated, the resulting adjusted peak overpressures are generally higher than those theoretically predicted. On the other hand, it is to be noted that the predicted values of the time of passage of the wave agree quite closely with those measured. For these reasons, it is felt that there is some nonlinearity in the pressure sensitivity of the transducers. It was previously noted that the transducers were calibrated using a pistonphone which had a pressure input of about 0.0045 psi, or only about 1 percent of the actual test values being measured. Future test work should utilize high-pressure calibration procedures, such as shock tube techniques.

One feature of measuring pressure signatures in this fashion is the rapidity with which they may be obtained. After the shot is fired, it is merely a matter of removing the Polaroid film from the oscilloscope camera. It is also to be noted that the form of the pressure signature generally indicates less distortion than the typical unadjusted wind tunnel signature presented in Figure 1.

Ballistic Model Description and Fabrication

Model fabrication. - Choice of the ballistic model configuration was dictated by several considerations. Because the nature of the subject investigation is one of feasibility, a simple configuration was decided upon, the size of which was chosen to be compatible with the 1.5-inch diameter of the launch tube. As the primary concern of the testing was to determine whether the model could be launched in a nonrolling nonoscillating flight path, considerable care was required to ensure the highest possible degree of accuracy in fabricating the models. This would result in minimizing asymmetries in the model such as misalignment of wing panels.

The basic configuration tested consisted of a parabolic nose and cylindrical after-body fuselage with a 60° swept delta wing and trapezoidal vertical tail, as shown in Figure 25. The stainless steel model was fabricated from three parts: wing, vertical tail, and fuselage (see Figure 26). The wing and tail panels were fitted into the fuselage by saw cuts in the fuselage, then pinned and soldered into place. To ensure uniformity from one model to the next, a fabricating jig was constructed for holding the model during final assembly as shown in Figure 27. Model tolerances were generally held to about 0.002 inch. A series of five "super" models was constructed holding tolerances to about 0.0005 inch. All tolerances were checked on a comparator which greatly magnifies the model shapes as shown in Figure 28. Considerable care was required in the machining of these models to hold the tolerances. One recurring problem was the wandering of the saw blade in making the cuts for the wing and tail in the fuselage. A new saw blade was required for each cut. Volume not filled by the wing and tail after the cuts were made was filled with silver solder (see Figure 26). This was found to be a rather unsatisfactory process. This problem was subsequently eliminated by using an electronic erosion process to produce the cuts. A completed model is shown in Figure 26. A total of about 25 manhours was required to fabricate and inspect each of the models. Casting processes were considered as a possible substitute for machining processes in order to reduce this time; however, casting tolerances are large, being, in general, about 0.010 inch. An appreciation of these tolerances can be gained by the following consideration. For a model launched at a Mach number of 3.0, operating at a lift coefficient of 0.10, a 0.002-inch lateral misalignment in wing planform results in a steady roll rate of about 3000 deg/sec. This would correspond to a total roll of about 90° during the model passage down the ballistic range.

Model aerodynamics. - The estimated aerodynamic characteristics of this model are presented in Figure 29. It can be seen from the pitching moment curve that the model is quite stable statically, having a static margin of about 29 percent. For reference in correlating test and theoretical overpressures, the model normal area distribution is shown in Figure 30.

Consideration of phugoid and short period modes indicates that the model has good longitudinal dynamic stability. References 12 and 13 present a simplified expression for the phugoid mode which is

$$T = \frac{2\pi}{\omega_n} t^*, \text{ sec} \tag{3}$$

where

$$t^* = \frac{\bar{c}}{2V} \tag{4}$$

$$\omega_n = \frac{C_{L_E}}{\sqrt{2}\,\mu} \tag{5}$$

Substituting the value of $\mu = 2W/S\big/g\rho\bar{c}$ into the expression for period, we obtain $T = 0.138\ V$. It is seen that the phugoid period is not a function of vehicle size. The 2-inch sonic boom ballistic model will then have approximately the same period as a full-scale supersonic aircraft at the same velocity. At a Mach number of 3.0, this corresponds to about 460 seconds which is very large compared to a test time in the range tank of about 0.03 second. On the other hand, phugoid damping is a strong function of model scale. Reference 12 states that the damping ratio is approximately

$$\zeta_P = \frac{1}{\sqrt{2}} \left(\frac{C_{D_E}}{C_{L_E}} \right) \tag{6}$$

For full-scale aircraft, $C_{D_E} \ll C_{L_E}$ so the phugoid is lightly damped. However, the ballistic models have a very high ratio of drag to lift at the equilibrium flight condition, resulting in a supercritical damping ratio on the order of 25.

The method of Reference 12, using stability derivatives from Reference 14, indicates that the short period has a frequency of about 9400 cps. The time to damp to half amplitude is about 0.6×10^{-4} seconds or slightly more than one-half cycle at 9400 cps.

Ballistic Model Testing

Sabot development. - Before launching the delta wing ballistic models, testing was conducted using simple slender cones to develop the proper sabot. The cone design used is shown in Figure 31. A copper nose was used in conjunction with an aluminum base to create a statically stable cone. Attempts to bring about a forward center of gravity by hollowing out the cone base were unsuccessful due to inadequate strength during the high launch accelerations.

The function of the sabot is primarily to protect the model during launch and to permit sufficient surface area for the driver gases to act upon during model acceleration. The sabot must, after leaving the gas gun, separate as cleanly as possible since minimum asymmetric forces are transmitted by the sabot to the model. The choice of sabot configurations resulted from the combined ballistic range experience of both Douglas and NASA Ames Research Center. A log of the cones fired, as well as the rifle shots and ballistic models, for the sabot development is presented in Appendix B. The various sabot configurations tested with the ballistic models are shown in Figures 32 and 33. The following table presents a description of these sabots.

TABLE I

Sabot Descriptions

Sabot Number	Description	Test Results
1	Made by casting polyurethane over the model. A polyethylene liner is used as the outer shell. Four quarter aluminum pushers form a base for the entire sabot. The finished sabot includes four integrated quarters.	Good
2	Cast in a fashion similar to Sabot No. 1, except no liner is used.	Good
3	Composed of two halves. The driving powder-gas pressure opens the sabot upon leaving the muzzle.	Good
4	Same basic design as No. 3, except that aluminum insert was added to increase the bearing strength.	Poor
5	This sabot uses the principle of minimum support in contrast to Sabot No. 1. A Lexan pusher is used to minimize the relative movement of the sabot quarters during launch.	Poor

TABLE I (Continued)

Sabot Number	Description	Test Results
6	Similar to the design of No. 3 sabot, except aerodynamic force is introduced to help open the front end of the sabot after it leaves the muzzle.	Poor
7	Similar to the design of No. 4, except that the aluminum insert was redesigned.	Poor
8	Minimum support principle has been used. The pusher is made of a solid, one-piece aluminum plate.	Very Good
9	Four quarters, complete support principle has been employed.	Good
	Note: All sabots are made of Lexan unless otherwise specified.	

Sabots 10, 11, and 12 were used in conjunction with the winged models and are discussed subsequently. Results described as poor were those shots wherein the cone did not enter the range tank or was damaged during launch. Representative of such a result was Sabot No. 5, shown in flight in Figure 34. The sabots which seemed the most promising were Nos. 3 and 8. Number 8, in particular, shown in Figure 35, is of a type which was successfully tested at the NASA Ames ballistic facility.

Delta wing models. - As a result of the sabot development testing, the initial sabot tested with the delta wing models was of the cantilever type (No. 10 in Figure 33) similar to No. 3 (shown in Figure 32). This sabot failed completely in that the model was destroyed before it entered the range tank. This was felt to be caused by the sabot not gripping the model firmly enough during launch. A second type of cantilever sabot (No. 12) was subsequently tested which held more of the model base and was machined from aluminum rather than Lexan plastic. This sabot also failed in that the model did not enter the range tank. Cantilever sabots were consequently discarded. Although Sabots Nos. 1, 2, and 9 gave good results using cone models, they were not tested with the delta wing models. This resulted from considerations of NASA Ames sabot experience indicating that the use of a minimum contact type of sabot gave the best results. Also, sabot types 1 and 2 were not particularly clean in that some of the polyurethane adhered to the model during the molding process. This, then, eliminated all but Sabot No. 8. Detail of this type of sabot used with the delta wing model can be seen in Figure 36. This sabot is referred to as No. 11 in Figure 33.

During the initial model testing the pressure transducers were not placed in the range tank as a precaution against impact damage from sabot or model fragments. This was unfortunate, however, as the first model launched with this type of sabot exhibited a very smooth flight path. As can be seen from Figure 37, there was no pitch or yaw motion to the model. Although it rolled slightly relative to the camera, it did not roll as a function of time. However, when this shot was repeated, a roll rate of at least 30,000 deg/sec was observed. In comparing the measured tolerances in these two models it was observed that the model of shot 16 actually had more asymmetry in the wing planform than the model of shot 17. The shot was repeated two more times and an even more irregular flight path was observed, exhibiting yaw, pitch and roll. Again, consideration of the measured model tolerance did not shed any particular light on the problem. Sample shadowgraphs for these shots are shown in Figure 38, and can be compared to the same configuration shown in Figure 37. Consideration of typical flash x-ray pictures of the model in flight (Figure 39) reveals that there is no observable damage to the model during launch. Examination of model traces on yaw cards further substantiates this belief. In order to ensure that the launch tube was not imparting any oscillating or rolling motion to the model and sabot during launch, the launch tube was rebored after the above described shots. Subsequent testing revealed that model motion was still of the type shown in Figure 38.

A series of the "super" models previously described was tested. A model with sharp leading edges was also launched on the theory that the relatively blunt leading edges of the other models was causing adverse effects on model stability. A series of models which were trimmed to a lift coefficient of approximately 0.06 were also tested. This trimming was accomplished by beveling the lower surface of wing leading and trailing edges and shifting the wing 0.075 inch forward as shown in Figure 40. All of these tests showed the same lack of repeatability discussed above.

Additional modifications were made to the basic sabot as a further attempt to improve model motion. On the theory that the sabot was separating from the model in an explosive fashion, the face angle of the sabot was made more shallow. In this way the pressures in the lateral direction were reduced permitting a more gentle separation. Sabot No. 11 was also modified to include a transverse shear pin (such as sabot No. 4, for example). The purpose of this pin was to reduce translational motion of one sabot quadrant relative to another in the belief that sabot separation would be more uniform. Another modification was to round off the outer edge of the bottom of the sabot quadrant so that, during separation, the quadrants would roll away from the pusher plate more smoothly. As with the changes in the model, repeatibility of good quality flights was not obtainable.

The most promising results were obtained by launching the models into the range tank at low pressures. Four such shots were fired: two at 7 psia, one at 1.9 psia, and one at 0.4 psia. In the 7-psia and 1.9-psia shots, the model exhibited roll and some pitch, but at reduced rates compared to those fired into atmospheric pressure. The model launched into the 0.4-psia (20-mm Hg) environment exhibited remarkably smooth flight with no observable pitch, yaw, or roll as can be seen in Figure 41. The sabot can also be seen clearly as it falls away from the model. Apparently more investigation is needed in this area. One problem coupled with testing at considerably reduced pressures is associated with the pressure transducers. Certainly the level of overpressure measured is much lower than that at atmospheric pressure, requiring that the transducers have suitably high sensitivity.

More importantly, the damping ratio of the transducer is considerably affected by environmental pressure. As seen in Figure 42, very high resonance peaks occur at substantially reduced pressures. Consequently, no pressure signatures were measured during the low pressure shots. Particular tailoring of the transducers could probably remedy these problems.

Once it was determined that there was no danger of sabot impact damage to the transducers, pressure signatures were measured for each of the model shots. It is felt that any attempt to correlate measured and theoretical pressures for models exhibiting the type of motion shown in Figure 38 would be quite fruitless. For this reason, only those signatures obtained from flights having a minimum of roll motion, and in particular that exhibited no large pitch or yaw oscillations are presented. Figures 43 through 46 present test signatures for these shots. Also included are the reduced signatures and the model shadowgraphs for each shot. The physical location of each shadowgraph station in relation to the transducer position is described in Figure 47. It should be noted that future testing could include a circumferential arrangement of several transducers. This technique would be of considerable assistance in properly evaluating the overpressures in the case of pure rolling motion by the model.

Due to the expense of fabricating each model, attempts were made to arrest the models at the end of the flight. It was found that by trying varying thicknesses of urethane foam the model could be stopped, but as shown in Figure 48, the structural integrity was completely lost. This experience is in general alignment with that of the NASA Ames facility in that a singular lack of success in arresting models has been noted.

Cone models. - Some additional testing was conducted measuring pressure signatures from cone models at varying Mach numbers. Two problem areas were introduced in testing at Mach numbers around 5.0: (1) the cones experienced an oscillating path (see Figure 49), and (2) sabot impact flash caused premature triggering of the optical system, resulting in failure to produce shadowgraphs for some of the shots. However, it should be noted that this high Mach number testing was done in an entirely cursory fashion. Additional test work should resolve these problems.

Representative shadowgraphs and pressure signatures measured through a range of Mach numbers are presented in Figures 50 through 53. Although no shadowgraphs were obtained for the Mach 5.14 shot, the pressure signature is nevertheless presented as an indication of the quality obtainable.

The theoretical and test pressure signatures have been compared on Figures 50 through 53. As with the case of the rifle bullets, the measured peak overpressures are seen to be higher than the predicted levels. In order to ensure that these higher pressures were not due to any amplification effects from the light gas gun, a shape was fabricated identical to the bullets fired from the .30-caliber rifle. This model, shown in a sabot in Figure 54, was balanced by boring out the aluminum afterbody, and adding a brass nose. Although the bullet shape demonstrated some pitching motion (see Figure 55), the resulting pressure signature agreed quite well with that of a bullet fired from the .30-caliber rifle. (Compare Figure 55c to Figure 24c.) One further test was conducted in this respect. The sweep on the scope was increased so as to observe any events possibly occurring before the cone leading wave passed over the transducer. Observation of the resulting cone pressure time history 10 milliseconds before the leading wave showed no change in pressure above ambient, as would be expected. (This corresponds to the time required for the cone to travel about 230 body lengths at M = 3.)

Emphasis is again placed on the need for calibrating the transducers at pressures more nearly compatible with the test levels.

The significant potential of testing at high Mach numbers using the ballistic technique can be gleaned from Figure 56. It is quite apparent that testing at high Mach numbers at any appreciable number of body lengths away is precluded in wind tunnels due to the short test section length. However, ballistic ranges offer considerable length — 100 feet, for example, in the current study.

CONCLUSIONS AND RECOMMENDATIONS

A series of tests has been conducted to investigate the feasibility of using small ballistic models to simulate sonic boom. The problems concerning model flight path, pressure transducers, and sabot design have been defined. The results of these tests indicate the following conclusions:

1. Commercially available pressure transducers can provide, in a rapid fashion, good quality pressure signatures resulting from shock wave systems of ballistic models in flight. Measured maximum overpressures were, in general, higher than theoretical levels. It is felt that this is primarily due to nonlinearity in transducer sensitivity.

2. Specially tailored transducers show promise of improvement in the quality of pressure signatures over those commercially available.

3. Motion of delta wing ballistic models varied from a smooth type of flight to one of highly erratic oscillatory motion. Consideration of model tolerances, sabot design, and light-gas gun tolerances revealed no significant parameters which would lead to the allowance of any degree of repeatability of model flight path. On those tests wherein model motion was of a non-oscillatory type, good shock wave pressure signatures were obtained.

4. Models launched into the ballistic range tank at reduced pressures exhibited a more acceptable type of motion.

5. Limited testing was conducted to explore the possibility of launching bodies of revolution at Mach numbers up to 5. Good quality pressure signatures were obtained.

In consideration of these conclusions, the following recommendations for additional research are made:

1. Conduct additional testing of ballistic models at reduced range tank pressures.

2. In conjunction with this testing, develop a transducer with suitable resonance damping at low pressures so that pressure signatures may be measured.

3. Utilize transducer calibration techniques which involve pressures more nearly compatible with test levels.

4. Conduct testing to explore the potential of sonic boom simulation by ballistic model bodies of revolution at high Mach numbers.

Douglas Aircraft Company
Aircraft Group
Long Beach, California

APPENDIX A

TRANSDUCER TAILORING

General Considerations

In order to develop a condenser microphone to record transient wave forms produced by weak shock waves, the following goals were established concerning the desired transducer characteristics:

1. Capability of being flush mounted
2. Small active area
3. High resonant frequency
4. Well damped resonance
5. Adequate sensitivity
6. Linearity at maximum sound pressure levels

The approach taken for this development was to modify the basic microphone shell to improve its high-frequency characteristics. This was accomplished by reducing the active diaphragm diameter to 0.10 inch. This modification allows the resonant frequency of the microphone to be increased to approximately 90 kc. Further reduction in the active area of the device was not considered at this point as a result of the loss in sensitivity. The diaphragm material used is 0.0001-inch-thick type 302 stainless steel. The microphone shell is constructed of type 302 stainless steel and has a maximum diameter of 0.300 inch. This shell can be directly flush mounted with or without an adaptor, as shown in Figure 7.

Particular concern was given to the transient response of the microphone during this development since the data to be recorded were to be in the time domain. For development purposes, it is convenient to compare the experimental systems to a mathematical model or analog, as previously discussed. A simple one-degree-of-freedom mechanical system with a mass m, a spring with a stiffness k, and a resistance with a value B, is quite adequate to describe the system to about one octave above the first resonant frequency of the diaphragm. The transient response of this model to a unit step function is given from Reference 15 as:

$$f(t) = 1 - \frac{e^{-\zeta 2\pi f_o t}}{\sqrt{1-\zeta^2}} \sin\left(2\pi f_o \sqrt{1-\zeta^2}\,t + \cos^{-1}\zeta\right) \qquad \text{(A-1)}$$

where: f_o is the natural resonant frequency $= \frac{1}{2\pi}\sqrt{\frac{k}{m}}$

ζ is the damping ratio $= \frac{\pi f_o B}{k}$

APPENDIX A

From plots of equation (A-1), one notes that the most acceptable transient response is obtained for ζ between 0.5 and 1.0. If $\zeta = 0.7$, which is usually considered optimum damping, a resonant frequency of 190 kc will suffice. On the other hand, if a resonant frequency of 1 mc could be obtained then a ζ of 0.13 would be satisfactory. It is to be noted that an overshoot of approximately 70 percent will occur in the second case.

In view of the above considerations concerning this model, it appears that methods to increase the resonant frequency as well as the damping are the primary areas of investigation.

Increasing Natural Resonant Frequency

From Reference 16, the first resonant frequency for a circular membrane is given as:

$$f_{o_{circ}} = \frac{0.382}{\alpha} \sqrt{\frac{T}{\sigma}} \qquad \text{(A-2)}$$

where: F is the tension in the membrane

α is the radius of the membrane

σ is the surface density of the membrane

The following values are applicable for the modified microphone:

$$F_{max} = 1.75 \times 10^{6} \text{ dynes/cm}$$

$$\alpha = 0.127 \text{ cm}$$

$$\sigma = 2.04 \times 10^{-3} \text{ grams/cm}^{2}$$

These values give a maximum f_o of 87 kc. This value was confirmed by experimental results.

The natural resonant frequency is raised for a diaphragm supported at the center. Theory for a circular membrane is given by Morse in Reference 17 and indicates that the addition of a center support will raise the resonance by a factor of about 2.3.

This effect was achieved by the following method. A groove was cut near the center of the backplate so as to leave a small circular area at the center approximately 0.01 inch in diameter. A small amount of a viscous silicon grease was attached to this area so that when the backplate is placed in the microphone shell, the grease will contact the diaphragm at its center. Since the grease is free to flow under static pressure, the normal spacing is achieved; however, the viscous effects are so large at frequencies of more than a few cps that the diaphragm is dynamically fixed. This method proved to be both simple to apply and very effective. The diaphragm resonance is raised by a factor of approximately 1.8. The discrepancy between this and the theoretical figure is apparently due to the grease adding some additional mass to the diaphragm and providing a slightly compliant support. A pressure signature for this type of transducer is shown in Figure 11.

If an insulating film is placed between the diaphragm and the backplate and the spacing eliminated, many small points of support will appear randomly distributed over the area of the backplate. These points of support are due to small irregularities in the diaphragm, the insulating film, and the backplate. The effect of these supports is to greatly raise the diaphragm resonant frequency. A result of using this type of diaphragm support is shown in Figure 12.

This technique was simplified by making the diaphragm a composite of 0.0001-inch-thick stainless steel and 0.00025-inch-thick mylar foil. The mylar lies between the stainless steel foil and the backplate and provides excellent electrical insulation. Resonant frequencies as high as 800 kc have been obtained by this method.

Resistive Damping

Damping is normally obtained in a condenser microphone by the resistive properties of the film of air between the diaphragm and the backplate. The mechanics of this damping action are presented by Crandall and by Robey, in References 18 and 19.

The following characteristics of the air film are of great importance in the design of condenser microphones:

1. The magnitude of the air film resistance increases rapidly as the diaphragm to backplate spacing is reduced. This effect seems to be approximately proportional to the inverse third power of the spacing.

2. The resistive part of the air film impedance becomes greatly diminished at the frequency where the inertia of the air prevents appreciable air flow during the maximum and minimum excursions of the diaphragm. Beyond this frequency the effect of the air film becomes reactive and adds to the total stiffness of the diaphragm.

For high-frequency damping purposes the reduced resistance at high frequencies is disappointing. This effect can usually be reduced by cutting a series of fine grooves in the backplate so that the length that the air must flow (hence, its effective mass) is reduced. To apply this technique to the backplate under present discussion would involve a difficult machining job.

These grooves should be approximately 0.003-inch wide and have a depth of 0.005-inch thickness in order to act as pressure relief points. When the spacing is further decreased to get additional damping at high frequencies, excessive damping occurs at low frequencies. This causes a droop in the frequency response characteristic at the mid frequencies. In the time domain, this excessive resistance causes the system output to fail to rise to the full output in the initial rise, as can be seen in Figure 12. This is particularly common in the case where a mylar stainless steel composite diaphragm is used. The reason for this is that the effective air film stiffness is very small.

Calibration Techniques

The calibration of microphones beyond 100 kc requires special techniques. Two methods used during this work were the transient (time domain) response of the microphone to a step function of pressure in a shock tube, and a frequency response characteristic determined with an electrostatic actuator.

The shock tube driver section is loaded with air at an overpressure of from 2 to 8 psi. An electrodynamic diaphragm rupturing device is used to give excellent repeatability with cellophane diaphragm material. With 4-psi overpressure, the frequency content of the shock wave at the microphone position contains frequencies well above 1 mc. The microphone to be calibrated is flush mounted in the end of the expansion section. The many small features which occur after the first 20 microseconds, as shown for example in Figure 11, are apparently reflected shocks occurring within the tube and are not due to the microphone response. Dual time bases of 100 and 10 microseconds were used for most tests.

A technique was developed to enable the pressure frequency response characteristic to nearly 1 mc to be measured. This device is composed of a clamp to hold the microphone and a fine screen element which can be placed parallel to and several thousandths of an inch away from the microphone diaphragm. When a driving voltage is placed between the screen element and the diaphragm, a force is applied to the diaphragm, simulating an applied sound pressure level. An example of frequency response characteristics obtained by an electrostatic actuator was previously presented in the Fourier analysis discussion.

APPENDIX B

TEST LOG

.30-Caliber Rifle Shots

Date	Shot Number	Transducer	Comments
10/13/65	1R	ARC LD 107#1	No good - poor focus in camera
	2R	ARC LD 107#1	Repeat of IR transducer on floor plates
	3R	ARC LD 107#1	Repeat of 2R,floor plates removed
	4R	ARC LD 107#1	Rubber shock mounting on base
	5R	ARC LD 107#1	Crimping ring on rifle bullet filled
	6R	ARC LD 107#2	Check #2 LD107
	7R	ARC LD 107#2	Repeat of 6R
	8R	ARC LD 107#4	Rubber shock mounting on base
	9R	ARC LD 107#1	Rubber shock mounting on base
	10R	ARC LD 107#1	Amplifier acoustically shielded
	11R	ARC LD 107#1	Amplifier uprange from transducer
	12R	ARC LD 107#1	Repeat of 11R
	13R	ARC LD 107#1	Repeat of 12R
	14R	ARC LD 107#1	Rubber shock mounting on amplifier
	15R	ARC LD 107#1	Uprange end of mounting sealed
	16R	ARC LD 107#1	Repeat of 15R
10/13/65	17R	ARC LD 107#1	Repeat of 16R
10/14/65	18R	ARC LD 107#1	Aluminum base on mounting
	19R	ARC LD 107#1	Repeat of 18R
	20R	ARC LD 107#1	Rubber base on mounting
	21R	LTV HTM-1	Checkout of LTV HTM-1
	22R	LTV HTM-1	Repeat of 21R
	23R	LTV HTM-1	Repeat of 22R
	24R	LTV HTM-1	Repeat of 23R
	25R	LTV HTM-1	Repeat of 24R
	26R	LTV HTM-1	Repeat of 25R
	27R	LTV HTM-1	Slow sweep to see rise time
	28R	LTV HTM-1	Repeat of 27R, slower sweep
10/14/65	29R	ARC LD 107#1	Reflecting plate isolated on top of card-board box
10/28/65	30R	ARC LD 107#1	Amplifier downrange of transducer
	31R	ARC LD 107#1	Amplifier uprange of transducer
	32R	ARC LD 107#1	Transducer mounting perpendicular to tank centerline
	33R	ARC LD 107#1	Repeat of 32R,amplifier moved uprange
	34R	ARC LD 107#1	Transducer moved to floorboard level
	35R	ARC LD 107#1	Transducer moved closer to centerline of tank
	36R	ARC LD 107#1	Repeat of 35R,crimping ring filled
	37R	ARC LD 107#1	Repeat of 34R,crimping ring filled
	38R	ARC LD 107#1	Repeat of 31R,crimping ring filled
	39R	ARC LD 107#1	Repeat of 38R,crimping ring filled
10/28/65	40R	Photocon Model 714	Checkout of Photocon Model 714

APPENDIX B

Date	Shot Number	Transducer	Comments
10/28/65	41R	Photocon Model 714	Repeat of 40R
10/29/65	42R	LTV HTM-2	Checkout of LTV HTM-2 cathode follower sitting in sponge rubber
	43R	LTV HTM-2	No reflecting plate
	44R	LTV HTM-2	Reflecting plate used
	45R	LTV HTM-2	Repeat of 44R
	46R	LTV HTM-2	Transducer in reflecting plate on aluminum mounting
	47R	LTV HTM-2	Transducer in reflecting plate sitting in cardboard box
	48R	LTV HTM-2	Repeat of 47R with 100 Ω resistor in cathode follower
	49R	LTV HTM-2	Repeat of 48R
10/29/65	50R	LTV HTM-2	Repeat of 49R
11/1/65	51R	Photocon Model 714	Externally triggered scope to obtain full trace
11/1/65	52R	ARC LD 107#1	Externally triggered scope to obtain full trace
11/3/65	53R	B & K	Flush metal mounting used
	54R	B & K	Repeat of 53R
	55R	B & K	Repeat of 54R
	56R	B & K	Repeat of 55R
	57R	B & K	Repeat of 56R; no good, no 'scope trace
	58R	LTV HTM-2	Externally triggered scope to obtain full trace
11/3/65	59R	LTV HTM-2	Repeat of 58R
11/15/65	60R	LTV HTM-3	Checkout of LTV HTM-3
	61R	LTV HTM-3	Repeat of 60R
	62R	LTV HTM-3	Repeat of 61R; slow sweep to obtain rise time
	63R	ARC LD 107#1	Repeat of 52R
11/15/65	64R	ARC LD 107#1	Repeat of 63R
11/16/65	65R	ARC LD 107#1	Repeat of 64R; slow sweep for rise time
	66R	Photocon Model 714	Checkout Photocon
	67R	Photocon Model 714	Repeat of 66R
	68R	B & K #101374	This shot starts series to see if ringing in B&K system is due to electronics or diaphragm
	69R	B & K #101374	Repeat of 68R
	70R	B & K #101374	Repeat of 69R; slow sweep for rise time
11/16/65	71R	B & K #101359	Repeat of 70R different transducer; same system

APPENDIX B

Date	Shot Number	Transducer	Comments
11/16/65	72R	B & K #107179	Repeat of 70R; different transducer, same system
	73R	B & K #107113	Repeat of 70R; different transducer, same system
	74R	B & K #107178	Repeat of 70R; different transducer, same system
	75R	B & K #107178	Repeat of 74R; transducer protruding 1/16" above reflecting plate
11/16/65	76R	B & K #107178	Repeat of 74R; transducer protruding 1/16" above reflecting plate
11/17/65	77R	B & K #107178	Repeat of 74R
	78R	B & K #107178	Repeat of 77R
	79R	B & K #107178	Repeat of 77R; slow sweep for rise time
	80R	B & K #107178	Symmetric bullet, unstable flight
	81R	B & K #107178	.30'06 bullet with nose sharpened
	82R	B & K #107178	.30'06 bullet with nose sharpened
	83R	B & K #107178	.30'06 bullet with nose sharpened
	84R	B & K #107178	Changed cathode follower unit
	85R	B & K #107178	Changed cathode follower unit
	86R	B & K #107178	Repeat of 78R with different power supply
	87R	B & K #107178	Repeat of 86R; gain on amplifier set at -10 db
	88R	B & K #107178	Repeat of 87R larger vertical scale
	89R	B & K #107178	Bypassed amplifier in power supply
	90R	B & K #107178	Repeat of 89R with amplifier gain different
11/17/65	91R	B & K #107178	Repeat of 90R; thin sheet of mylar over transducer
11/30/65	92R	LTV HTM-4	Transducer produced no output
	93R	B & K #107113	Acrylic reflecting plate, close tolerances
	94R	B & K #107113	Repeat of 93R
	95R	B & K #107113	Repeat of 94R
	96R	B & K #107113	Repeat of 94R
	97R	B & K #107113	Used power supply with 40 kc filter
	98R	B & K #107113	Repeat of 96R with 100k resistor and amplifier bypassed
11/30/65	99R	B & K #107113	Repeat of 99R; resistor closer to scope
11/30/65	100R	B & K #107113	Repeat of 99R; resistor connected directly to scope
	101R	B & K #107113	Repeat of 99R; 6" of cable between scope and resistor
12/1/65	102R	B & K #107113	Original system; scope moved to door of test section
	103R	B & K #107113	Repeat of 102R
	104R	B & K #107113	Repeat of 102R
	105R	LTV HTM-5	Checkout of LTV HTM-5

APPENDIX B

Date	Shot Number	Transducer	Comments
12/1/65	106R	LTV HTM-5	Repeat of 105R
	107R	B & K #107113	Checking out timing system
	108R	B & K #107113	Reduced powder charge in bullet
	109R	B & K #107113	Reduced powder charge in bullet
	110R	B & K #107113	Pointed nose bullet
12/1/65	111R	B & K #107113	Repeat of 110R
12/8/65	112R	LTV HTM-4	Checkout of LTV HTM-4
	113R	LTV HTM-4	Rerun of 112R
	114R	B & K #107113	Closer tolerance metal fittings
	115R	B & K #107113	Aluminum plate with rubber seat for cartridge
	116R	B & K #107113	Repeat of 115R
	117R	B & K #107113	Same plate as 115R with nylon seat
	118R	B & K #107113	Repeat of 117R
	119R	B & K #107113	Repeat of 114R;repeatability shot
	120R	B & K #107113	Aluminum base repeatability shot
	121R	B & K #107113	Rubber base nylon seat in aluminum plate
	122R	B & K #107113	Repeat of 122R with gap around transducer sealed
	123R	ARC LD 107#1	Columbia research cathode follower used
	124R	ARC LD 107#1	Repeat of 123R
	125R	ARC LD 107#1	Repeat of 124R cathode follower reorientation
	126R	ARC LD 107#1	Repeat of 125R; shielded output cable
12/8/65	127R	ARC LD 107#1	Repeat of 126R; moved cathode follower upstream
12/17/65	128R	B & K #107113	Remachined nylon seat
	129R	B & K #101359	Metal mounting counter didn't work
	130R	B & K #101359	Repeat of 129R
	131R	B & K #107113	Repeat of 128R
	132R	B & K #107113	Pictures no good
	133R	B & K #107179	No times
	134R	B & K #107179	Repeat of 133R;no times
	135R	B & K #107179	Repeat of 133R
	136R	B & K #107178	Repeat of 132R
	137R	B & K #107374	No scope trace
	138R	B & K #107374	Repeat of 137R
	139R	Kistler Model 717L	Checkout shot; transducer on cardboard box
	140R	Kistler Model 717L	Repeat of 139R; transducer on metal box
12/17/65	141R	LTV HTM-6	Checkout of LTV HTM-6
5/27/66	142R	B & K #107178	Checkout shot
	143R	B & K #101359	Checkout shot

APPENDIX B

Date	Shot Number	Transducer	Comments
5/27/66	144R	B & K #101359	Checkout shot
	145R	B & K #101359	Checkout shot
	146R	B & K #101359	Checkout shot
	147R	B & K #101359	Checkout shot
5/31/66	148R	B & K #107178	Checkout shot
	149R	B & K #107178	Checkout shot
	150R	B & K #107178	Checkout shot
	151R	B & K #107178	Checkout shot
	152R	B & K #107178	Checkout shot
6/1/66	153R	B & K #107178	Checkout shot
	154R	B & K #107178	Checkout shot
	155R	B & K #107178	Checkout shot
	156R	B & K #107179	Checkout shot
	157R	B & K #107179	Checkout shot

Ballistic Model Shots

Date	Run Number	Model	Sabot	Range Tank Pressure	Remarks
12/13/65	1	15° cone	1	Atm	Slight angle of attack
12/14/65	2	15° cone	1	Atm	Good shot*
12/17/65	3	15° cone	2	Atm	Good shot
12/21/65	4	15° cone	2	Atm	Shot o.k.; instruments malfunctioned
12/21/65	5	15° cone	3	Atm	Good shot
12/27/65	6	15° cone	4	Atm	Bad shot **
12/28/65	7	15° cone	4	Atm	Bad shot
12/29/65	8	15° cone	3	Atm	Bad shot. Pins fit too tight
12/30/65	9	15° cone	3	Atm	Good shot
12/30/65	10	15° cone	6	Atm	Bad shot
01/03/66	11	15° cone	5	Atm	Model tumbled
01/04/66	12	15° cone	7	Atm	Bad shot
01/05/66	13	15° cone	8	Atm	Good shot
01/05/66	14	Plane	10	Atm	Bad shot
01/06/66	15	15° cone	8	Atm	Good shot
01/10/66	16	Plane	11	Atm	Good shot. No roll
01/11/66	17	Plane	11	Atm	Good shot. Rolled at 45°/ 10 ft.
01/11/66	18	Plane	11	Atm	Good shot. Model has roll, yaw, and pitch

APPENDIX B

Date	Run Number	Model	Sabot	Range Tank Pressure	Remarks
01/12/66	19	Lexan Cylinder	None	Atm	Check loading condition
01/12/66	20	Lexan Cylinder	None	Atm	Check loading condition
01/12/66	21	Lexan Cylinder	None	Atm	Check loading condition
01/13/66	22	Plane	11	Atm	Good shot. Model rolled
01/17/66	23	15^{o} cone	8	Atm	Good shot
01/17/66	24	15^{o} cone	8	Atm	Good shot
01/18/66	25	15^{o} cone	8	Atm	Good shot
01/18/66	26	15^{o} cone	8	Atm	Good shot
02/01/66	27	15^{o} cone	8	Atm	Good shot. New launch tube
02/01/66	28	15^{o} cone	8	Atm	Good shot
02/01/66	29	Plane	11	Atm	Good shot. Model rolled
02/02/66	30	Super Plane	11	Atm	Good shot
02/02/66	31	Plane	11	Atm	Good shot. Model rolled and yawed
02/02/66	32	Super Plane	11	Atm	Good shot. Roll and yaw
02/03/66	33	Plane	11	Atm	Good shot. Model rolled
03/03/66	34	Plane	11	20mm Hg	Perfect flight
02/04/66	35	15^{o} cone	8	Atm	Bad shot
02/04/66	36	15^{o} cone	8	Atm	Bad shot
02/07/66	37	15^{o} cone	8	Atm	Bad shot
02/07/66	38	15^{o} cone	8	Atm	Bad shot
02/08/66	39	15^{o} cone	8	Atm	Bad shot
02/08/66	40	15^{o} cone	8	Atm	Good shot. Model yawed
02/09/66	41	15^{o} cone	8	Atm	Good shot.
02/09/66	42	Plane	11	Atm	Good shot. Slight roll
02/09/66	43	Super Plane	11	Atm	Good shot.
02/10/66	44	15^{o} cone	8	Atm	Bad shot
02/10/66	45	15^{o} cone	8	Atm	Bad shot
02/11/66	46	Super Plane	11	Atm	Good shot. Model yawed
02/11/66	47	Super Plane	11	Atm	Perfect shot
02/14/66	48	Super Plane	11	Atm	Good shot. Model yawed
02/14/66	49	Super Plane	11	Atm	Good shot, slight yaw and roll
02/15/66	50	15^{o} cone	8	Atm	Good shot. No shadow-graph
02/16/66	51	15^{o} cone	8	Atm	Good shot. No shadow-graph
02/16/66	52	Trimmed Plane	11	Atm	Good shot. Model Rolled
02/17/66	53	Trimmed Plane	11	Atm	Bad shot
02/17/66	54	Trimmed Plane	12	Atm	Bad shot

APPENDIX B

Date	Run Number	Model	Sabot	Range Tank Pressure	Remarks
02/18/66	55	Trimmed Plane	11	Atm	Good shot. Model rolled
02/21/66	56	Sharp L.E. Plane	11	7 psia	Good shot. Model rolled and pitched
02/21/66	57	Plane	11	7 psia	Good shot. Model rolled
02/22/66	58	Plane	11	100 mm Hg	Good shot. Slight roll
05/27/66	59	15^{o} cone	8	Atm	Good shot. Model pitched
	60	15^{o} cone	8	Atm	Good shot.
	61	15^{o} cone	8	Atm	Good shot.
05/31/66	62	15^{o} cone	8	Atm	Good shot. Slow scope sweep
	63	.30-06 armor piercing shape	8	Atm	Good shot. Model pitched and yawed
	64	.30-06 armor piercing shape	8	Atm	Good shot.
06/1/66	65	.30-06 armor piercing shape	8	Atm	Good shot. Model pitched and yawed slightly
	66	.30-06 armor piercing shape	8	Atm	Good shot. Model pitched down, no yawing

*Good shot indicates that model has been successfully launched and the velocity and model integrity have been verified.

**Bad shot indicates that model breaks up or did not enter the range tank.

REFERENCES

1. Anon.; Some Considerations of Sonic Boom. Federal Aviation Agency, Office of Plans, May 1961.

2. Lyster, H. N. C.; A Review of Theoretical and Experimental Information Relating to the Sonic Boom. National Research Council of Canada, Aeronautical Report LR-313, September 1961.

3. Maglieri, Domenic J.; and Carlson, Harry W.; The Shock-Wave Noise Problem of Supersonic Aircraft in Steady Flight. NASA Memo 3-4-59L, April 1959.

4. Carlson, H. W.; Correlation of Sonic-Boom Theory with Wind-Tunnel and Flight Measurements. NASA TR R-213, December 1964.

5. Whitham, G. B.; The Flow Pattern of a Supersonic Projectile. Communications on Pure and Applied Mathematics, Vol. V, 1952, pp. 301-348.

6. Walkden, F.; The Shock Pattern of a Wing-Body Combination, Far from the Flight Path. The Aeronautical Quarterly, March 1957, pp. 164-194.

7. Callaghan, J. G.; The Simulation of Sonic Boom by Ballistic Models. Technical Proposal 902T, Douglas Aircraft Company, 16 August 1963.

8. Kuethe, A. M.; and Schetzer, J. D.; Foundations of Aerodynamics. Second Printing, John Wiley & Sons, Inc., 1955.

9. DeRose, Charles E.; and Boissevain, Alfred G.; An Exploratory Investigation in a Ballistic Range of the Stability Derivatives of a Simple Airplane Configuration at Low Supersonic Speeds. NASA TND-139, December 1959.

10. Warren, H. R.; Templin, R. J.; and Cheers, B.; Aeroballistics Range Measurements of the Performance and Stability of Supersonic Aircraft. IAS Pre-print 788, January 1958.

11. Wylie, C. R., Jr.; Advanced Engineering Mathematics. Second Edition, McGraw-Hill Book Company, Inc., 1960.

12. Etkin, B.; Dynamics of Flight. John Wiley & Sons, Inc., 1959.

13. Perkins, C. D.; and Hage, R. E.; Aircraft Performance, Stability and Control. John Wiley & Sons, 1956.

14. Ellison, D. E.; USAF Stability and Control Datcom. 1960.

15. D' Azzo and Houpis; Control System Analysis and Synthesis. McGraw-Hill Book Company, 1960.

16. Olson, H. F.; Acoustical Engineering. D. Van Nostrand Company, 1957.

17. Morse, P. M.; Vibration and Sound. McGraw-Hill Book Company, 1948.

18. Crandall, I. B.; Theory of Vibrating Strings and Sound. D. Van Nostrand Company, 1954.

19. Robey, D. H.; Theory of a Thin Air Film on the Vibrations of a Stretched Circular Membrane. Journal Acoust. Soc. America, Vol. 26, pp. 740, 1954.

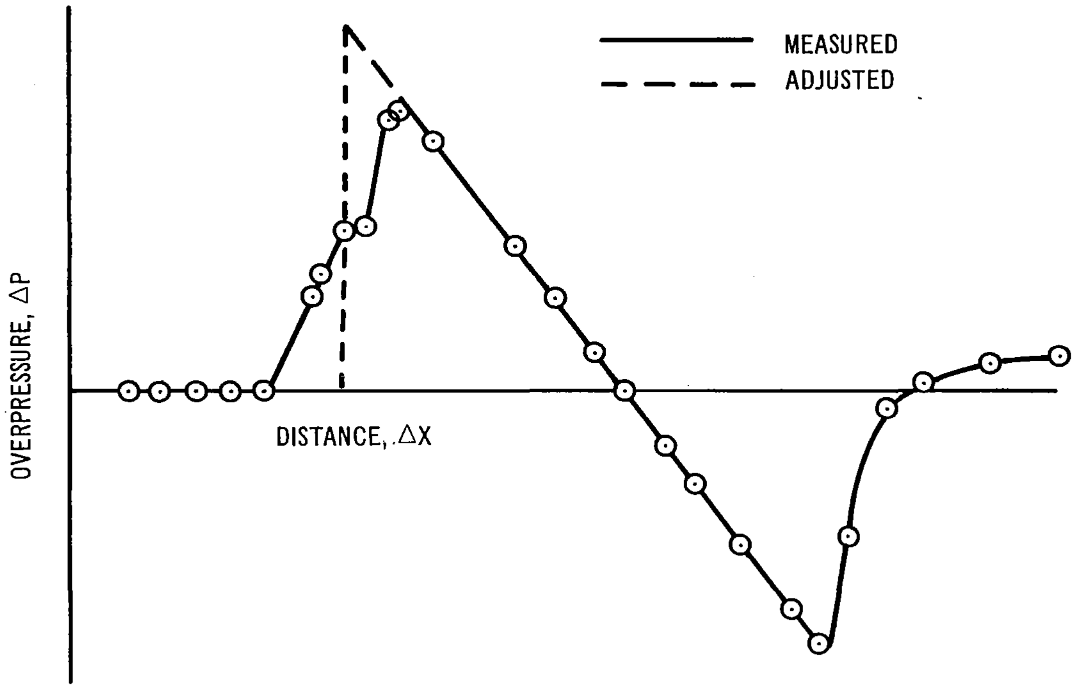

FIGURE 1. TYPICAL MEASURED PRESSURE SIGNATURE FROM STING SUPPORTED WIND TUNNEL MODEL

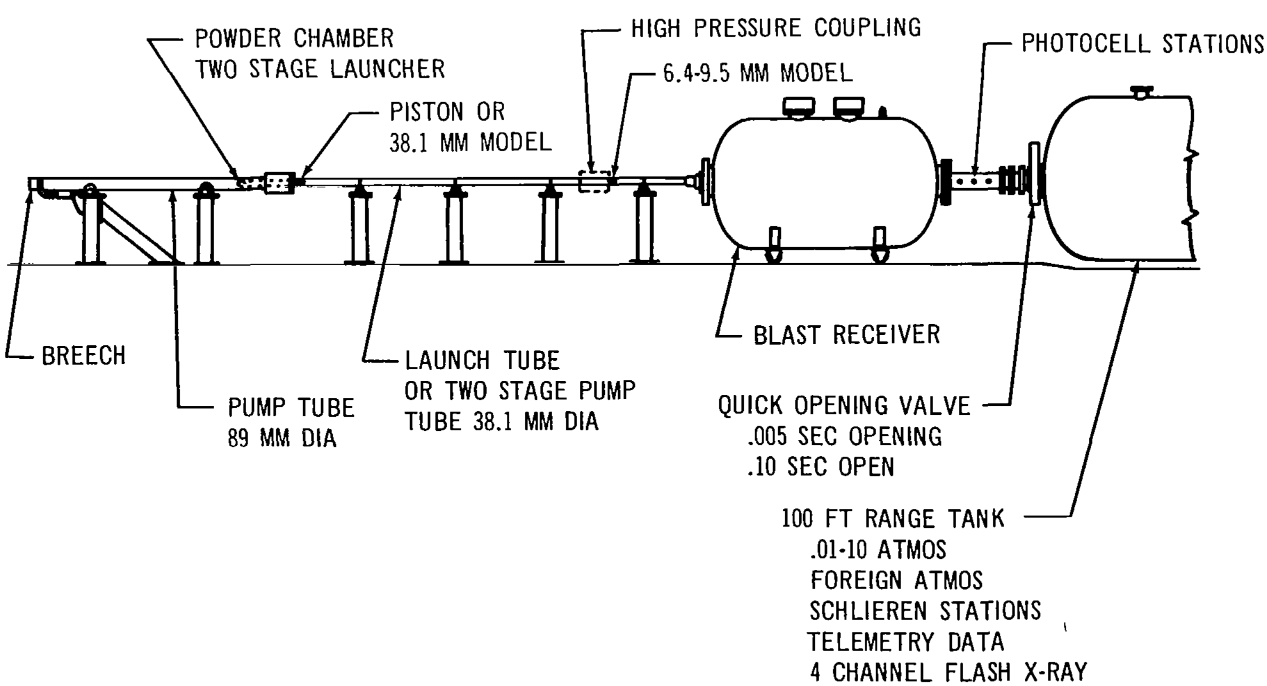

FIGURE 2. LIGHT GAS GUN – BALLISTIC RANGE

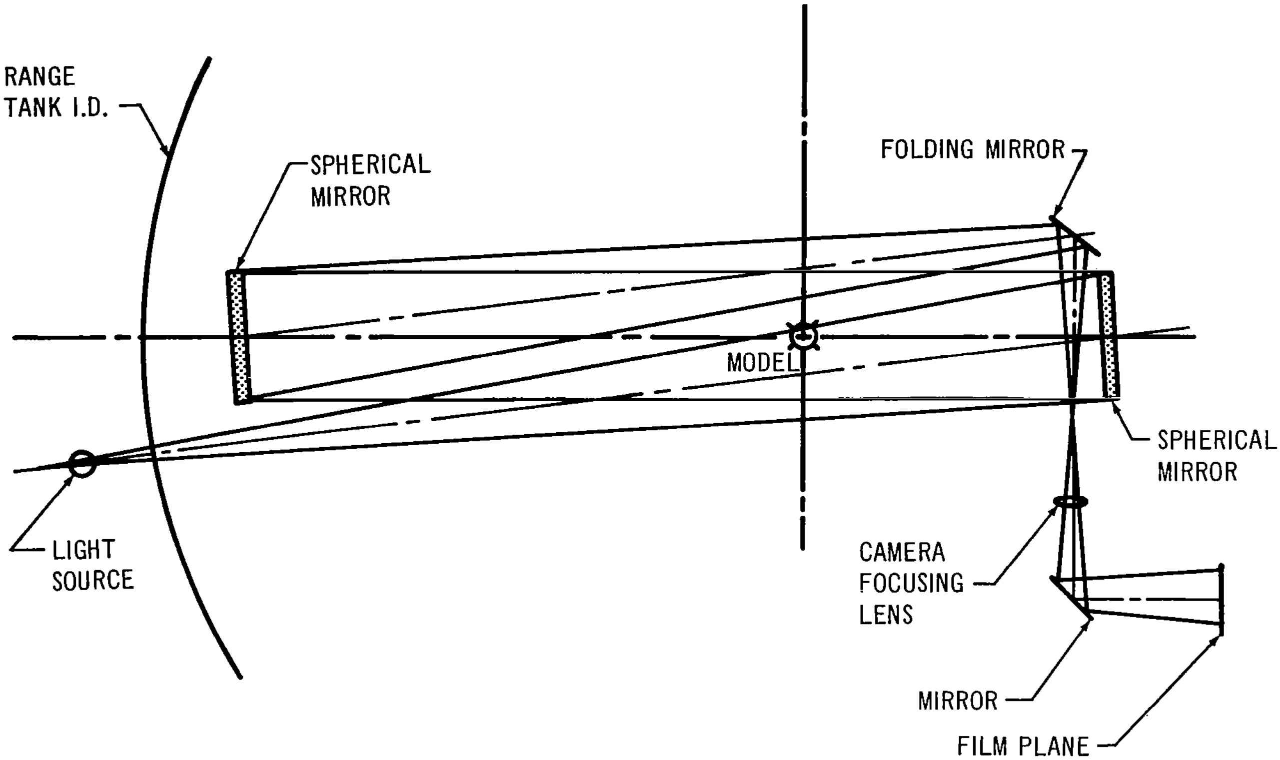

FIGURE 3. SHADOWGRAPH OPTICAL ARRANGEMENT

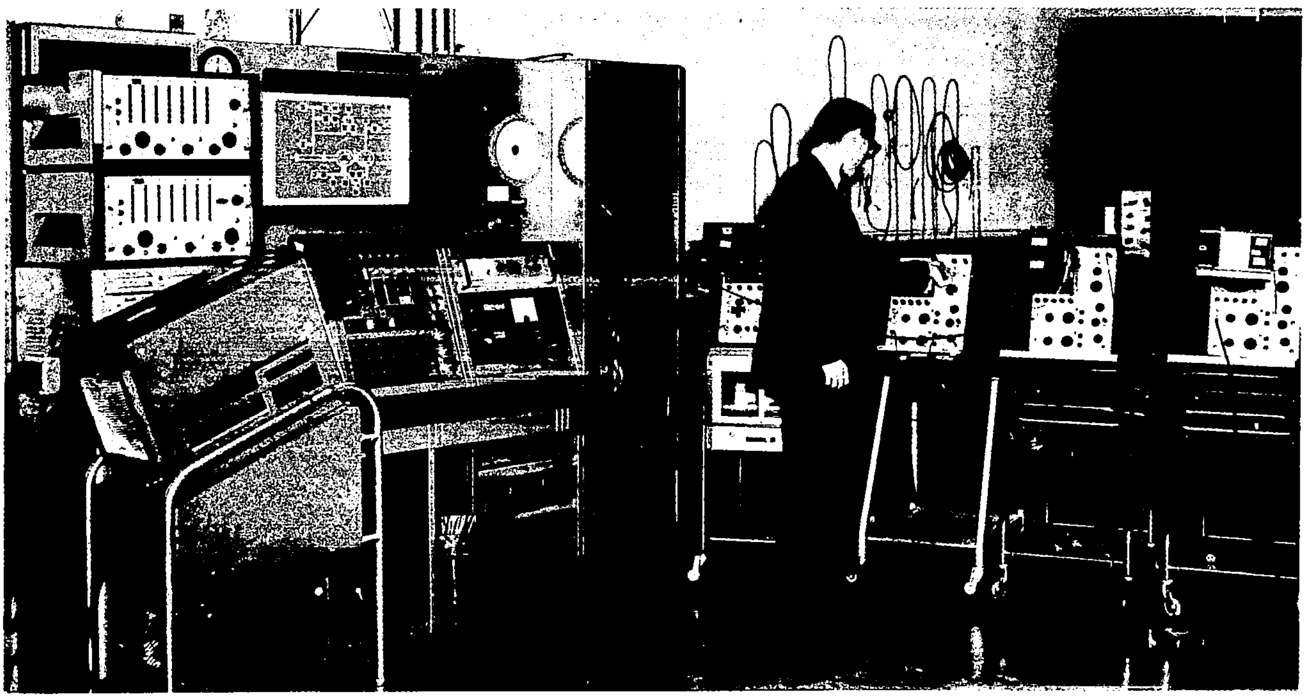

FIGURE 4. BALLISTIC RANGE CONTROL CONSOLE

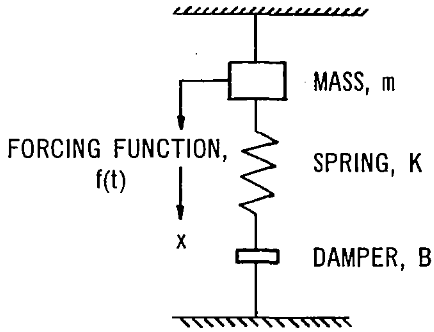

$$m\ddot{x} + K\dot{x} + Bx = f(t)$$

FIGURE 5. TRANSDUCER MECHANICAL ANALOG

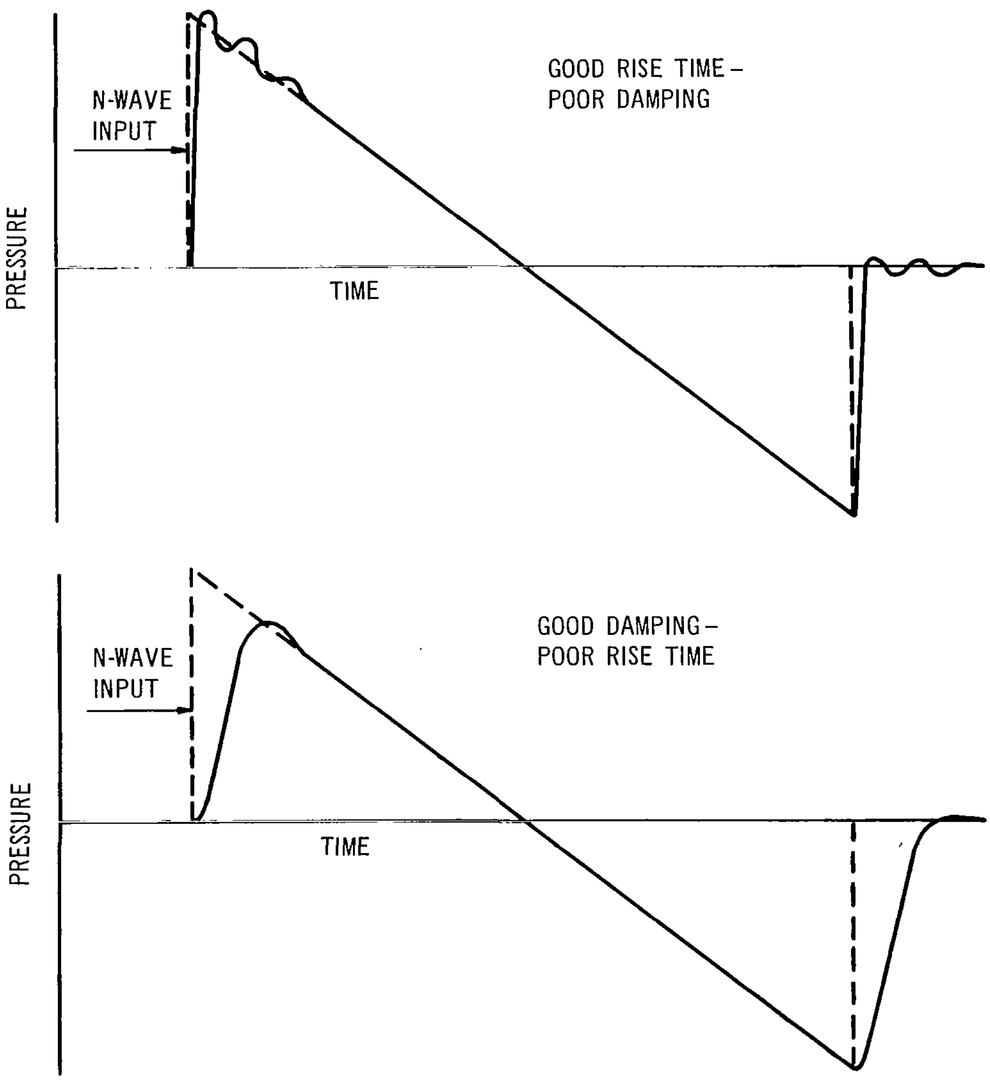

FIGURE 6. REPRESENTATIVE TRANSDUCER RESPONSE CHARACTERISTICS

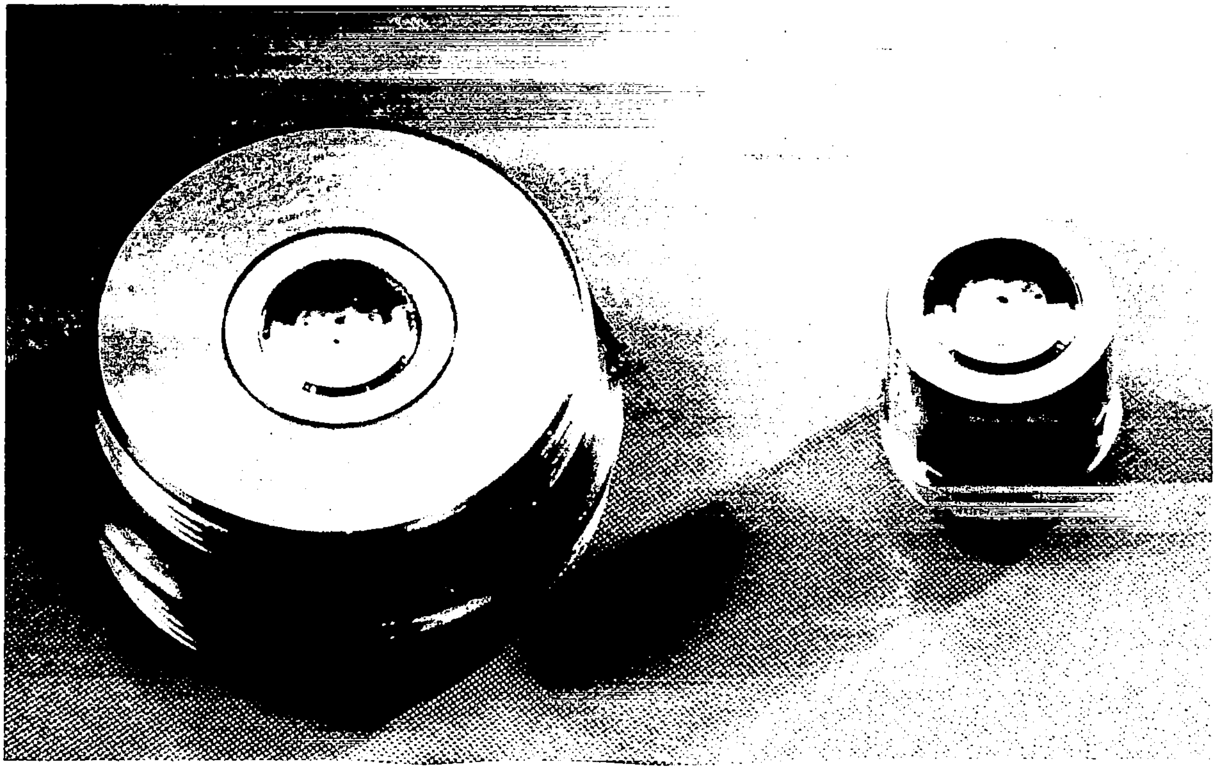

FIGURE 7. TAILORED TRANSDUCERS

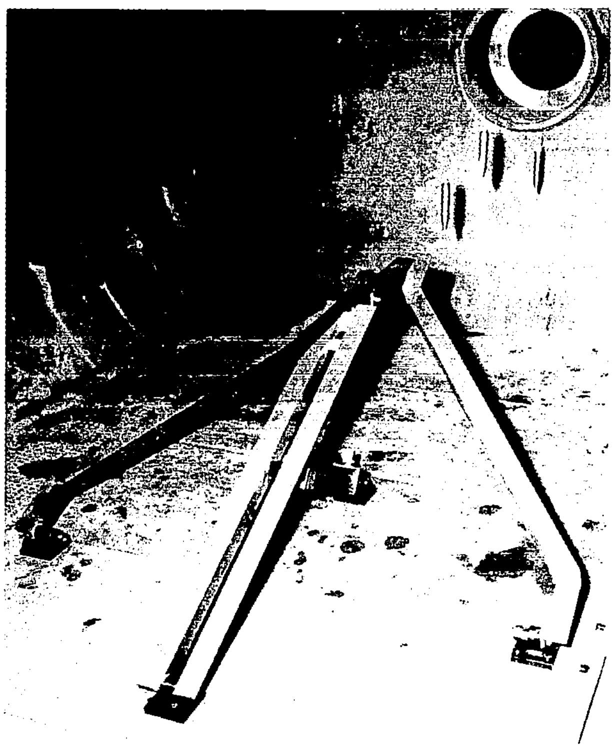

FIGURE 8. .30-CALIBER RIFLE INSTALLED IN RANGE TANK

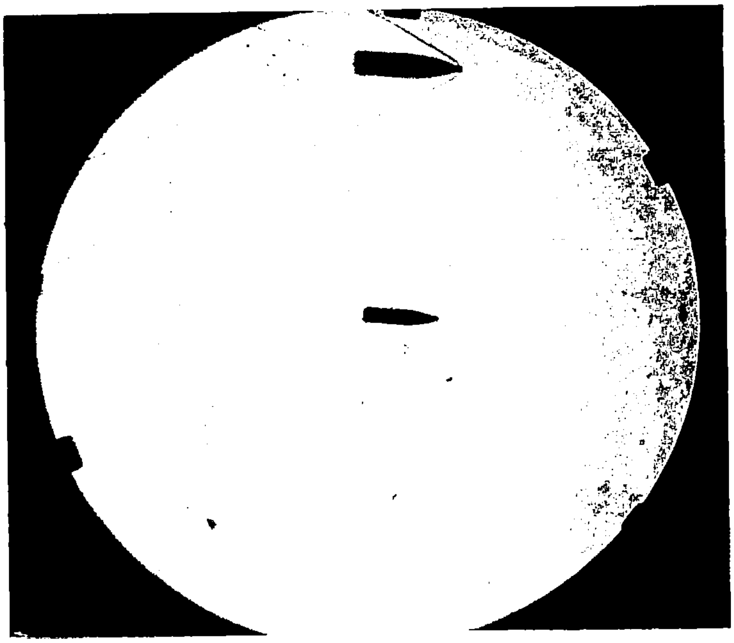

FIGURE 9. SHADOWGRAPH OF .30-CALIBER RIFLE BULLET; VELOCITY = 2650 FT/SEC; SHOT 17R

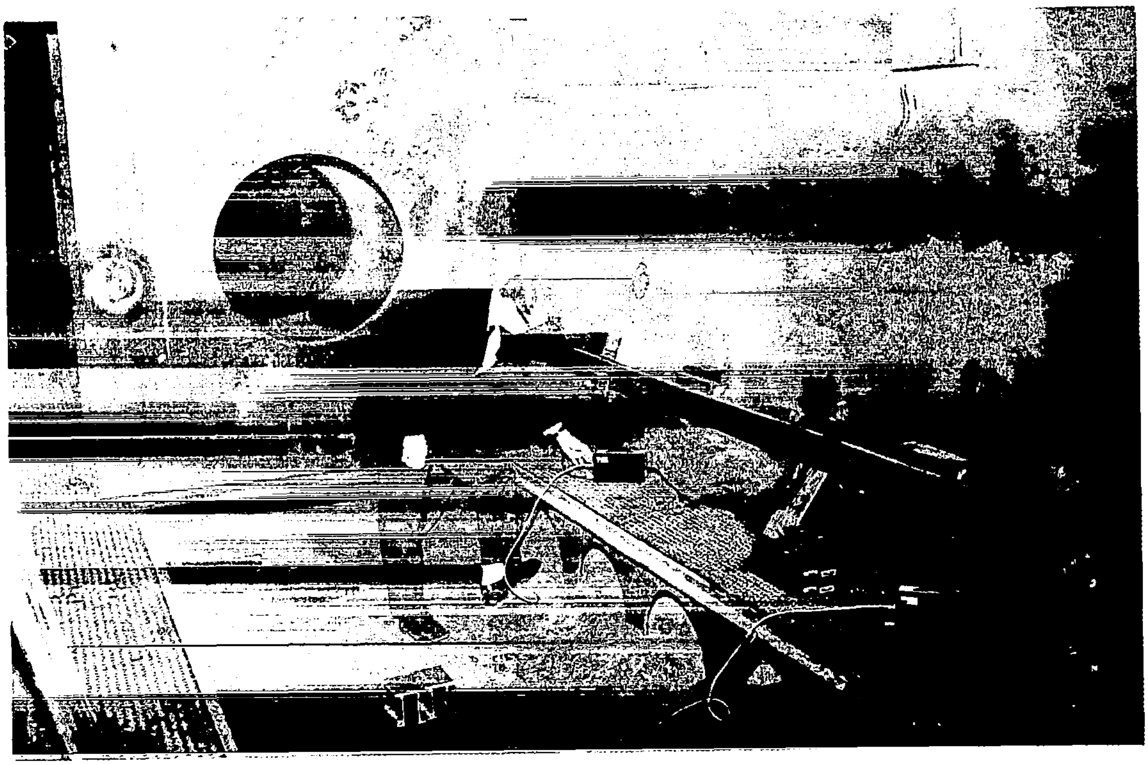

FIGURE 10. TEST ARRANGEMENT IN RANGE TANK

1 VOLT/CM

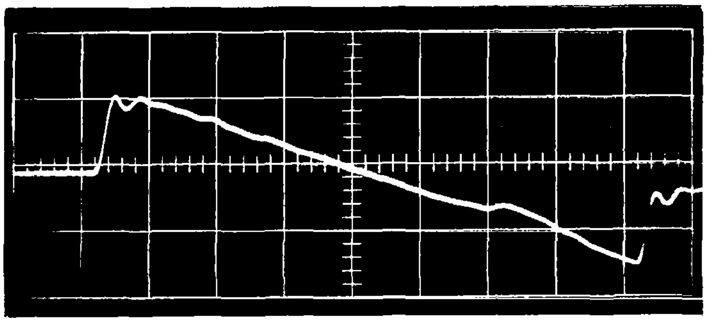

.30-CALIBER RIFLE BULLET SIGNATURE; SHOT 105R

20 μ SEC/CM

100 μ SEC/CM

10 VOLTS/CM

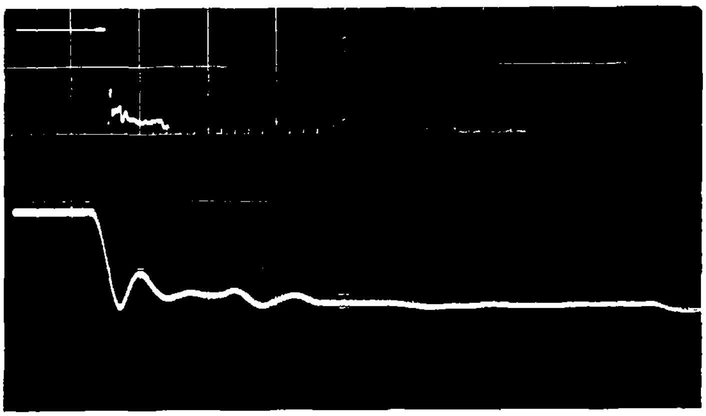

SHOCK TUBE SIGNATURE

10 μ SEC/CM

FIGURE 11. TAILORED TRANSDUCER PRESSURE SIGNATURE; CENTER SUPPORT DIAPHRAGM

0.5 VOLTS/CM

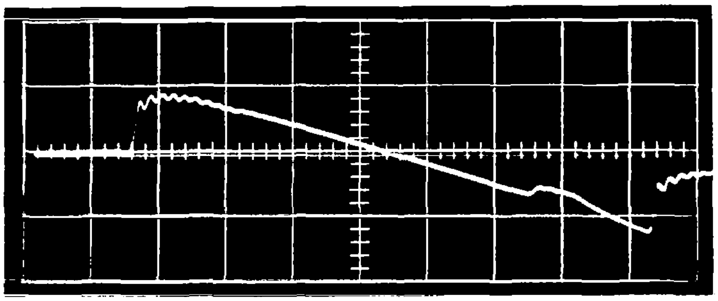

.30-CALIBER RIFLE
BULLET SIGNATURE;
SHOT 113R

20 μ SEC/CM

FIGURE 12. TAILORED TRANSDUCER PRESSURE SIGNATURE; MULTIPLE SUPPORT DIAPHRAGM

0.1 VOLTS/CM

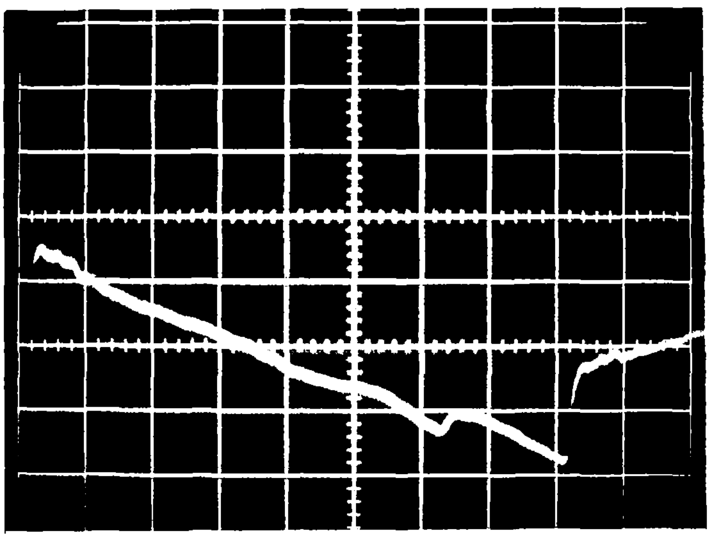

.30-CALIBER RIFLE
BULLET SIGNATURE;
SHOT 16R

20 μ SEC/CM

.05 VOLTS/CM

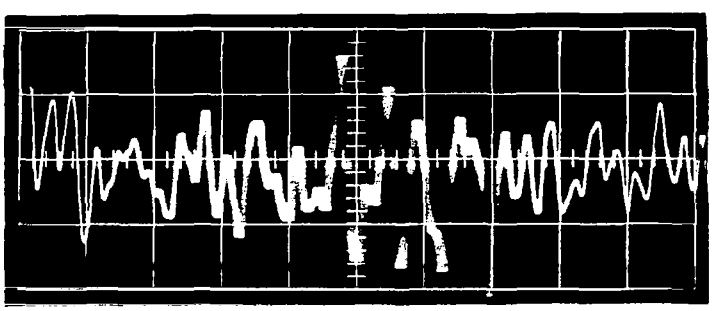

.30-CALIBER RIFLE
BULLET SIGNATURE;
SHOT 139R

20 μ SEC/CM

FIGURE 13. REPRESENTATIVE SIGNATURES FROM COMMERCIALLY AVAILABLE PIEZOELECTRIC TYPE TRANSDUCERS

0.5 VOLT/CM

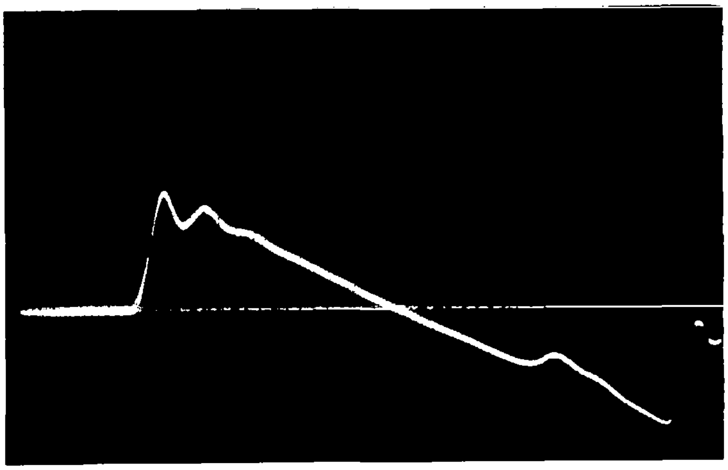

.30-CALIBER RIFLE BULLET PRESSURE SIGNATURE; SHOT 51R: INSUFFICIENT DAMPING FOR CURRENT STUDY

20 μ SEC/CM

1 VOLT/CM

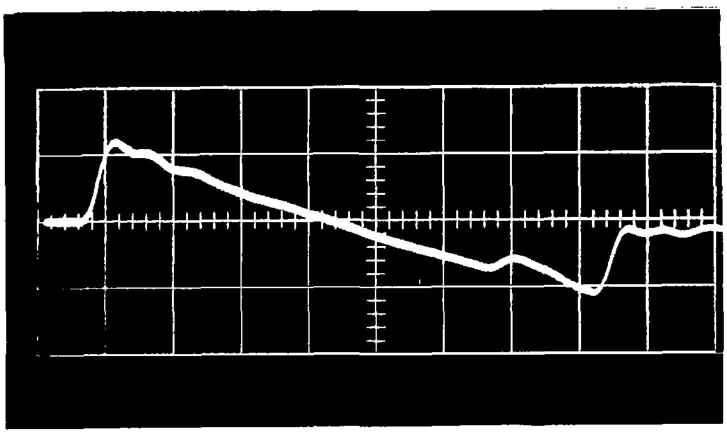

.30-CALIBER RIFLE BULLET PRESSURE SIGNATURE; SHOT 82R: TRANSDUCER USED FOR RECORDING BALLISTIC MODEL PRESSURE SIGNATURES

20 μ SEC/CM

FIGURE 14. PRESSURE SIGNATURES FROM COMMERCIALLY AVAILABLE CAPACITANCE TRANSDUCERS

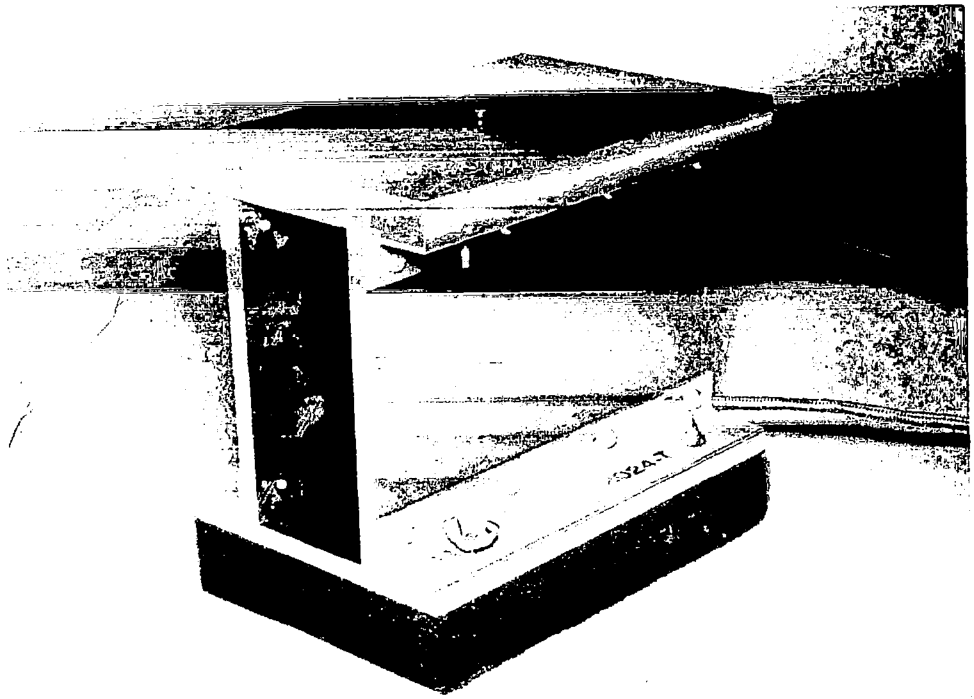

FIGURE 15. TYPICAL TRANSDUCER MOUNTING BOX

1 VOLT/CM

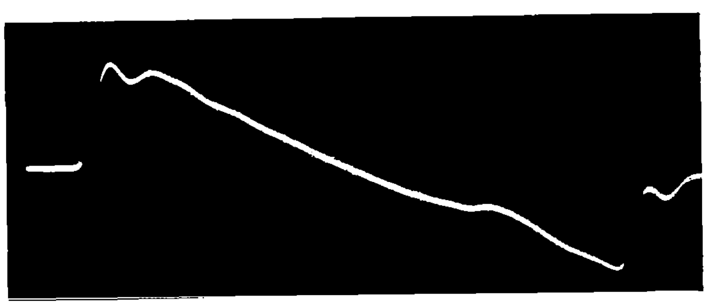

.30-CALIBER RIFLE BULLET SIGNATURE; SHOT 115R

20 μ SEC/CM

FIGURE 16. EFFECT OF SOFT RUBBER INSULATING SEAT AROUND TRANSDUCER

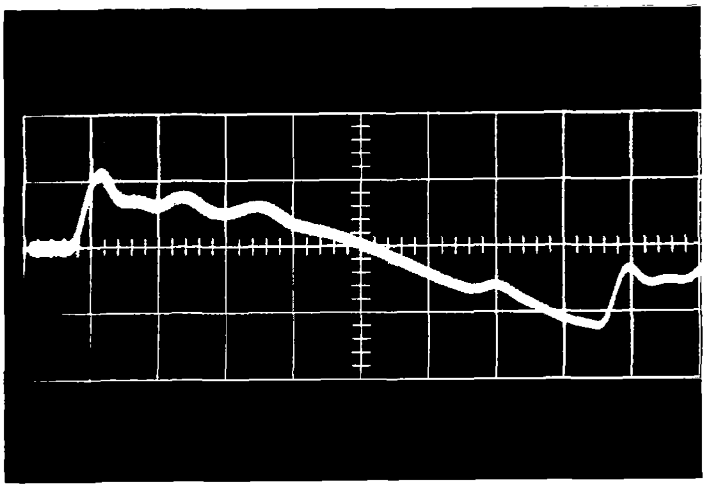

FIGURE 17. EFFECT OF 0.1 INCH GAP BETWEEN TRANSDUCER AND REFLECTING PLATE

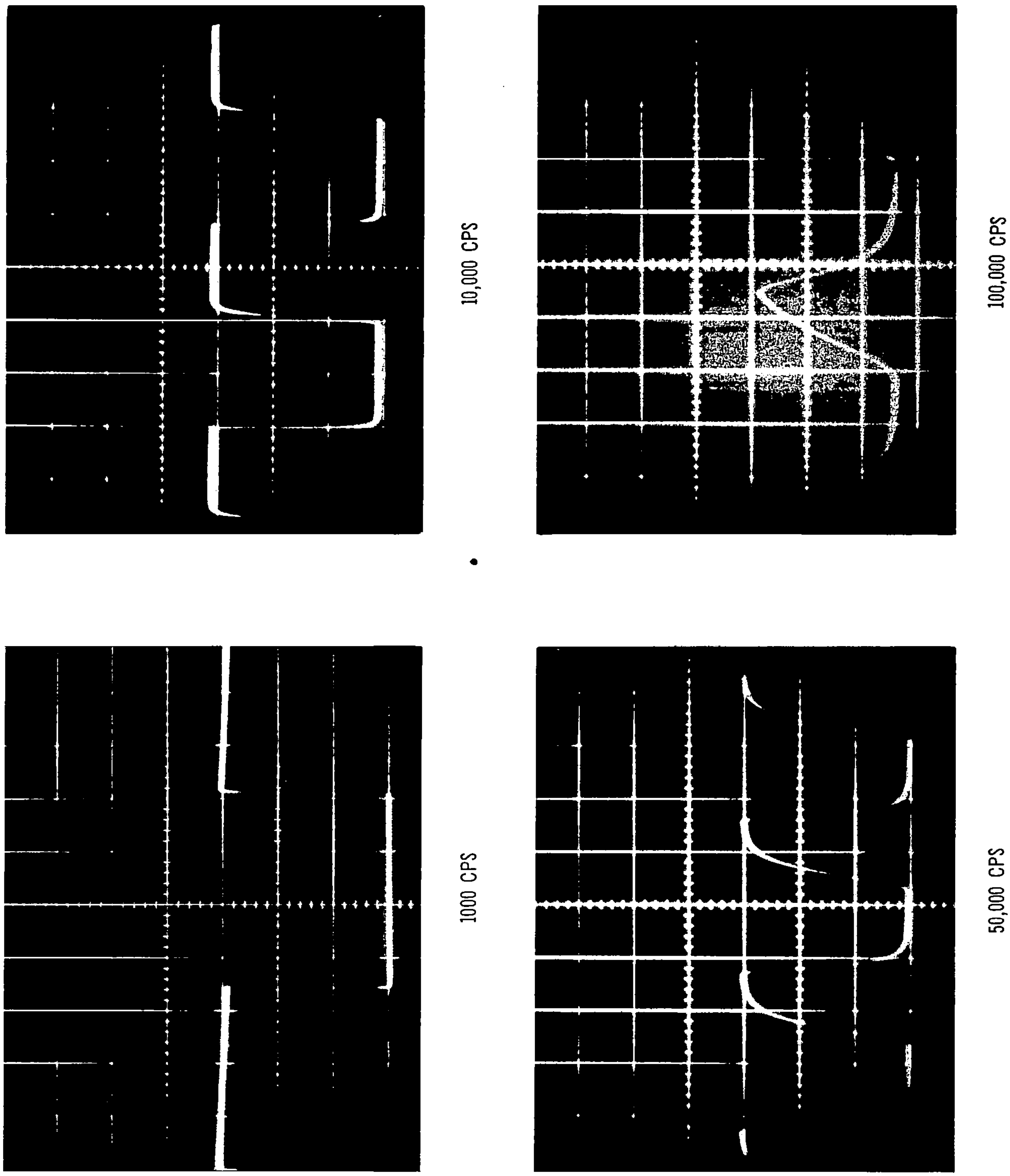

FIGURE 18. SQUARE WAVE INPUT INTO TRANSDUCER CATHODE FOLLOWER

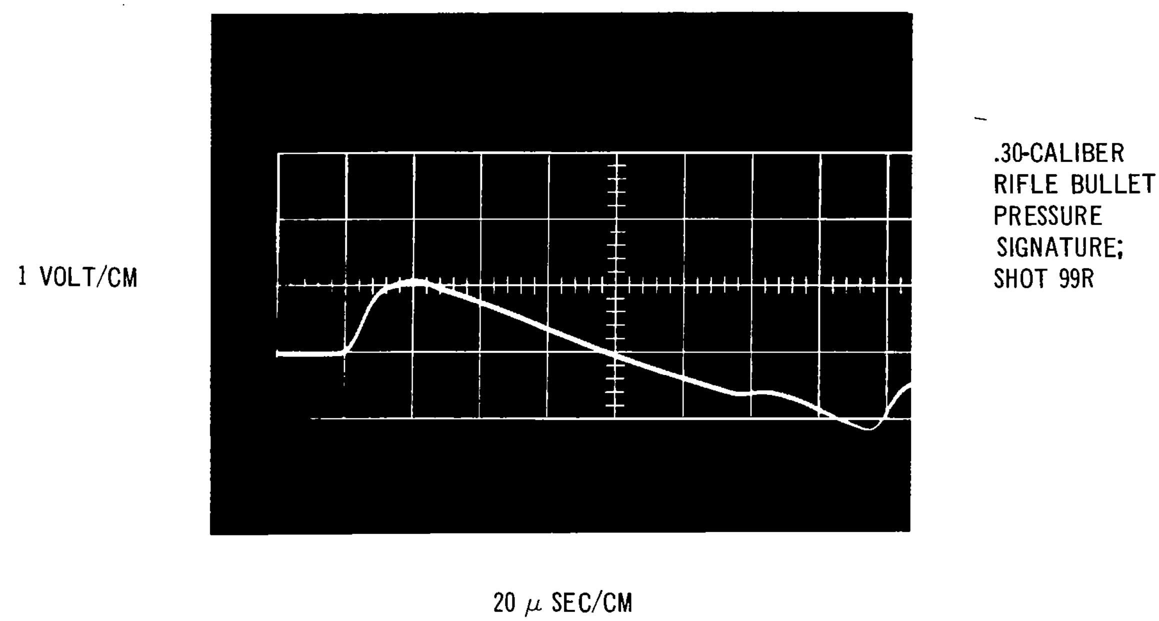

FIGURE 19. EFFECT OF 50,000 CPS FILTER
ON PRESSURE SIGNATURE

.01 VOLTS/CM

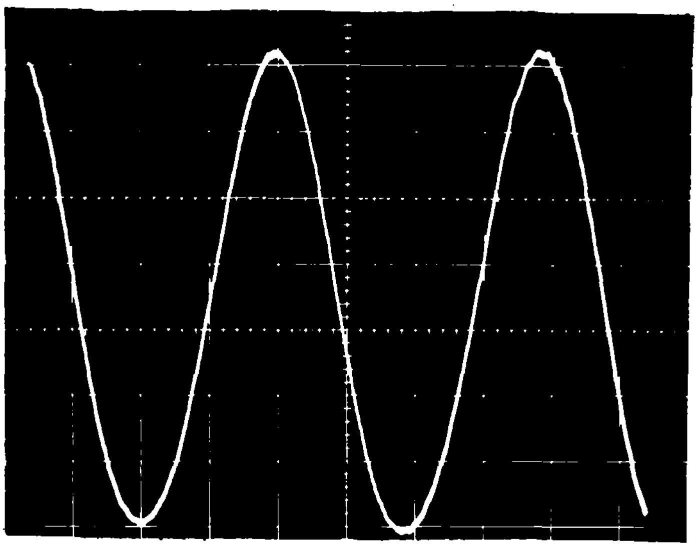

1 MSEC/CM

$$\text{TRANSDUCER SENSITIVITY} = \frac{\text{R.M.S. electrical output, volts}}{\text{pressure input, psi}}$$

$$\text{PRESSURE INPUT FROM PISTONPHONE} = 123.82\text{ dB}$$
$$= .00451\text{ psi}$$

$$\text{R.M.S. ELECTRICAL OUTPUT} = \frac{1}{\sqrt{2}}\left(\frac{3.18 + 3.18}{3.90 + 4.05}\right)(.01)\text{ VOLTS}$$
$$= .0253\text{ VOLTS}$$

$$\therefore\ \text{SENSITIVITY} = \frac{.0253\text{ volts}}{.00451\text{ psi}} = 5.61\text{ volts/psi}$$

FIGURE 20. SAMPLE TRANSDUCER CALIBRATION

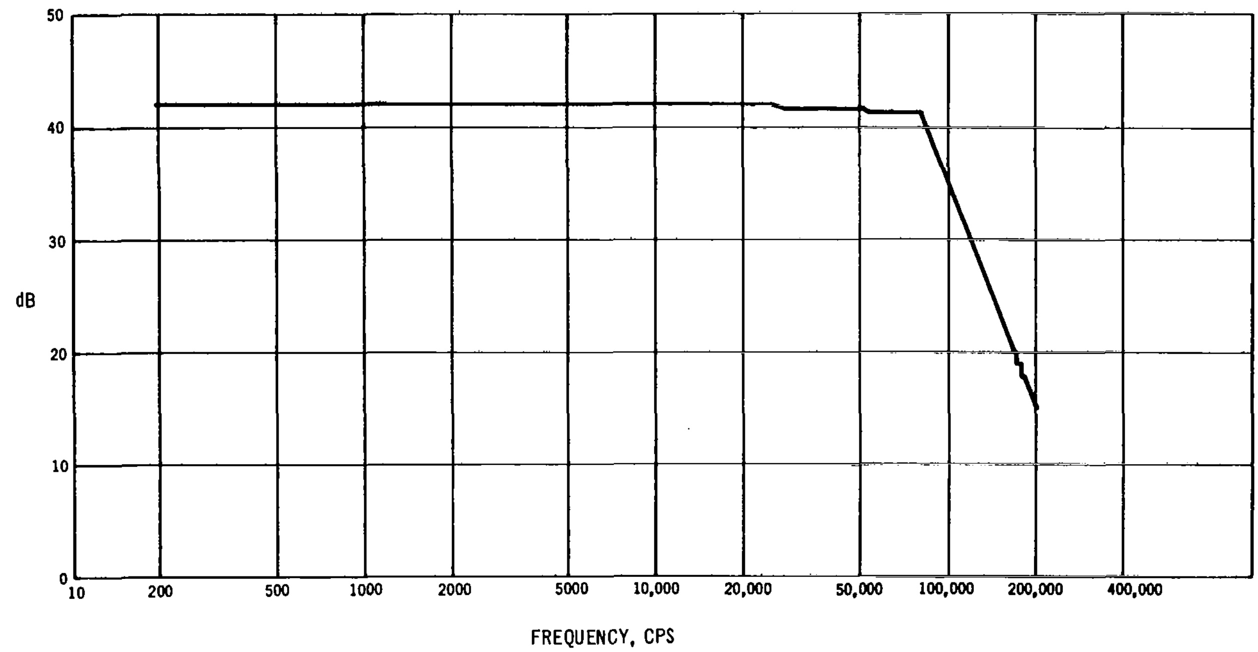

FIGURE 21. REPRESENTATIVE FREQUENCY RESPONSE CHARACTERISTICS FOR PRESSURE TRANSDUCER

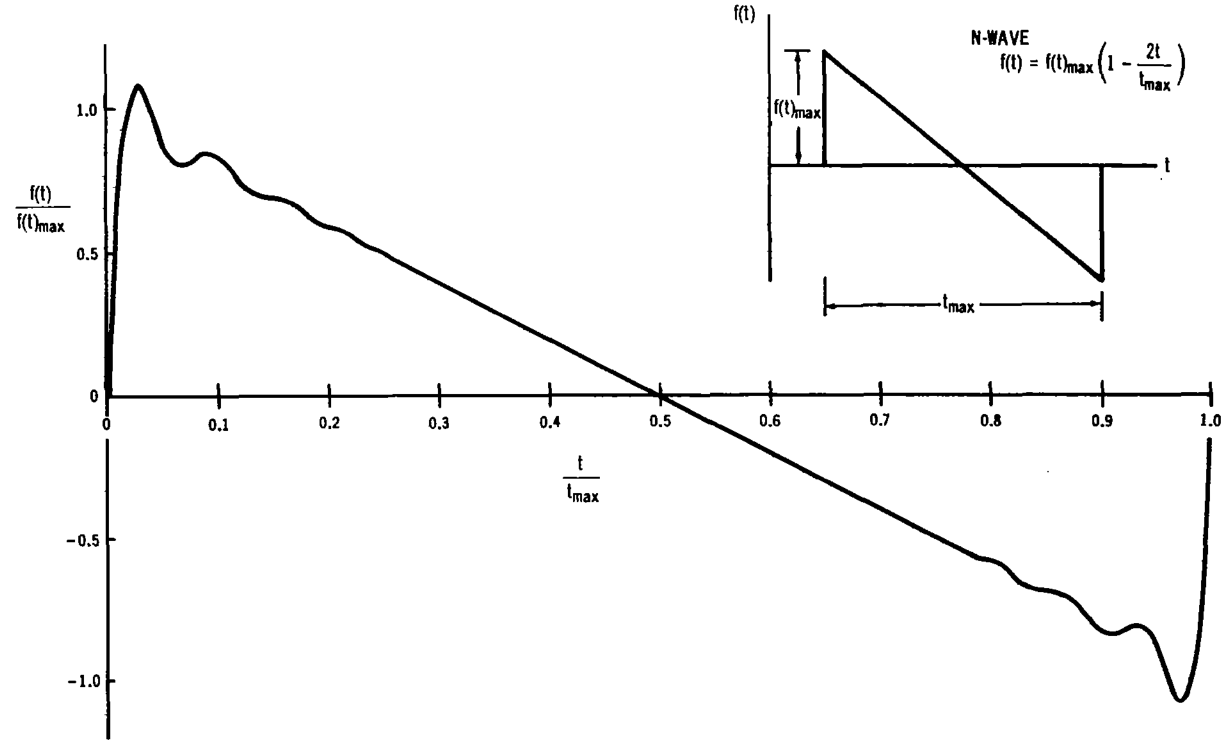

NOTE: FREQUENCY RESPONSE CHARACTERISTICS FROM FIGURE 21 USED. FOURIER SYNTHESIS CUT OFF AT 180,000 CPS, GIVING A TOTAL OF 29 HARMONICS.

FIGURE 22. FOURIER SYNTHESIS OF N-WAVE

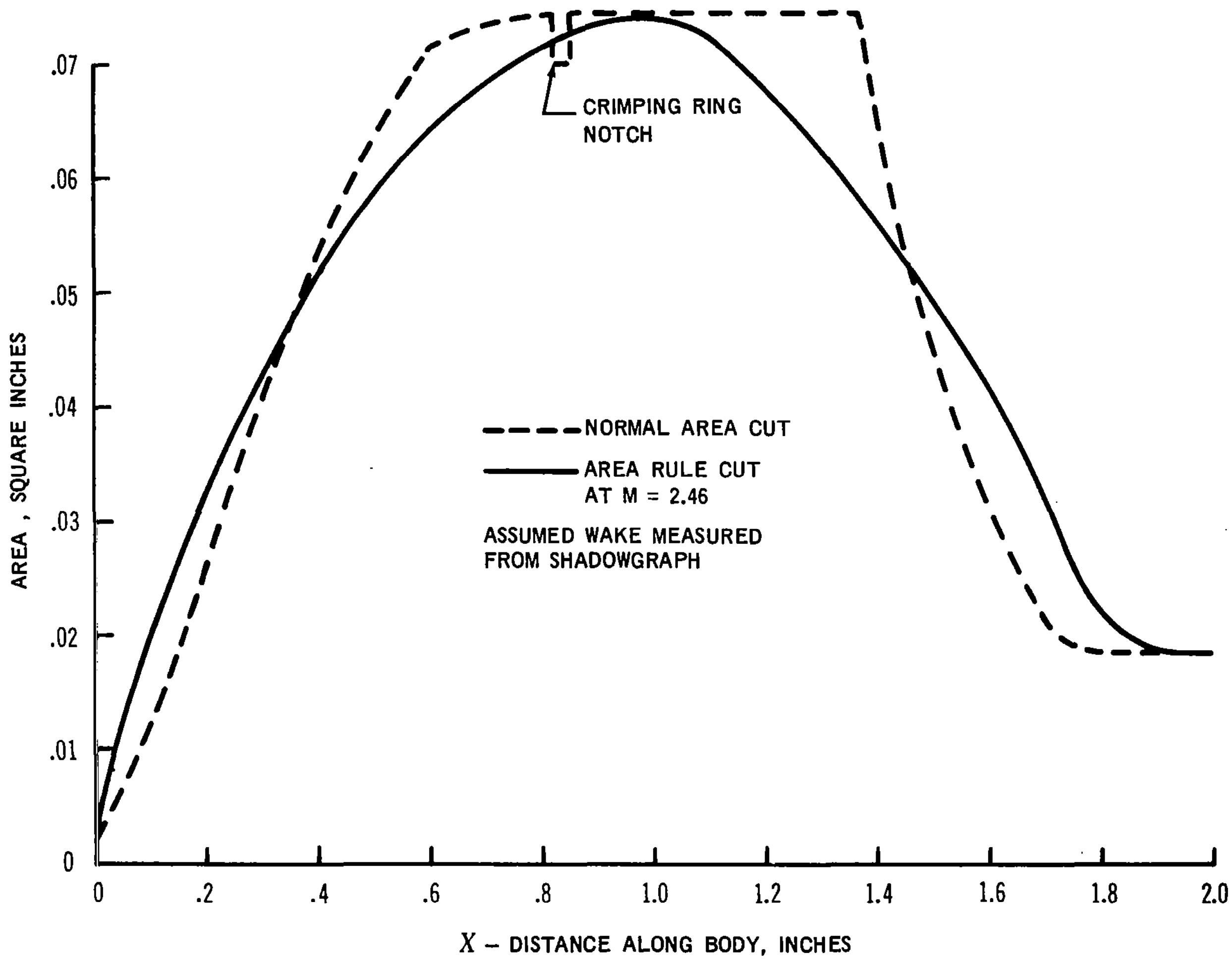

FIGURE 23. AREA DISTRIBUTION FOR .30-CALIBER RIFLE BULLET

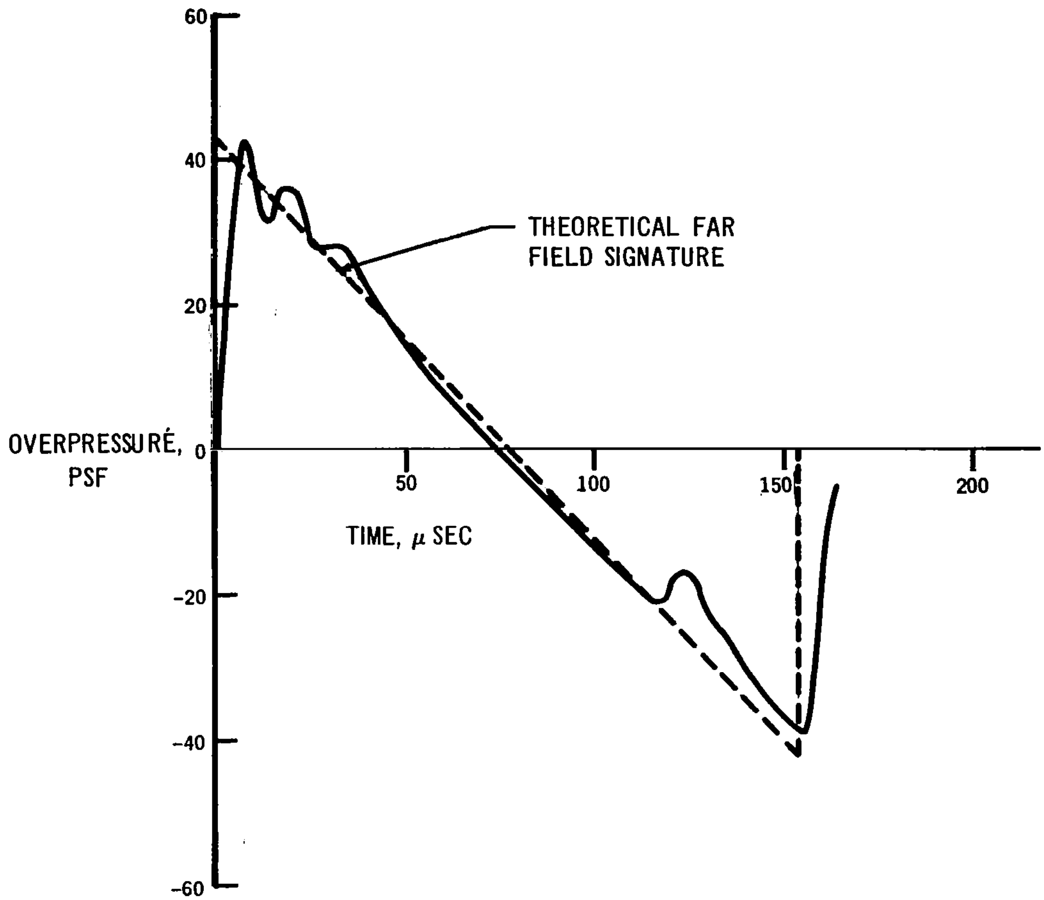

TRANSDUCER SENSITIVITY = 4.41 VOLTS/PSI

1 VOLT/CM

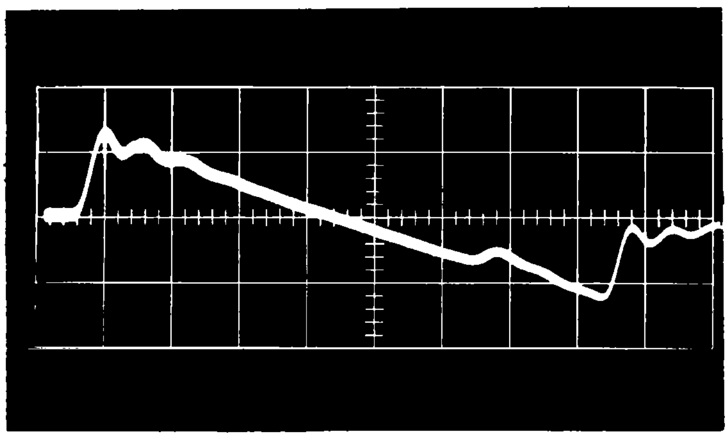

20 μ SEC/CM

FIGURE 24(a). PRESSURE SIGNATURE FROM A .30-CALIBER RIFLE BULLET; SHOT 69R: M = 2.5

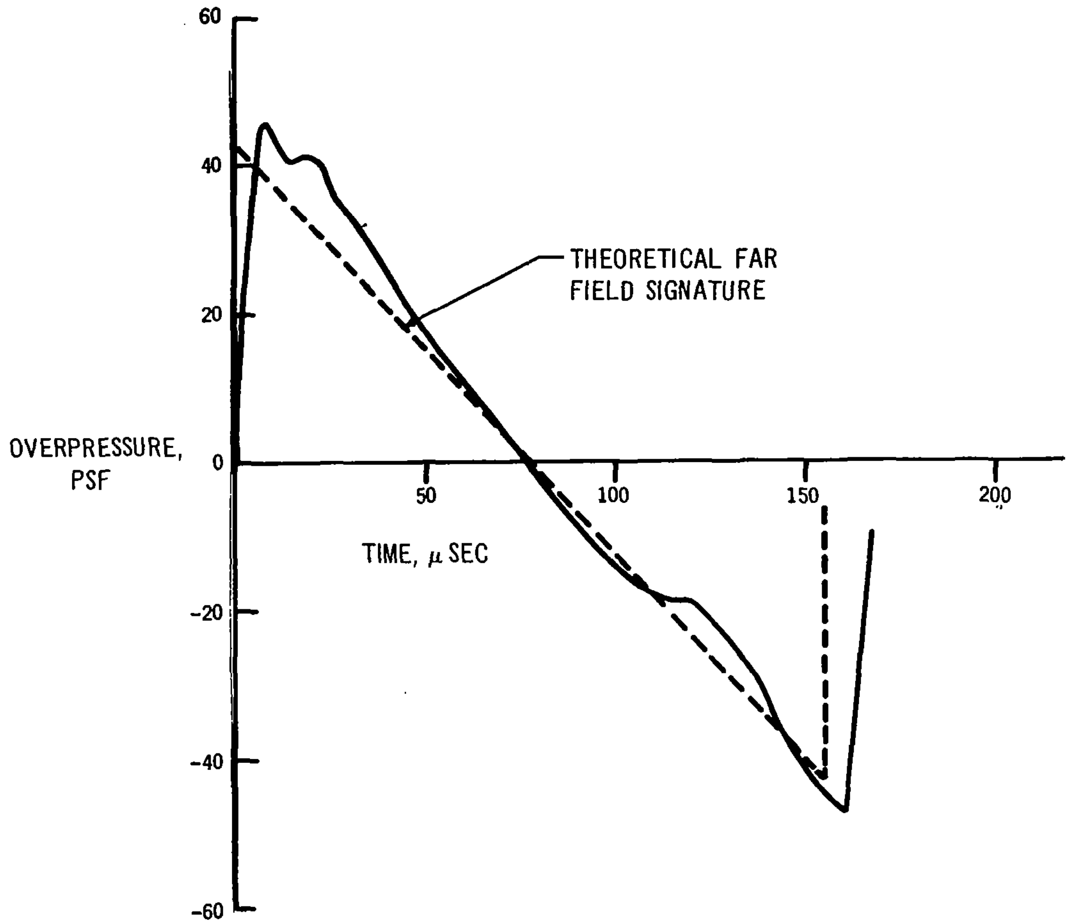

TRANSDUCER SENSITIVITY = 4.56 VOLTS/PSI

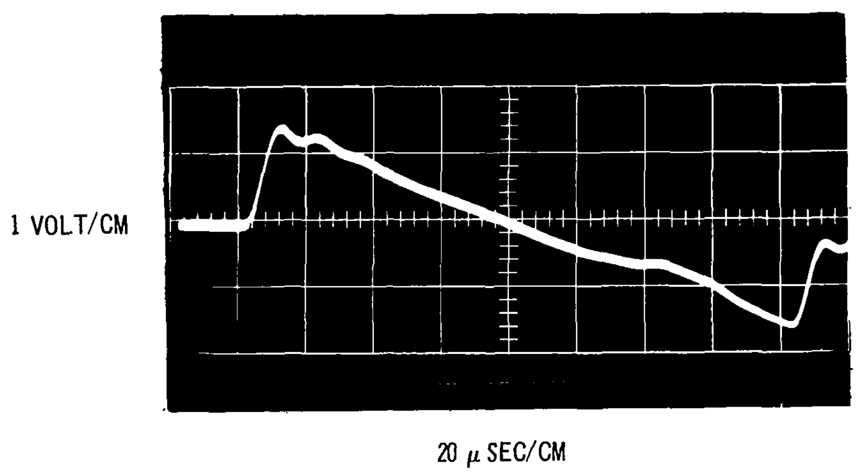

FIGURE 24(b). PRESSURE SIGNATURE FROM A .30-CALIBER RIFLE BULLET; SHOT 130R: M= 2.46

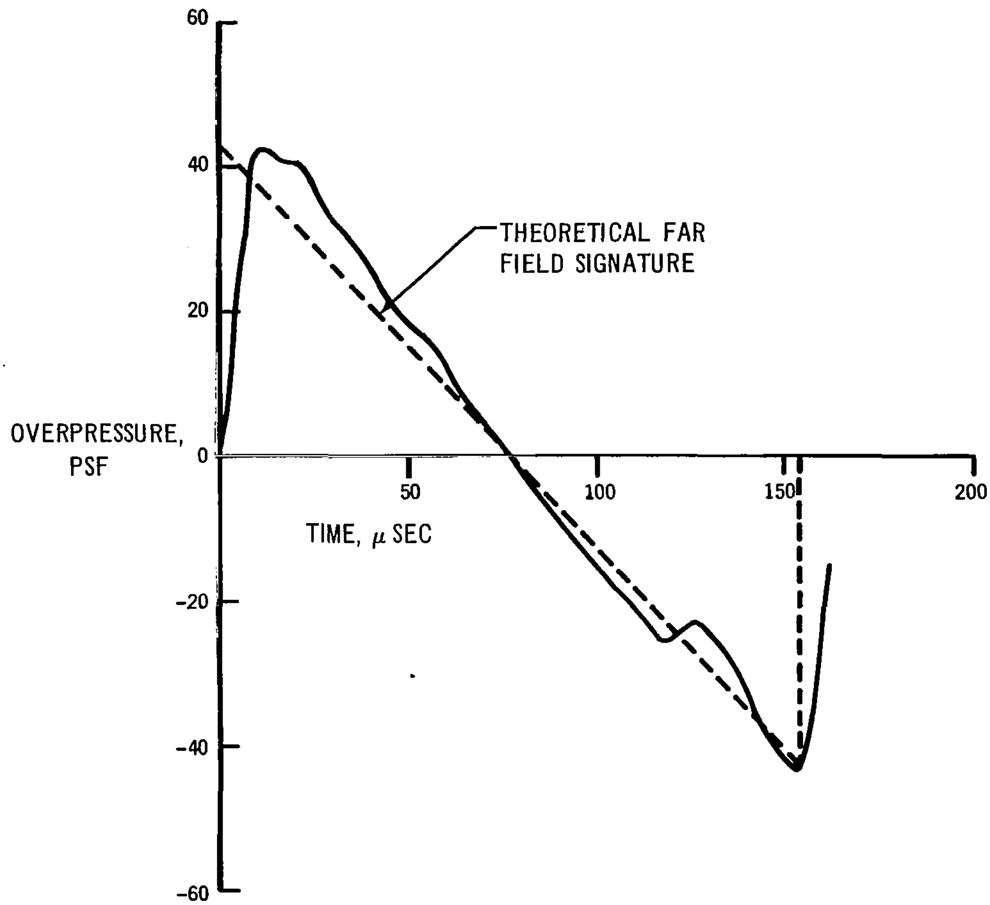

TRANSDUCER SENSITIVITY = 5.61 VOLTS/PSI

1 VOLT/CM

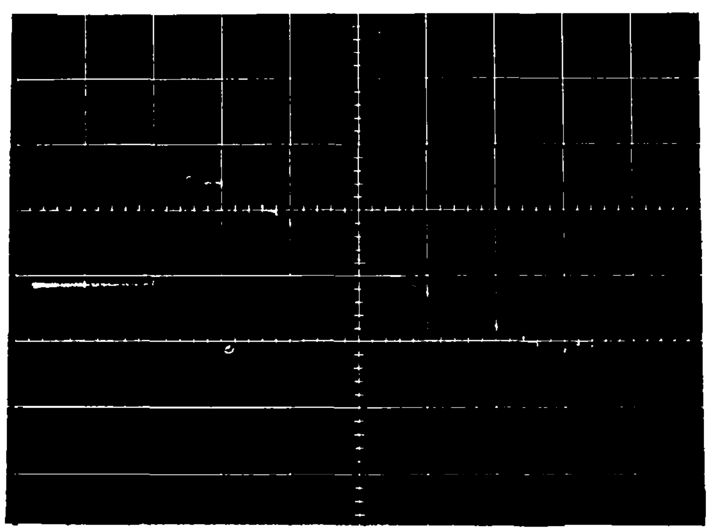

20 μ SEC/CM

FIGURE 24(c). PRESSURE SIGNATURE FROM A .30-CALIBER RIFLE BULLET; SHOT 152R: M = 2.5

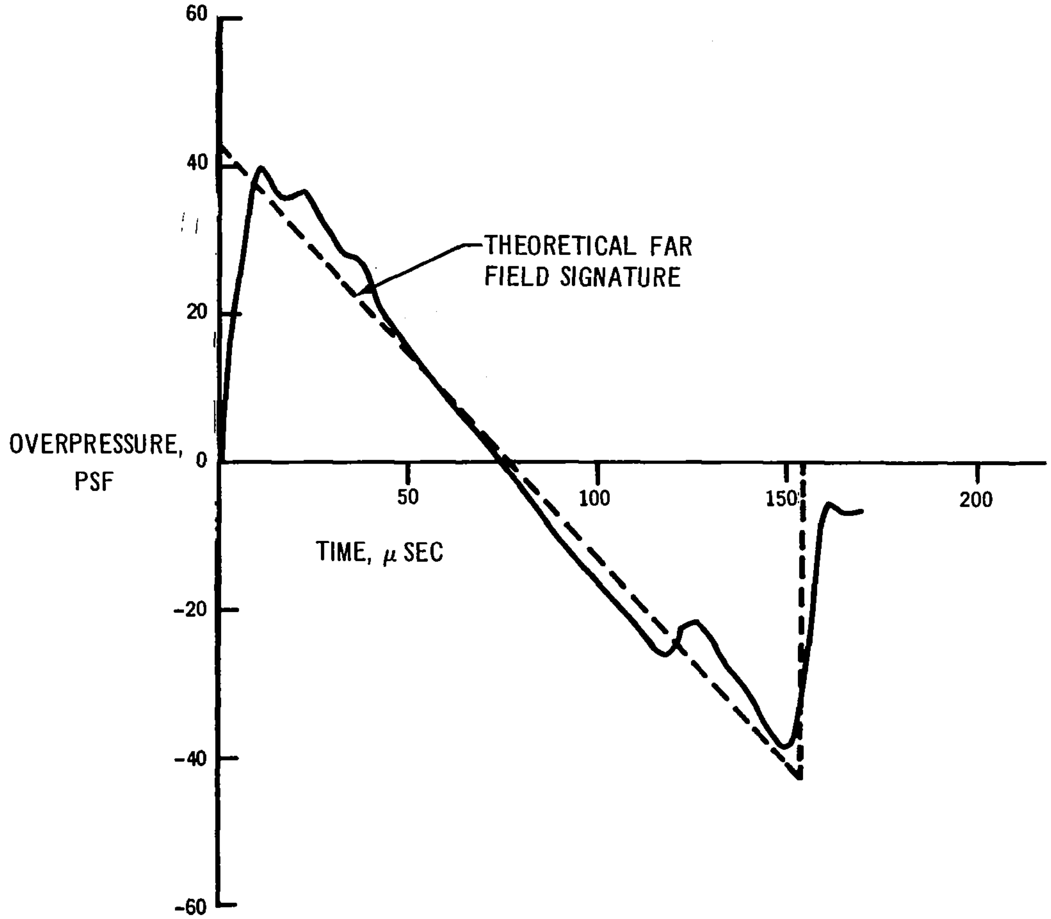

TRANSDUCER SENSITIVITY = 6.06 VOLTS/PSI

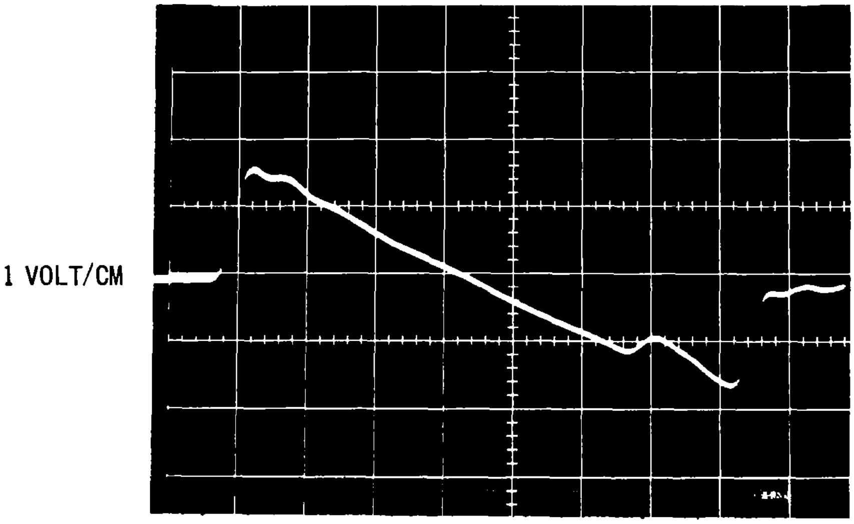

FIGURE 24(d). PRESSURE SIGNATURE FROM A .30-CALIBER RIFLE BULLET; SHOT 145R: M = 2.5

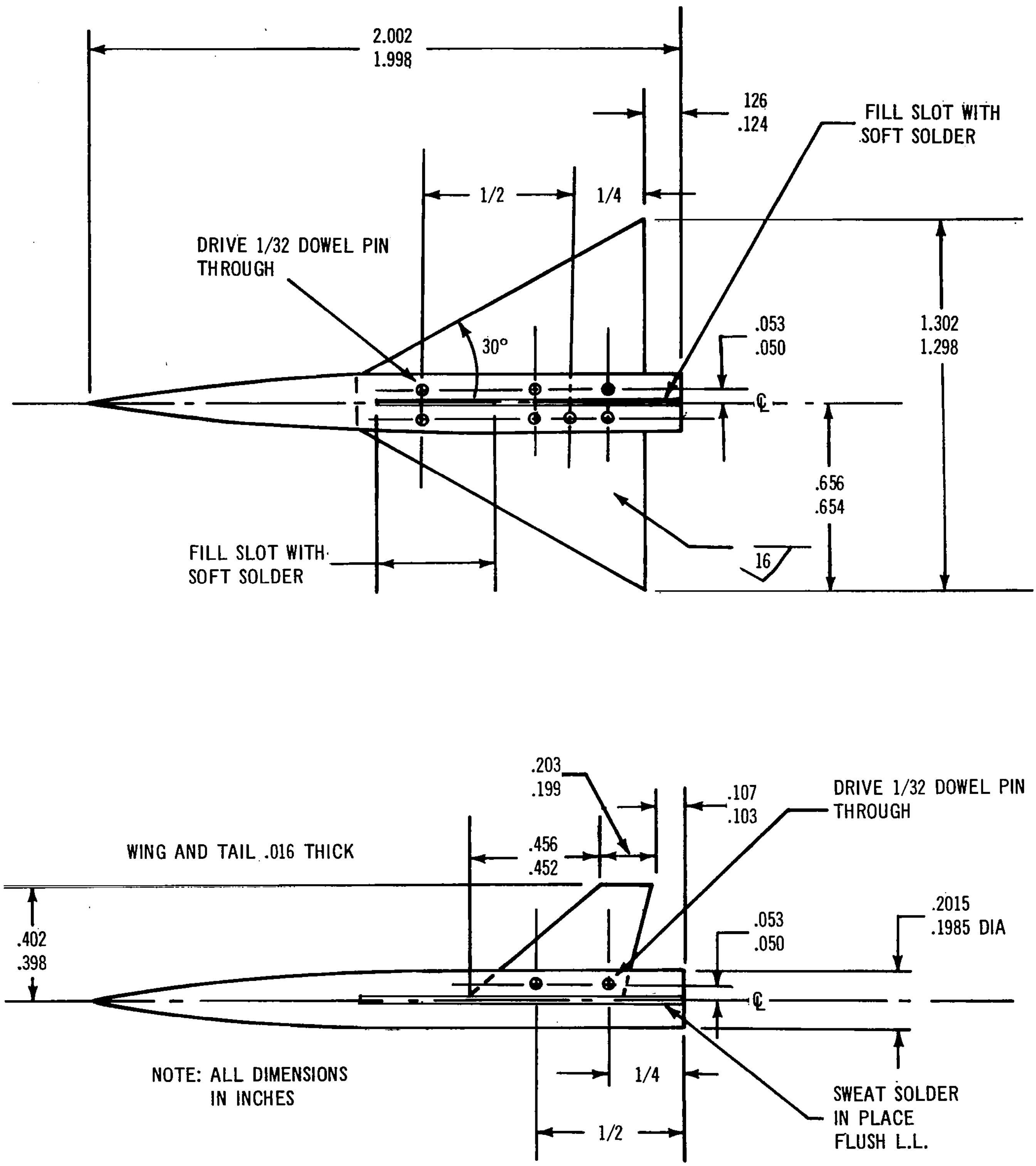

FIGURE 25. DETAIL OF DELTA WING BALLISTIC MODEL

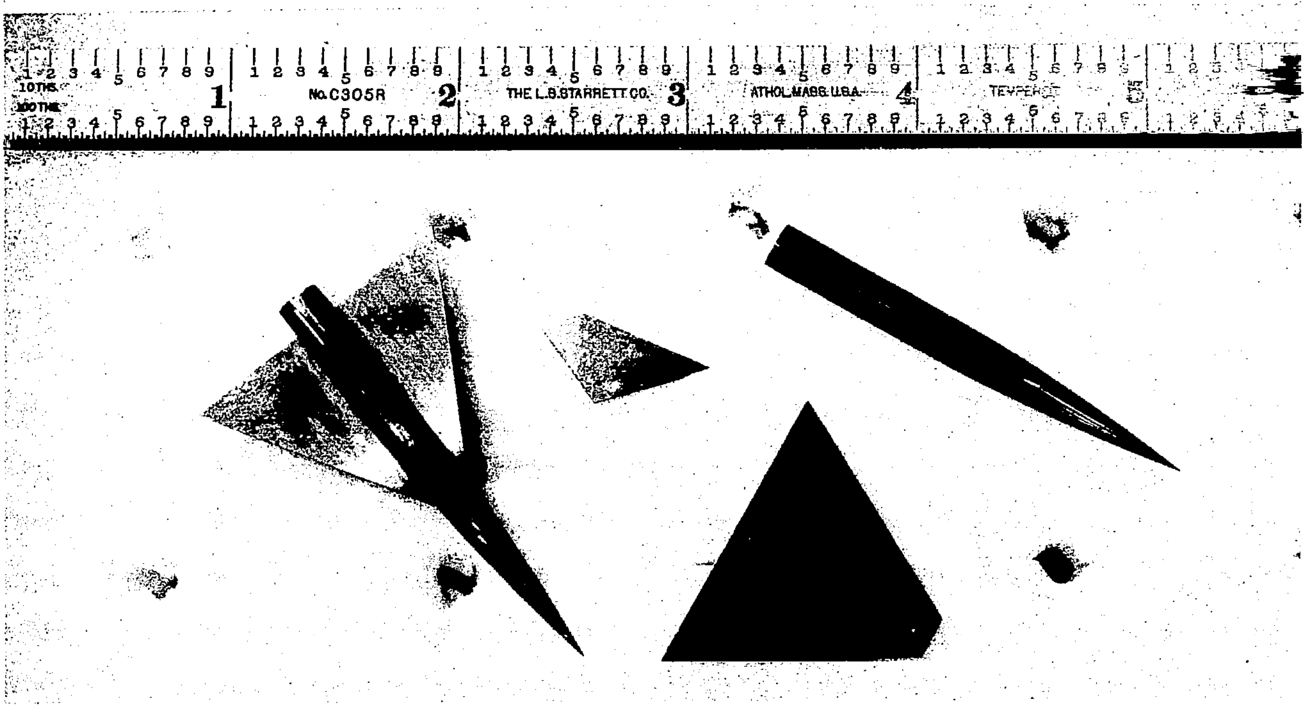

FIGURE 26. BALLISTIC MODEL COMPONENTS AND COMPLETED MODEL.

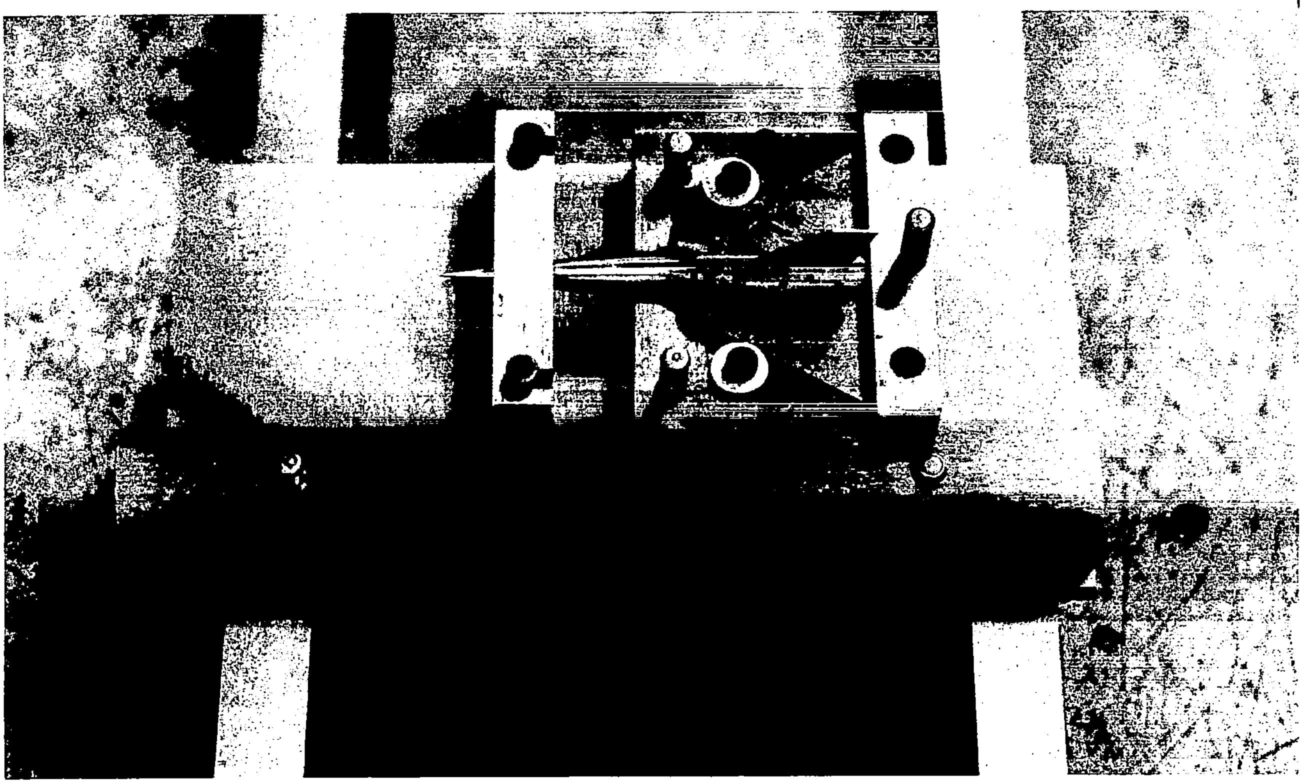

FIGURE 27. BALLISTIC MODEL CONSTRUCTION JIG

FIGURE 28. BALLISTIC MODEL IN INSPECTION COMPARATOR

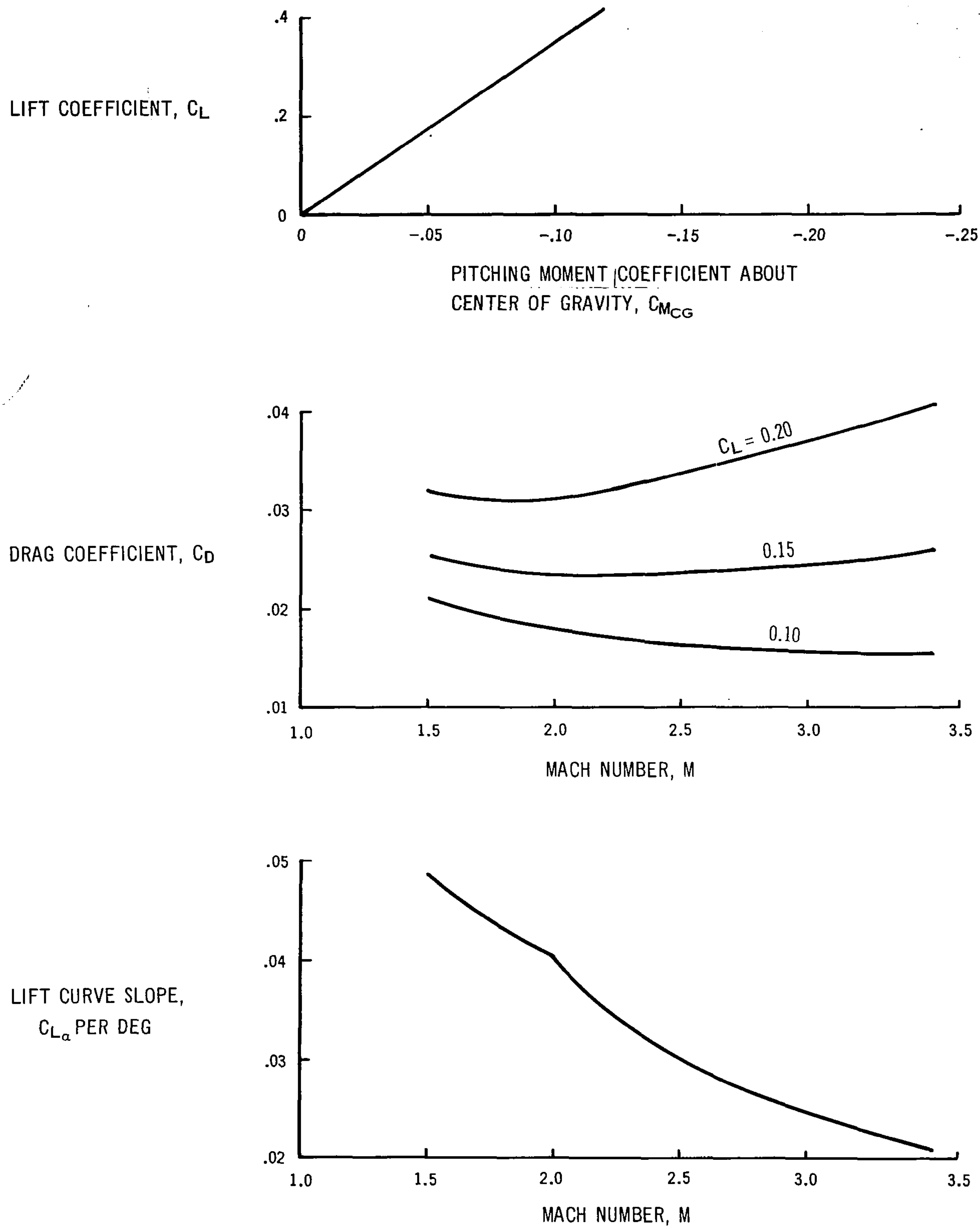

FIGURE 29. BALLISTIC MODEL AERODYNAMIC CHARACTERISTICS

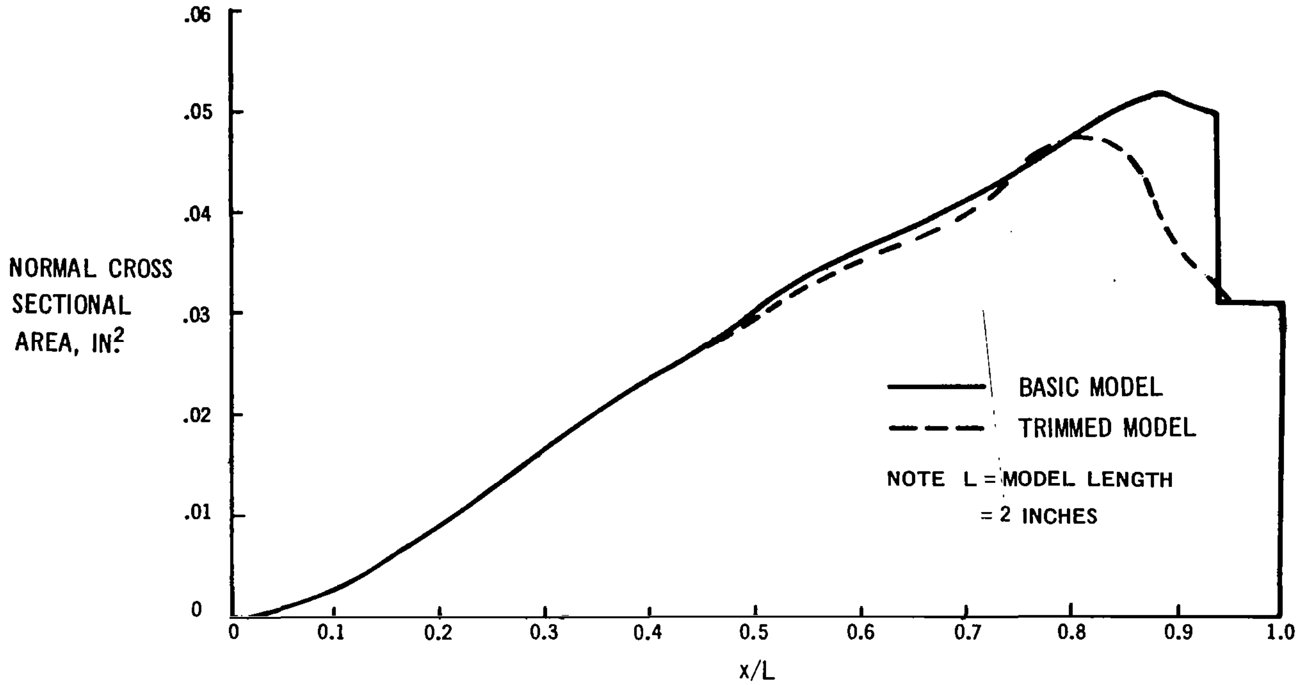

FIGURE 30. BALLISTIC MODEL AREA DISTRIBUTION

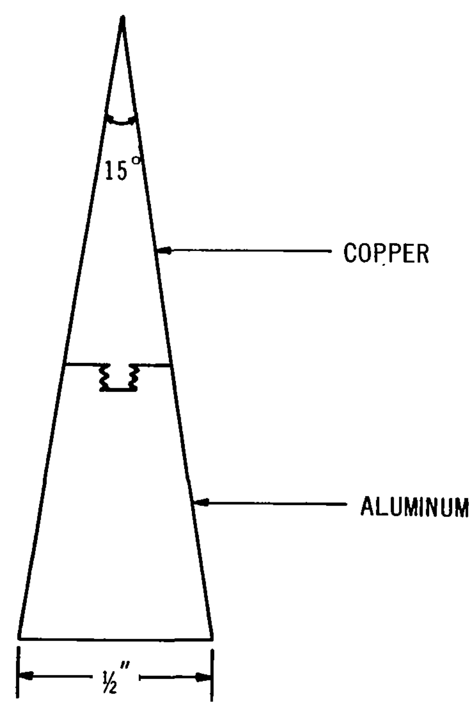

FIGURE 31. CONE MODEL

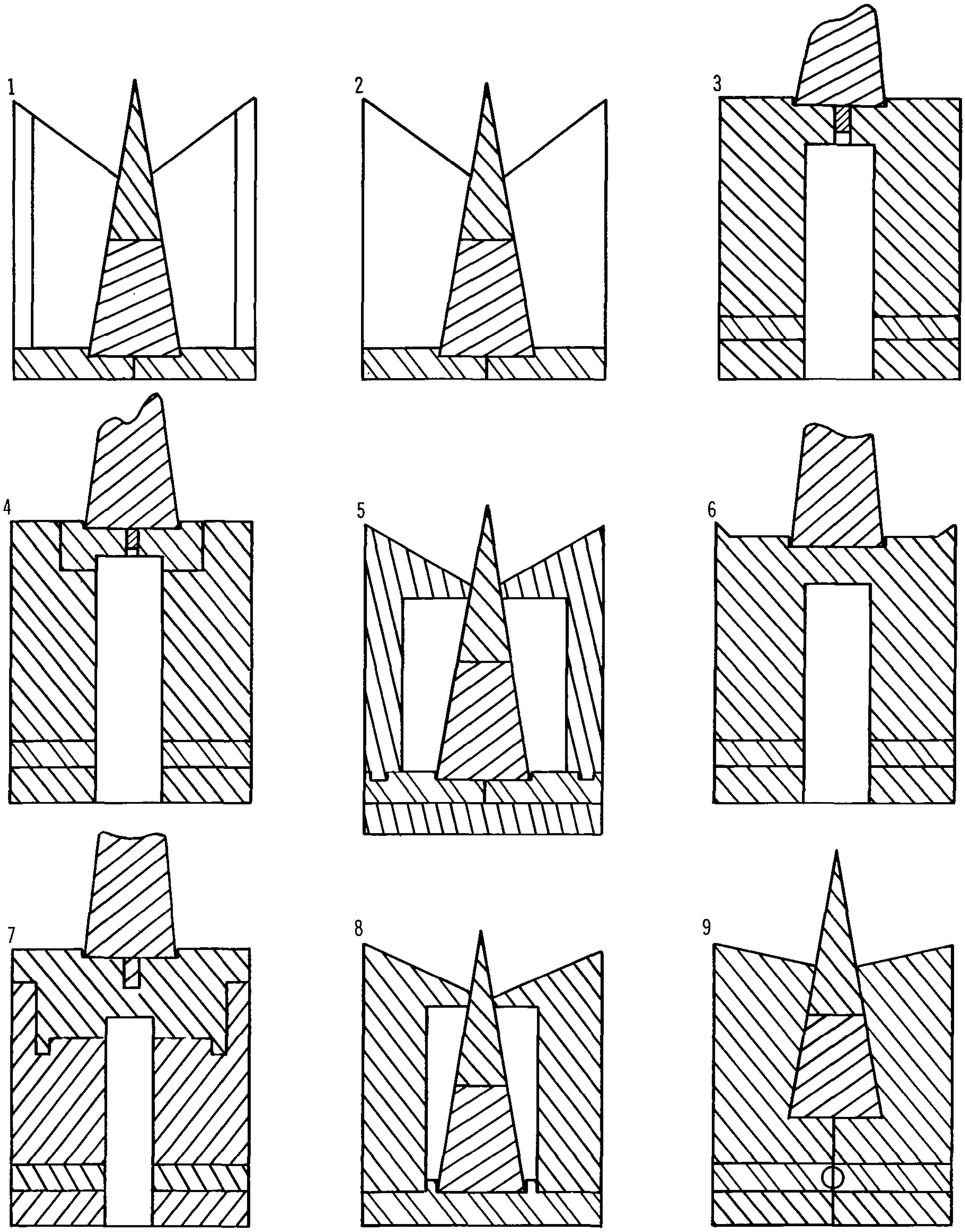

FIGURE 32. CONE SABOT DESIGNS

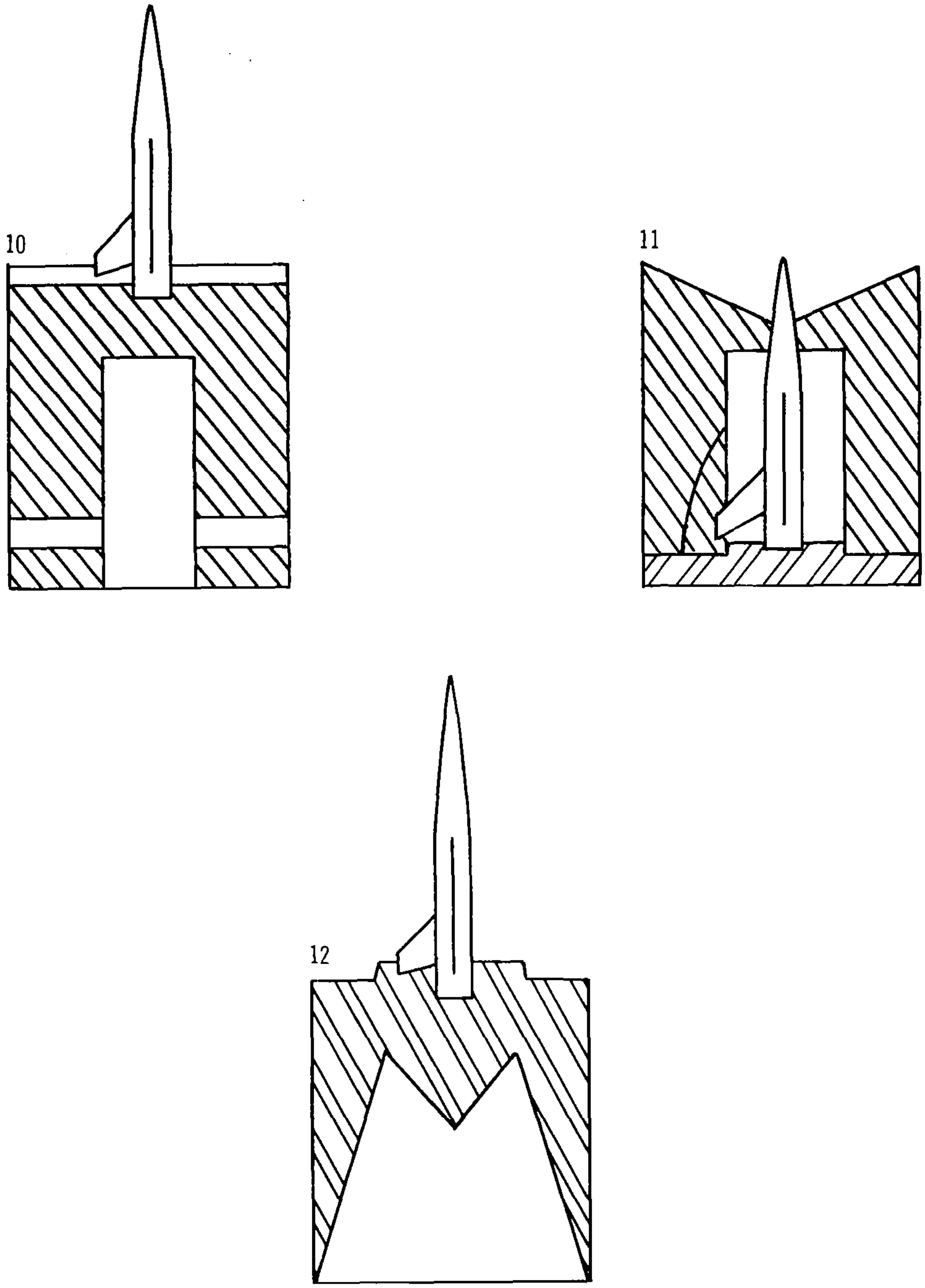

FIGURE 33. DELTA WING MODEL SABOTS

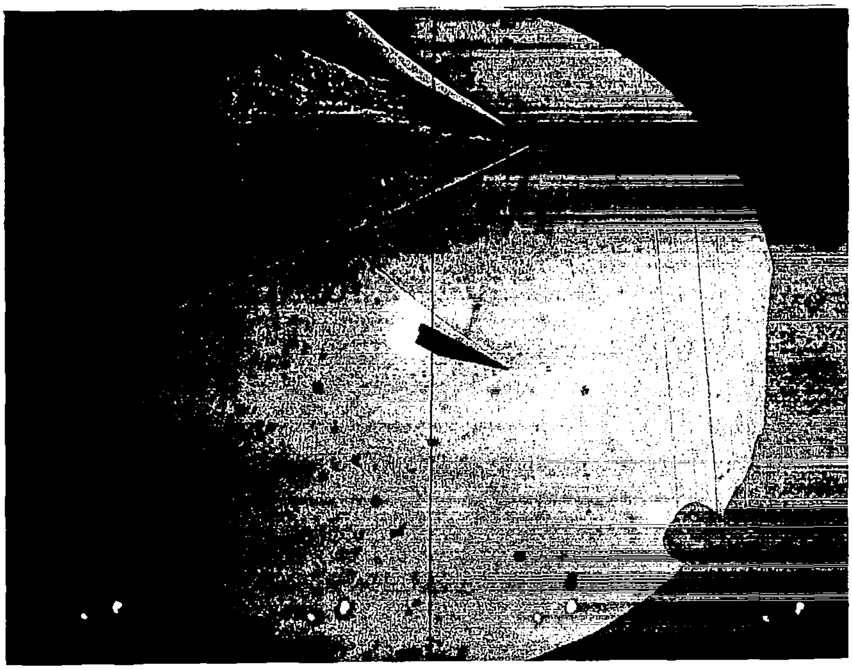

VERTICAL
VIEW –
STATION 3

VERTICAL
VIEW –
STATION 4

FIGURE 34. REPRESENTATIVE RESULT USING SABOT NUMBER 5;
SHOT 11: M = 3

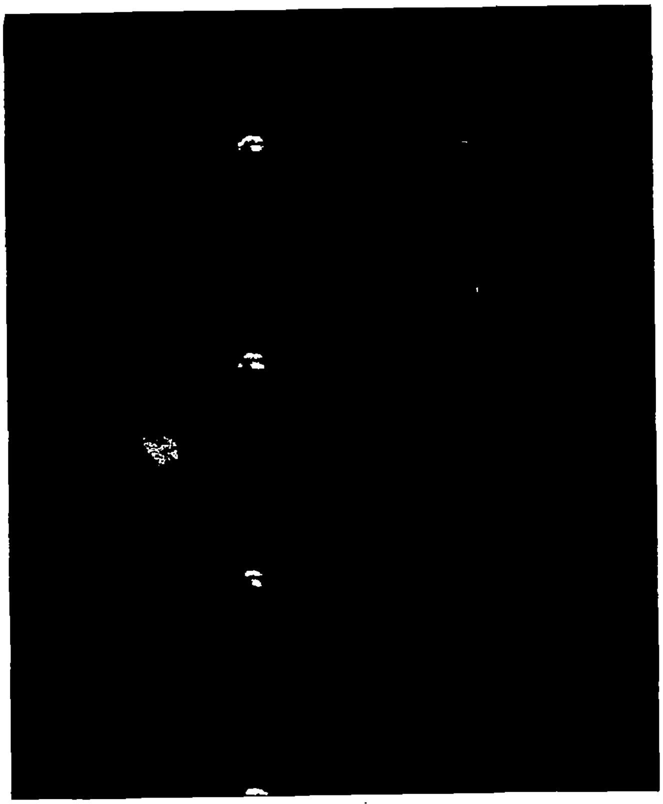

HORIZONTAL VIEW – STATION 5

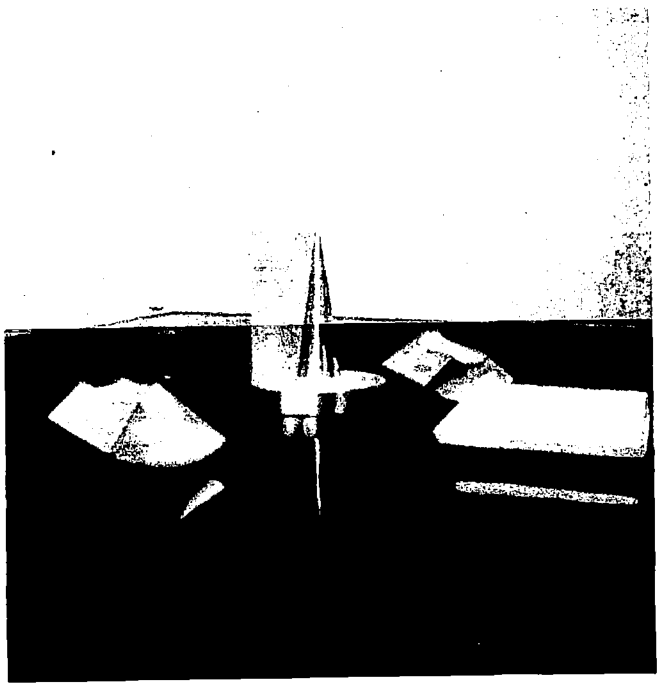

FIGURE 35. SABOT NUMBER 8 LAUNCHED WITH CONE MODEL; SHOT 13: M = 3

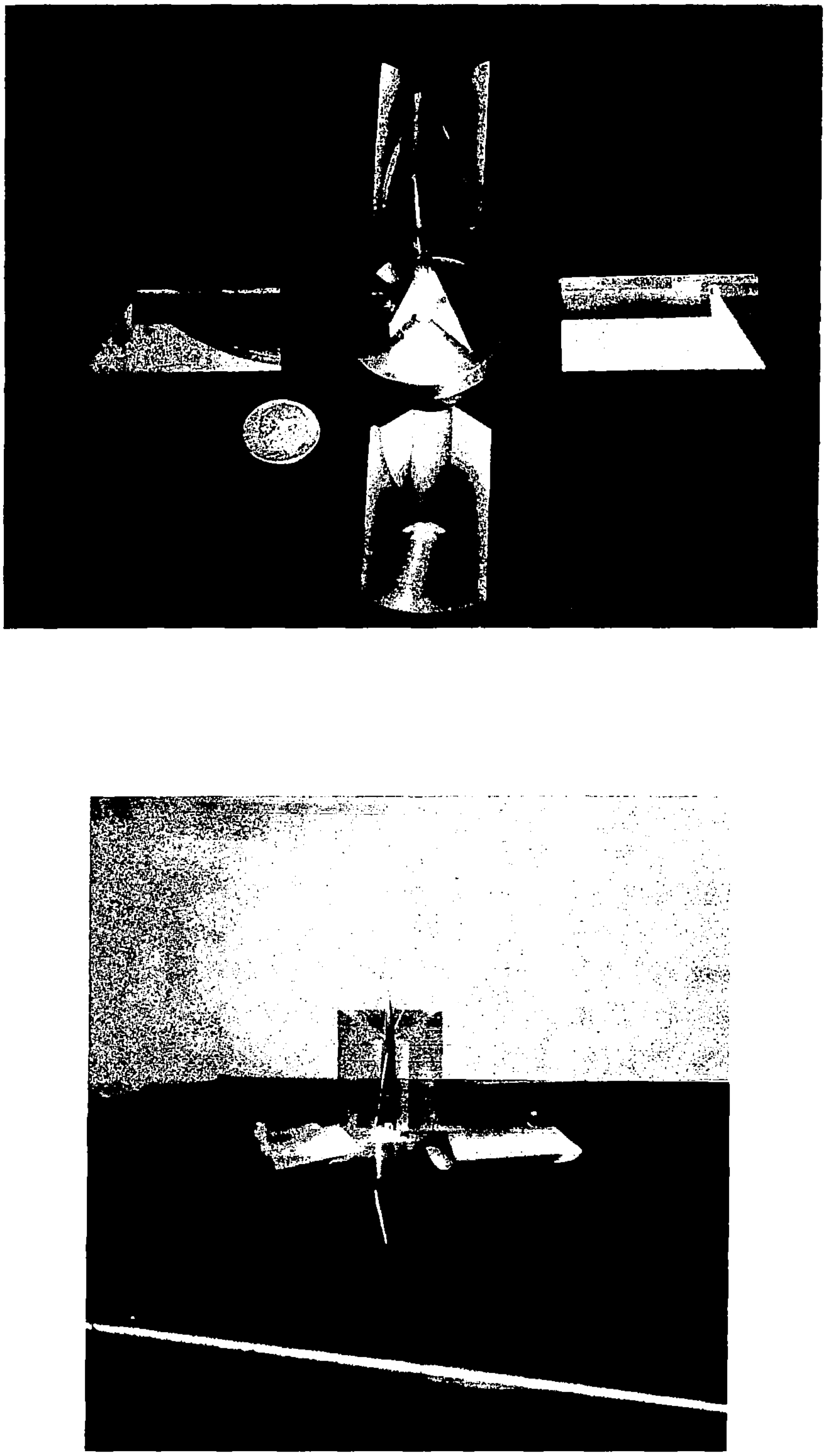

FIGURE 36. DELTA WING BALLISTIC MODEL MOUNTED IN SABOT NUMBER 11

VERTICAL
VIEW –
STATION 3

VERTICAL VIEW –
STATION 4

VERTICAL VIEW –
STATION 5

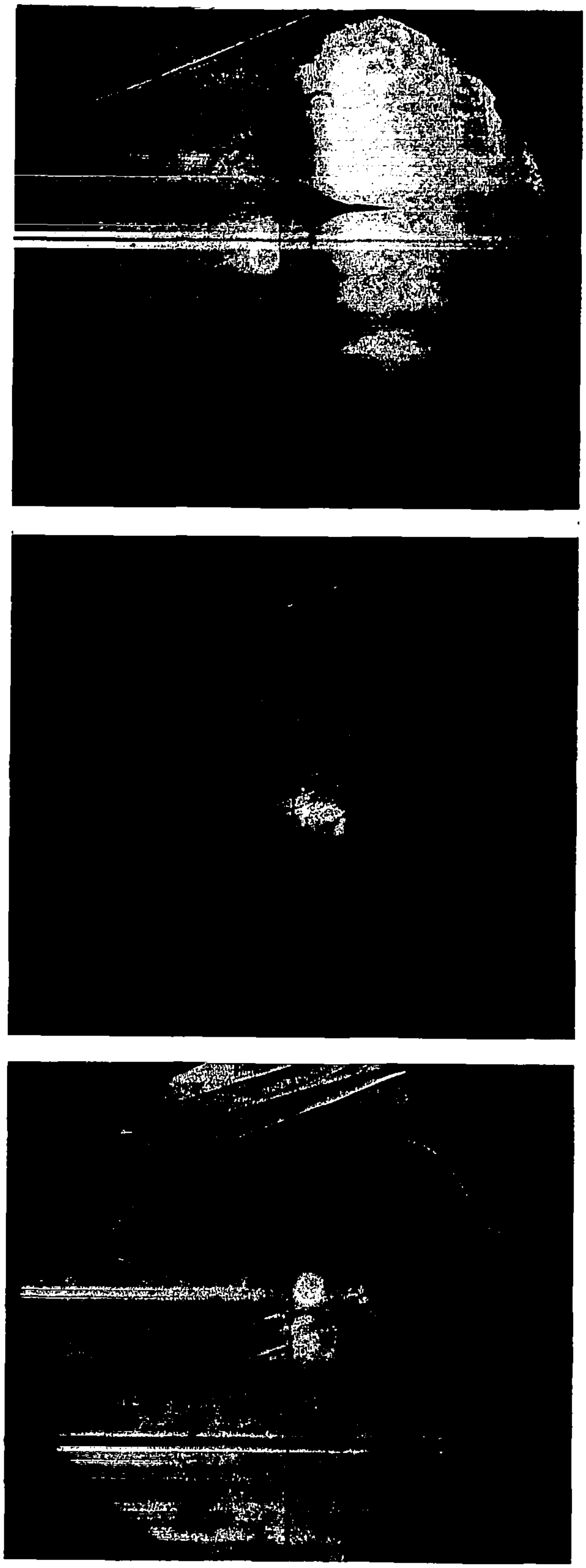

FIGURE 37. INITIAL RESULT USING SABOT NUMBER 11; SHOT 16: M = 3

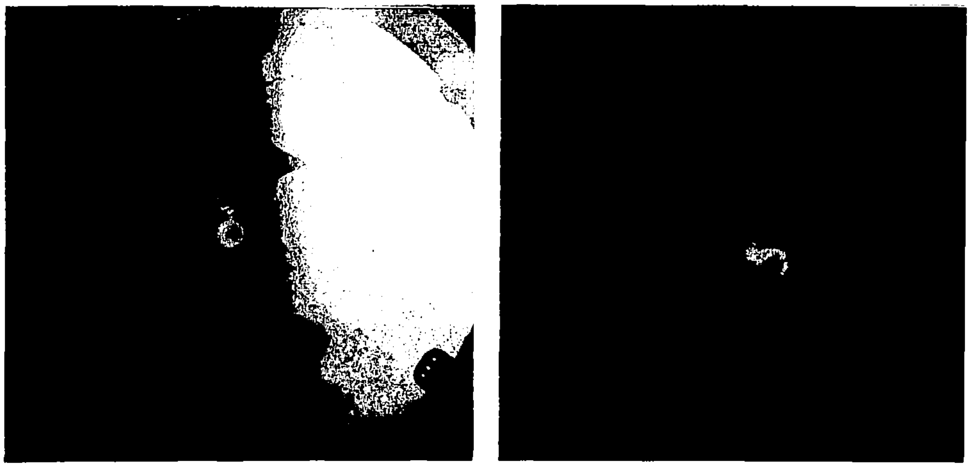

SHOT 17:

VERTICAL VIEW – STATIONS 3 AND 4

SHOT 18:

VERTICAL VIEW – STATIONS 3 AND 4

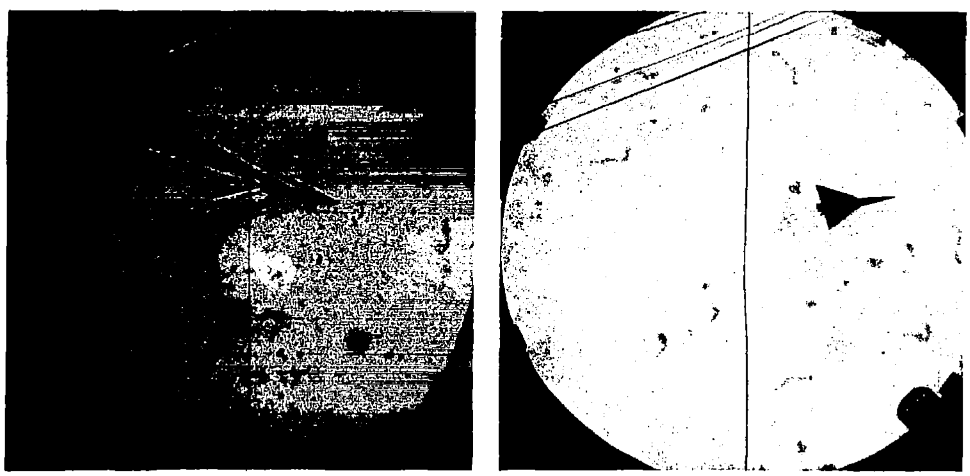

SHOT 22:

VERTICAL VIEW – STATIONS 4 AND 5

FIGURE 38. REPEATIBILITY RESULTS USING SABOT 11; M = 3

SHOT 18

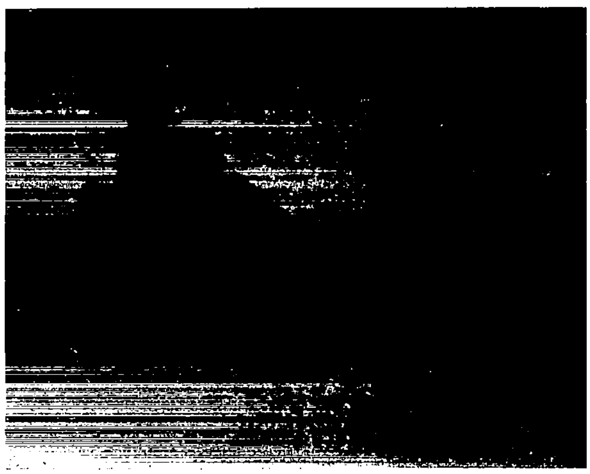

SHOT 48

FIGURE 39. REPRESENTATIVE FLASH X-RAY RADIOGRAPHS; M = 3

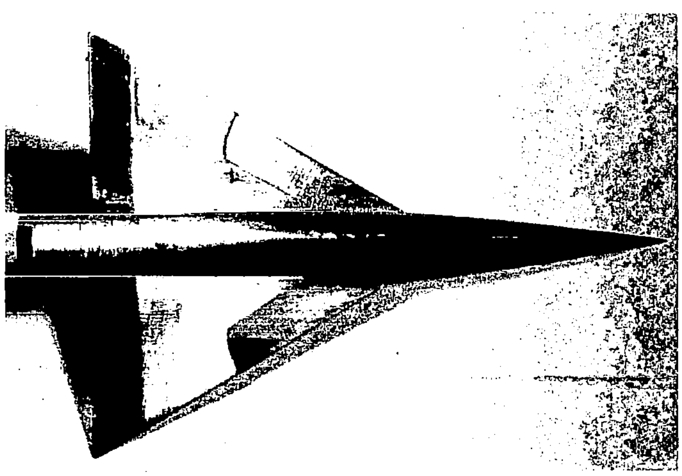

FIGURE 40. TRIMMED DELTA WING MODEL

STATION 3

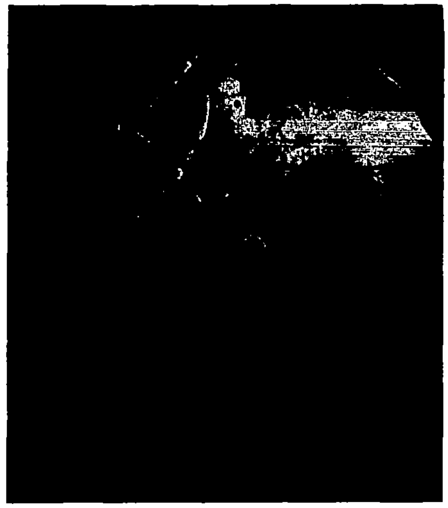

STATION 4

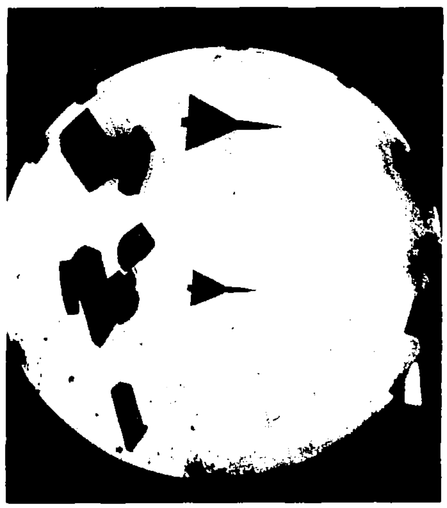

STATION 5

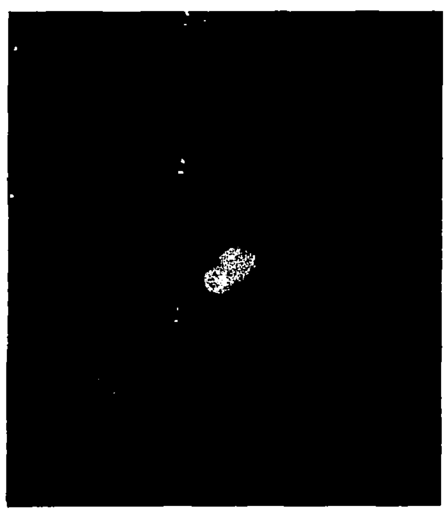

FIGURE 41. EFFECT OF LAUNCHING MODEL INTO RANGE TANK EVACUATED TO 20mm Hg; SHOT 34: M = 3

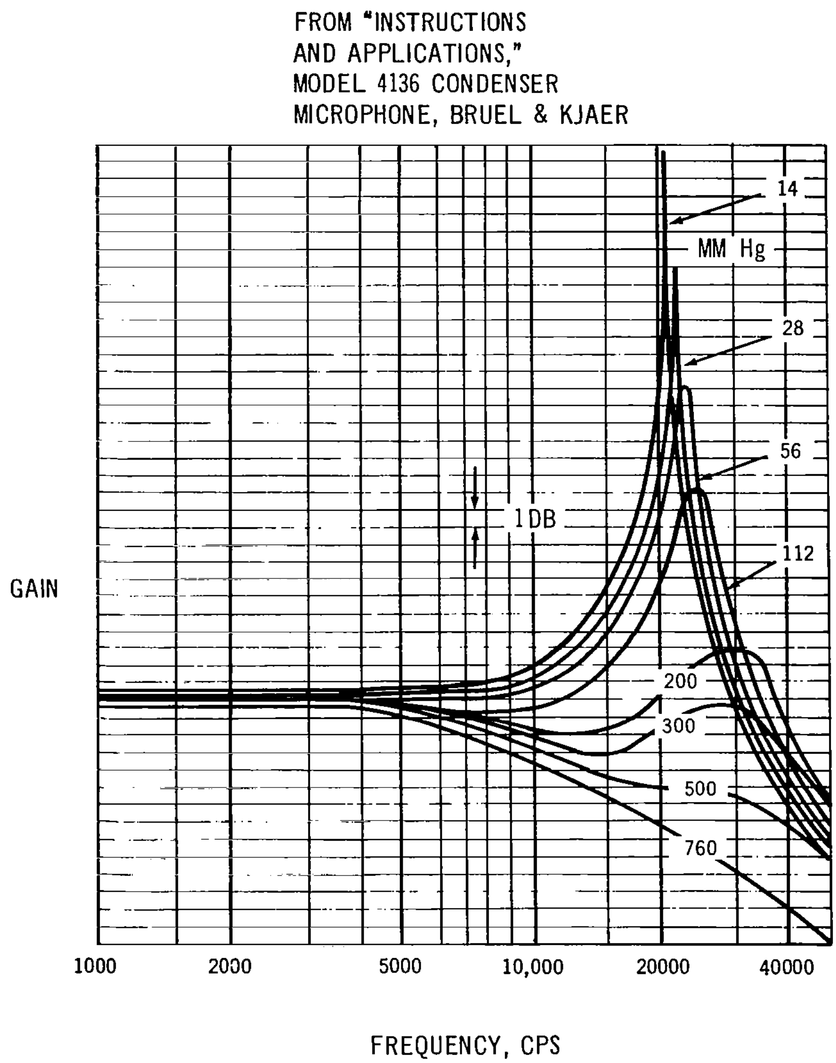

FIGURE 42. EFFECT OF LOW PRESSURES ON TRANSDUCER DAMPING

STATION 3

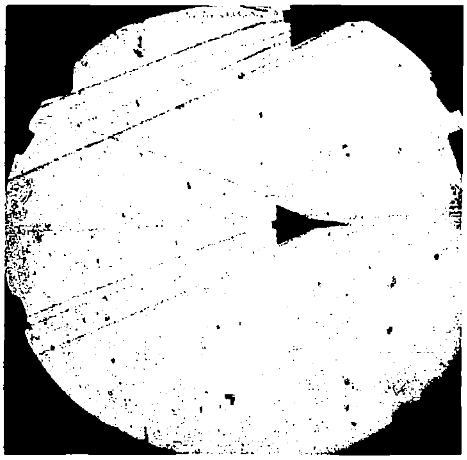

STATION 4

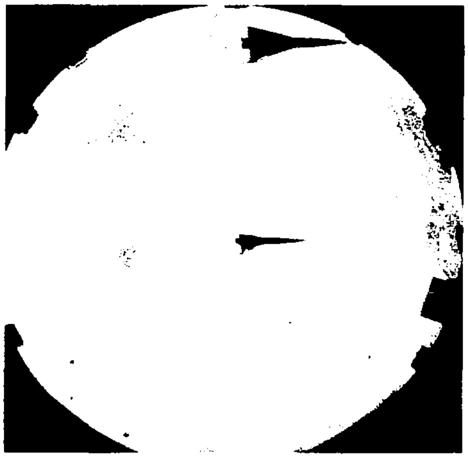

STATION 5

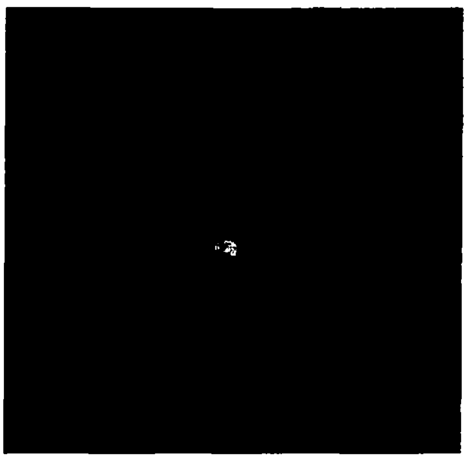

FIGURE 43 (a). SHOT 42: HORIZONTAL VIEW SHADOWGRAPHS; M = 2.84

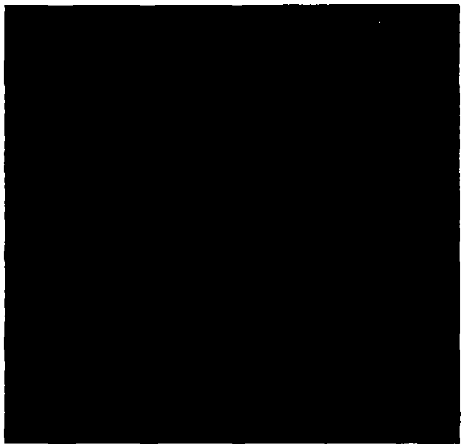

STATION 3

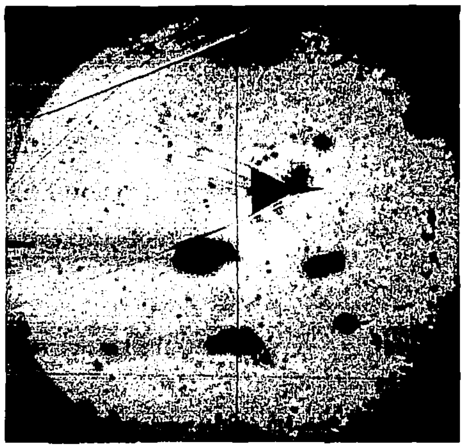

STATION 4

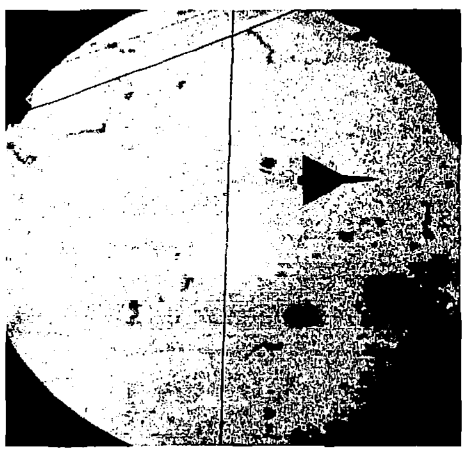

STATION 5

FIGURE 43 (b). SHOT 42: VERTICAL VIEW SHADOWGRAPHS; M = 2.84

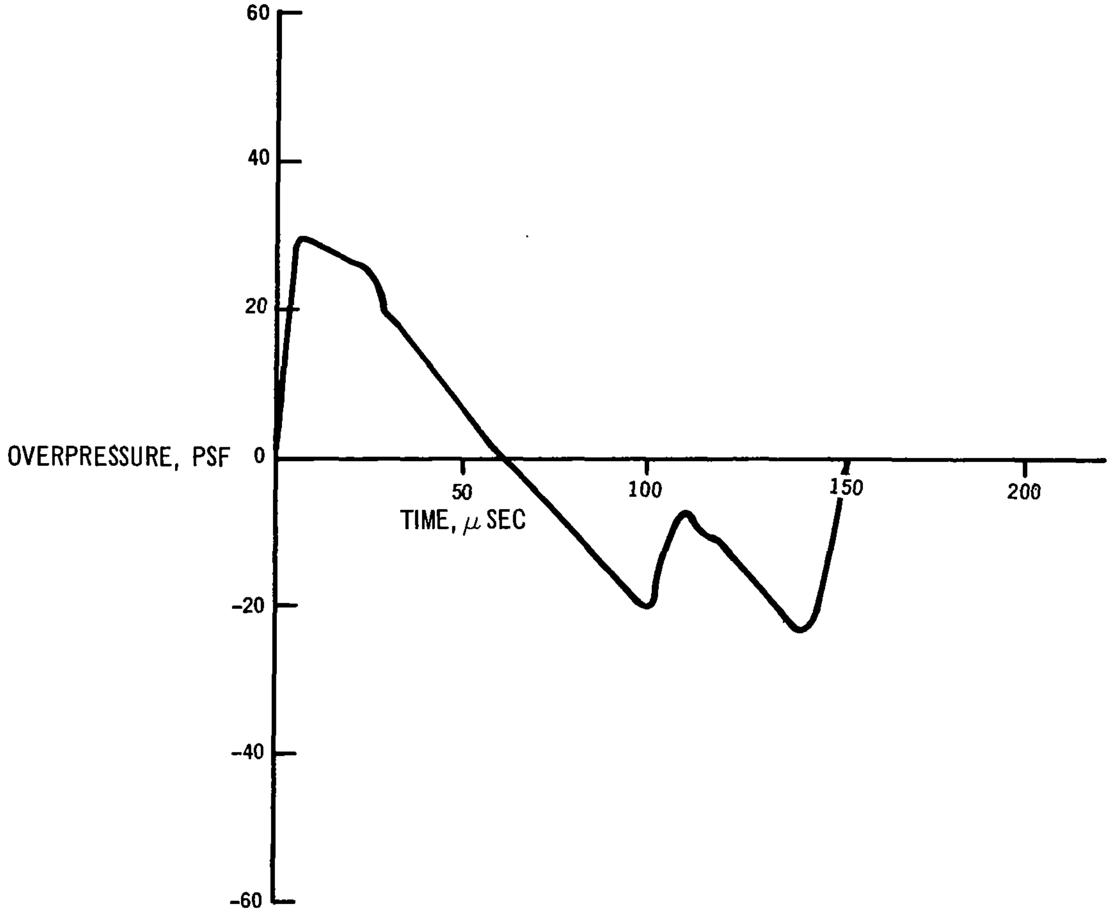

TRANSDUCER SENSITIVITY = 5.61 VOLTS/PSI

1 VOLT/CM

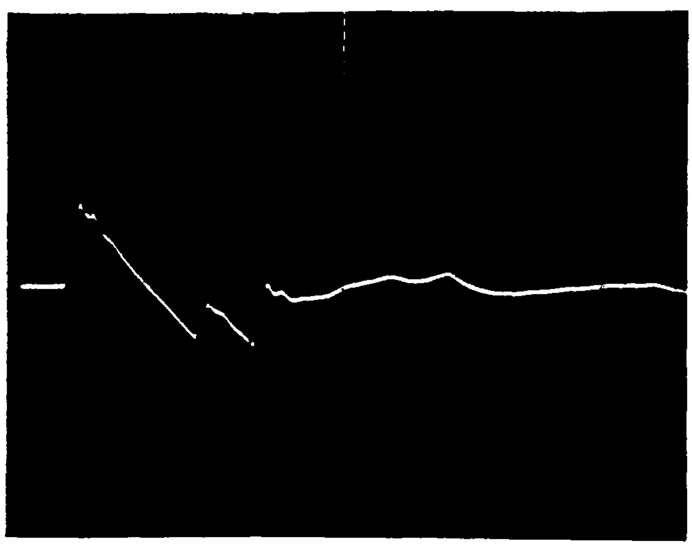

50μ SEC/CM

FIGURE 43 (c). SHOT 42: BALLISTIC MODEL PRESSURE SIGNATURE; M = 2.84

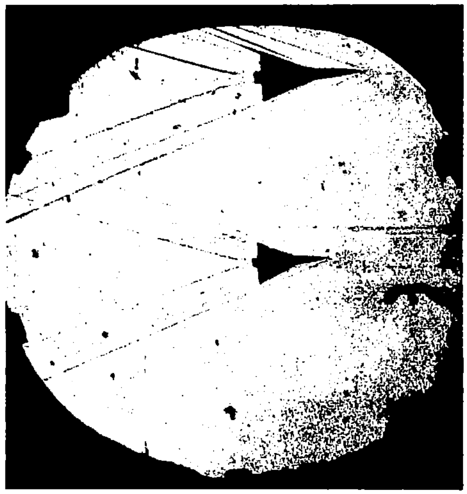

STATION 3

SHADOWGRAPH
NOT AVAILABLE
FOR THIS STATION

STATION 4

STATION 5

FIGURE 44 (a). SHOT 43: HORIZONTAL VIEW SHADOWGRAPHS; M = 2.86

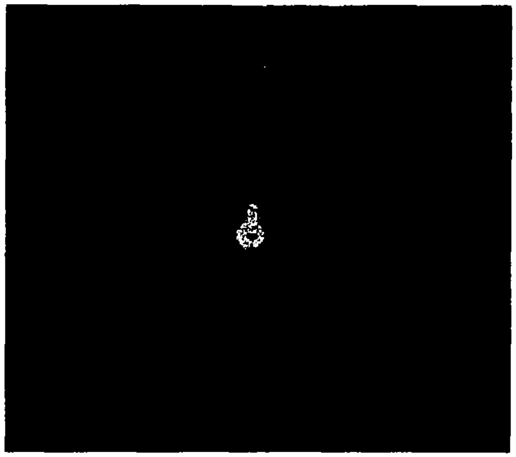
STATION 3

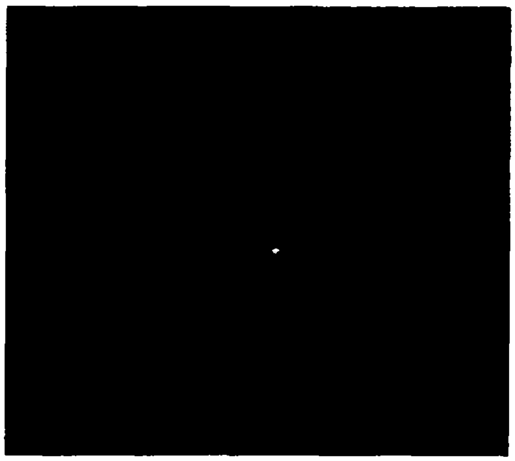
STATION 4

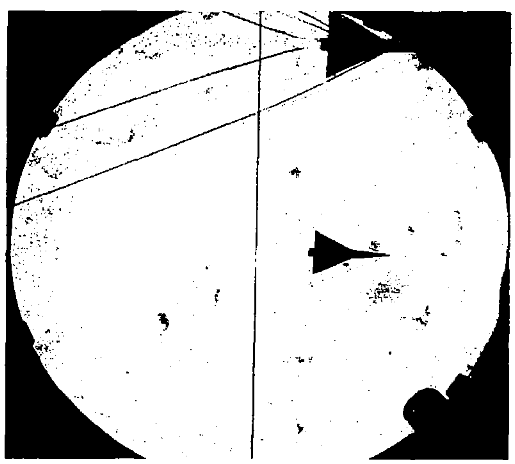
STATION 5

FIGURE 44 (b). SHOT 43: VERTICAL VIEW SHADOWGRAPHS; M = 2.86

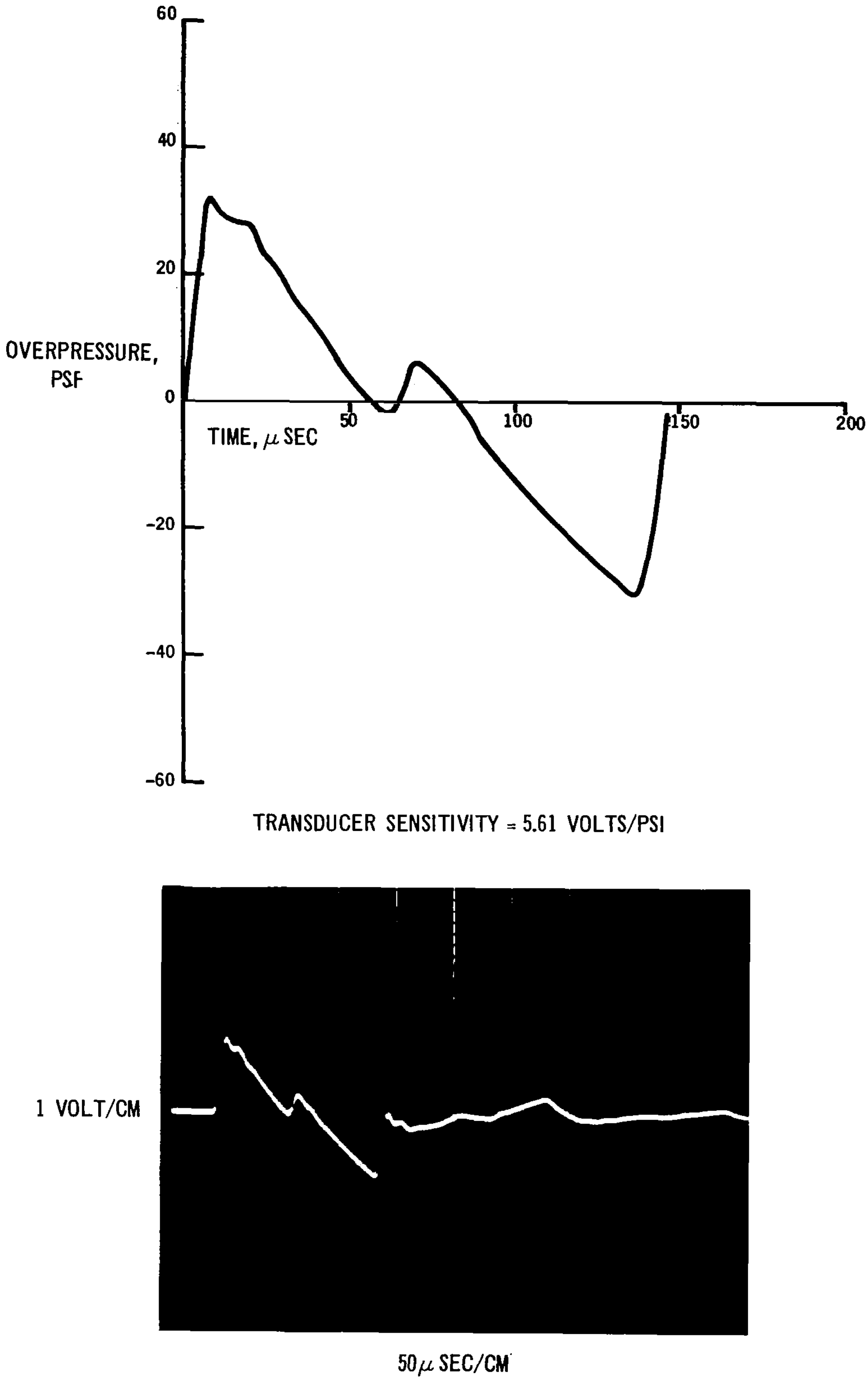

FIGURE 44 (c). SHOT 43: BALLISTIC MODEL PRESSURE SIGNATURE; M = 2.84

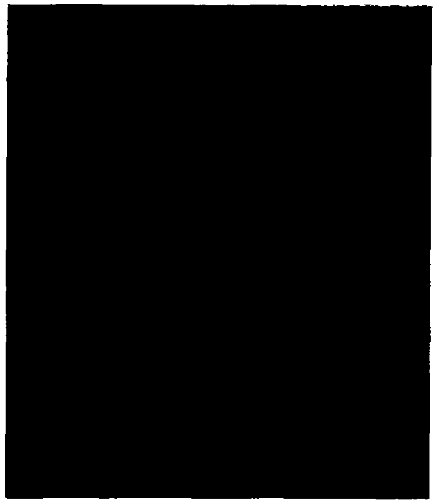

STATION 3

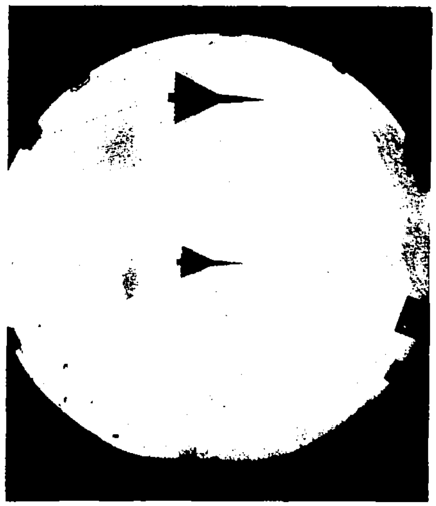

STATION 4

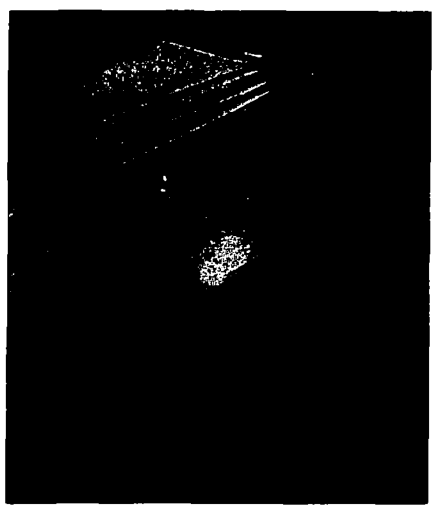

STATION 5

FIGURE 45 (a). SHOT 47: HORIZONTAL VIEW SHADOWGRAPHS; M = 3.00

STATION 3

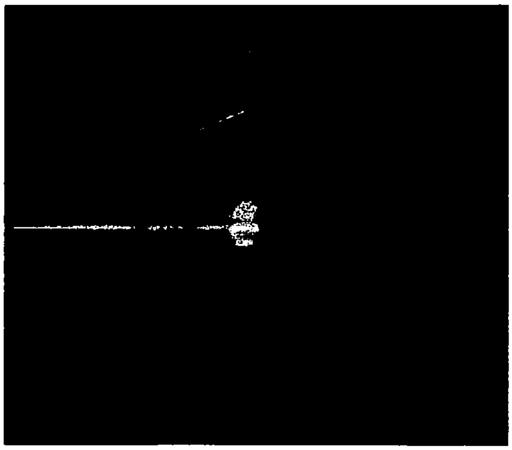

STATION 4

SHADOWGRAPH
NOT AVAILABLE
FOR THIS STATION

STATION 5

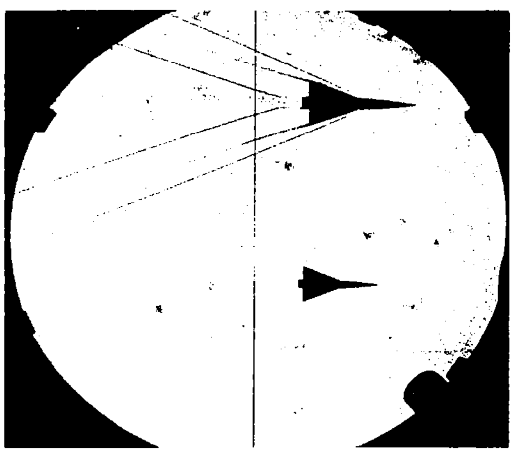

FIGURE 45 (b). SHOT 47: VERTICAL VIEW SHADOWGRAPHS; M = 3.00

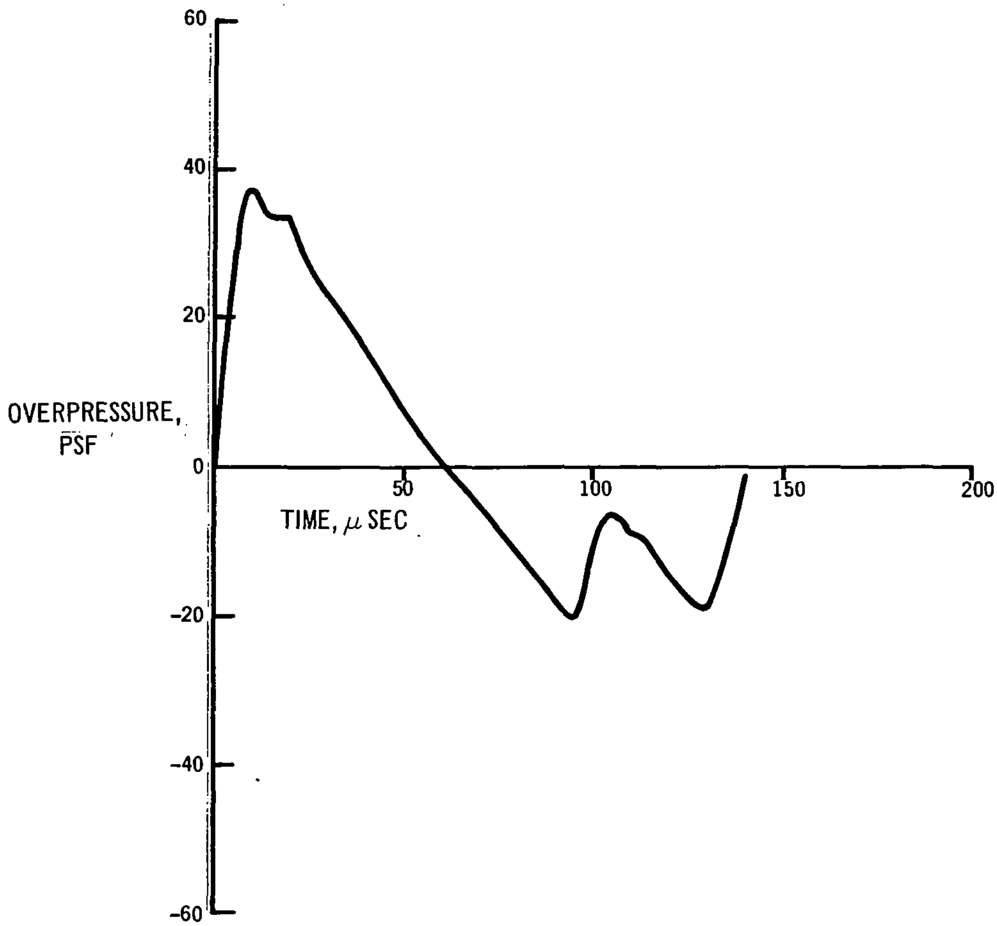

TRANSDUCER SENSITIVITY = 5.61 VOLTS/PSI

1 VOLT/CM

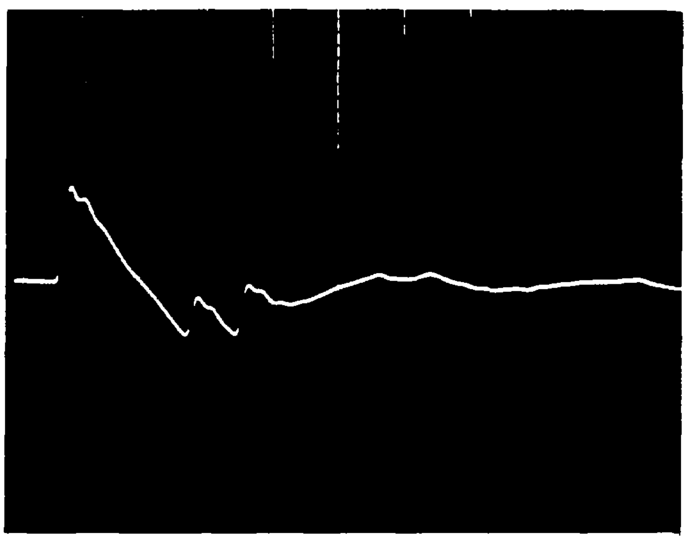

50μ SEC/CM

FIGURE 45 (c). SHOT 47: BALLISTIC MODEL PRESSURE SIGNATURE; M = 3.00

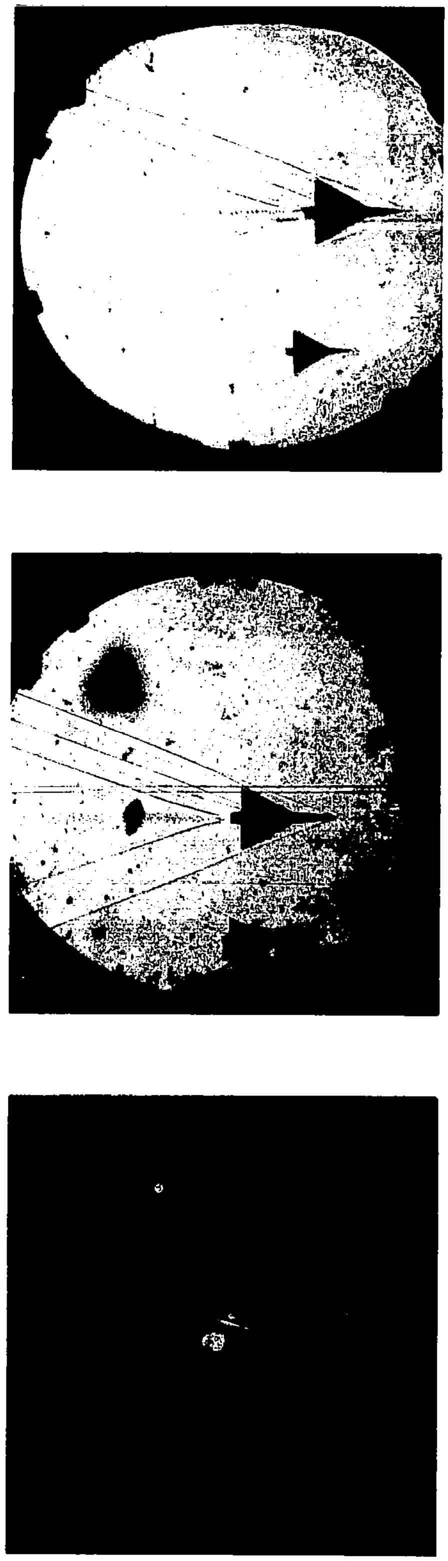

STATION 3

STATION 4

STATION 5

FIGURE 46(a). SHOT 52: HORIZONTAL VIEW SHADOWGRAPHS; M = 2.92

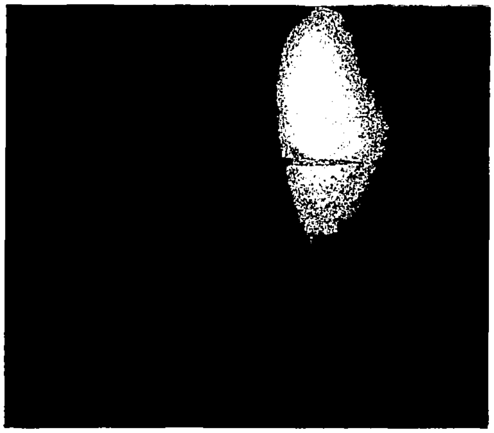

STATION 3

STATION 4

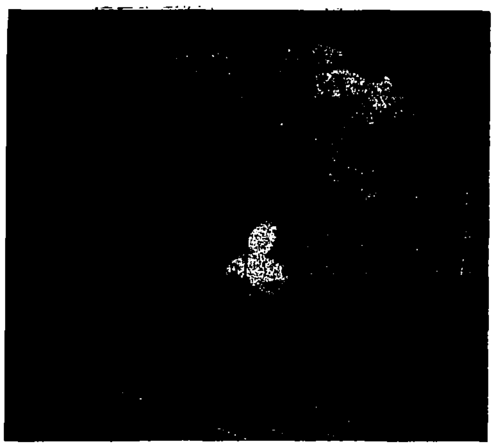

STATION 5

FIGURE 46(b). SHOT 52: VERTICAL VIEW SHADOWGRAPHS; M = 2.92

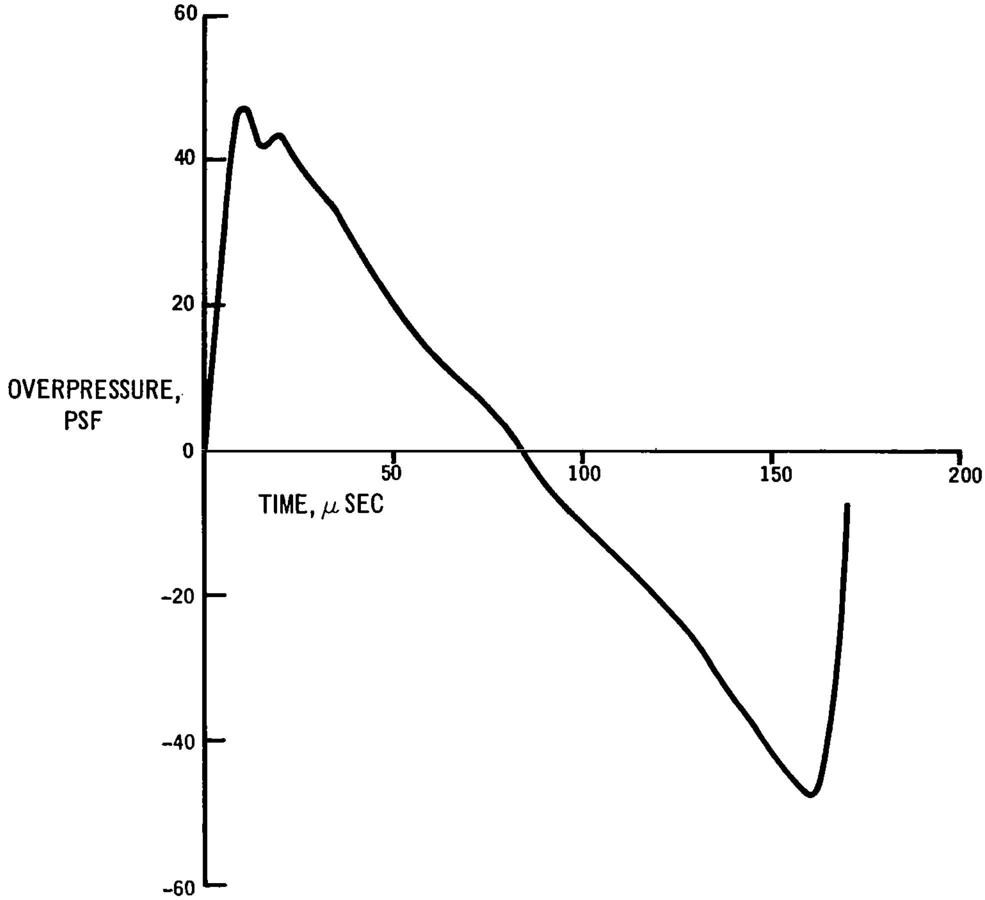

TRANSDUCER SENSITIVITY= 5.61 VOLTS/PSI

1 VOLT/CM

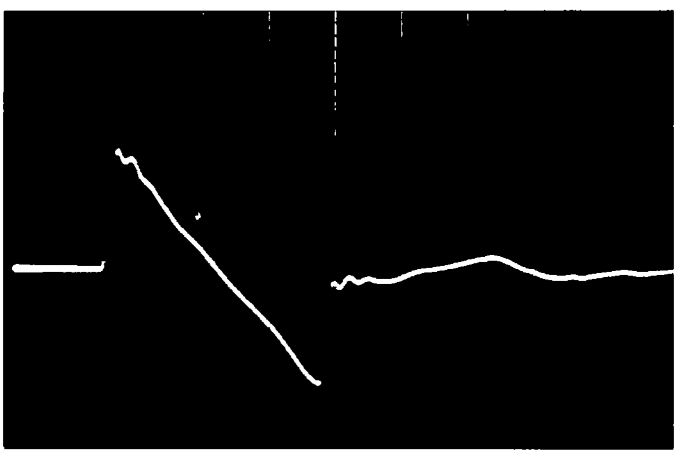

50μ SEC/CM

FIGURE 46 (c). SHOT 52: BALLISTIC MODEL PRESSURE SIGNATURE; M = 2.92

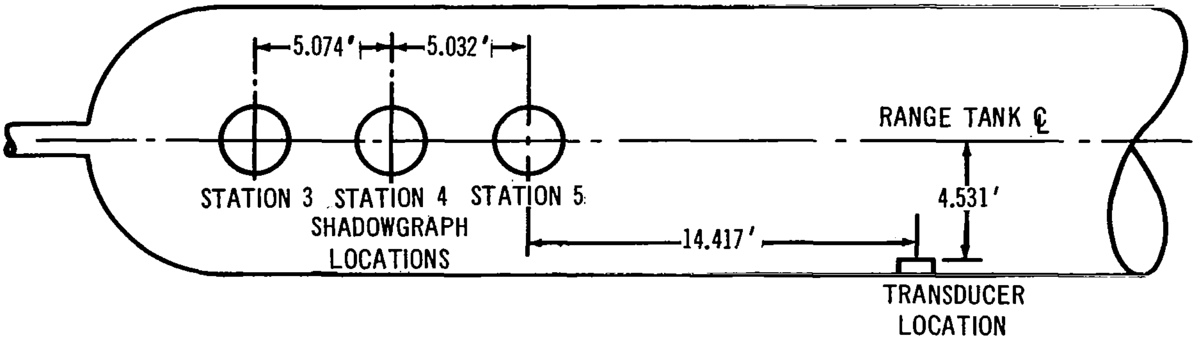

FIGURE 47. INSTRUMENTATION LOCATION IN RANGE TANK

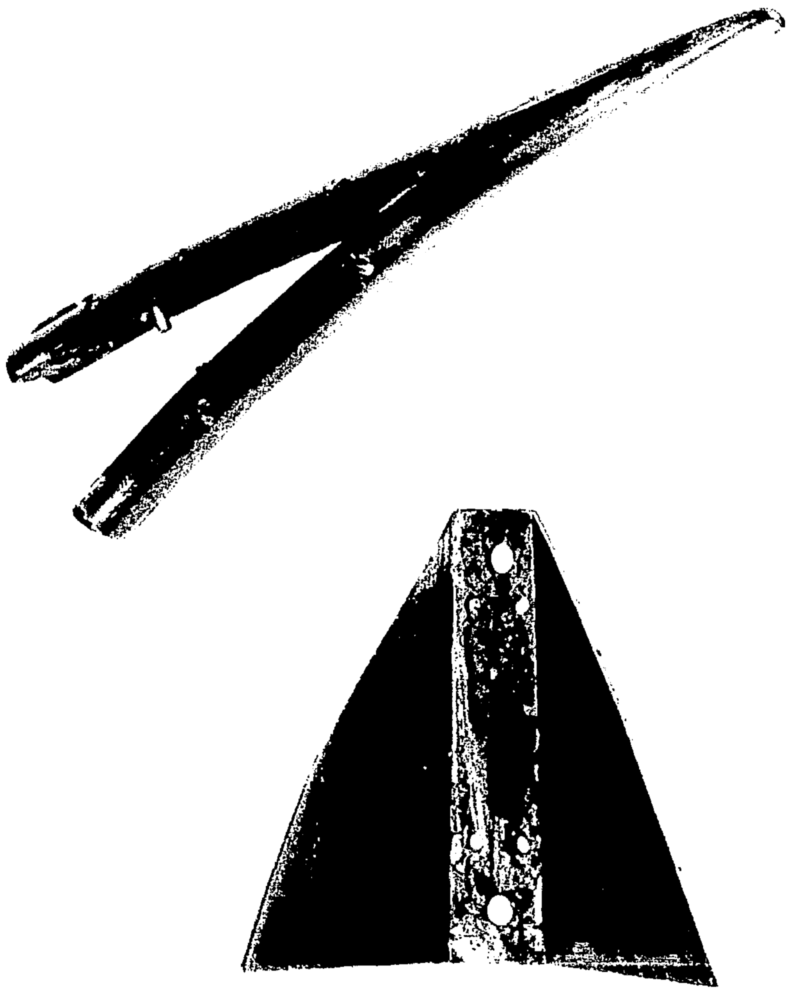

FIGURE 48. BALLISTIC MODEL ARRESTED FROM M = 3 FLIGHT IN EIGHT FEET OF URETHANE FOAM.

VERTICAL VIEW –
STATION 4

HORIZONTAL VIEW –
STATION 4

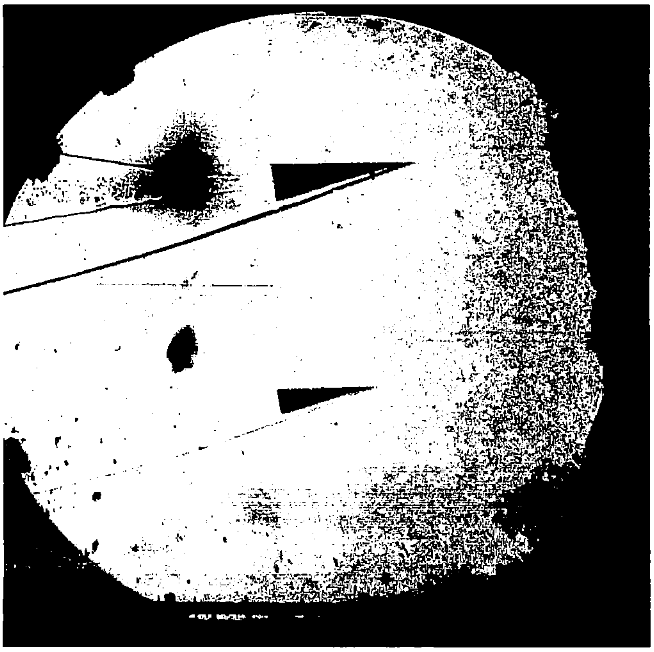

FIGURE 49. SHOT 40: CONE MODEL IN FLIGHT AT M = 5.0

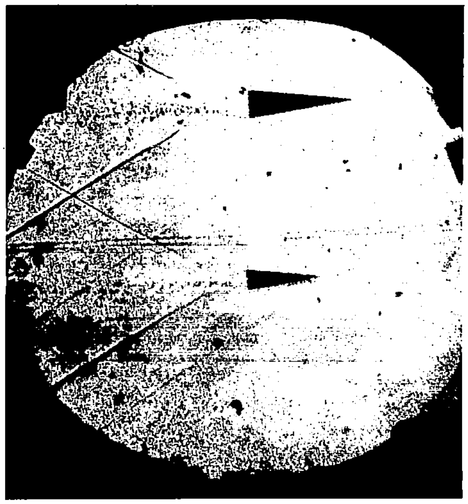

STATION 3

SHADOWGRAPH
NOT AVAILABLE
FOR THIS STATION

STATION 4

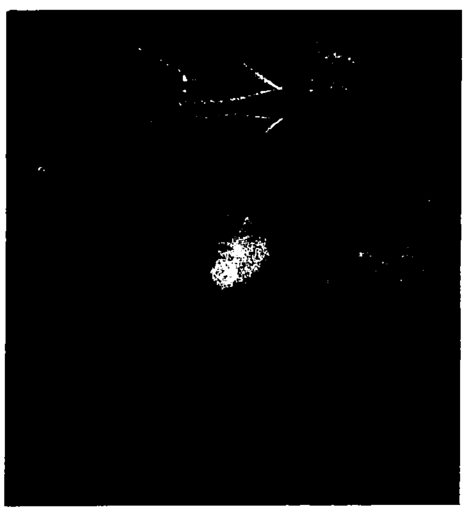

STATION 5

FIGURE 50 (a). SHOT 28: HORIZONTAL VIEW SHADOWGRAPHS; M = 1.83

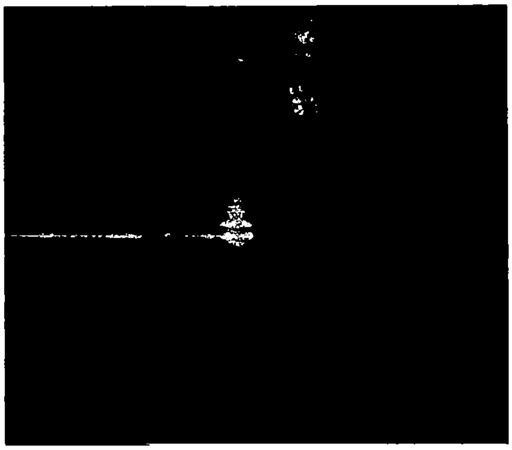
STATION 3


STATION 4

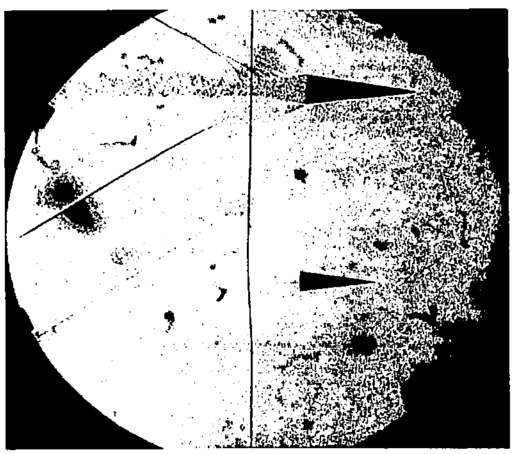
STATION 5

FIGURE 50 (b). SHOT 28: VERTICAL VIEW SHADOWGRAPH; M = 1.83.

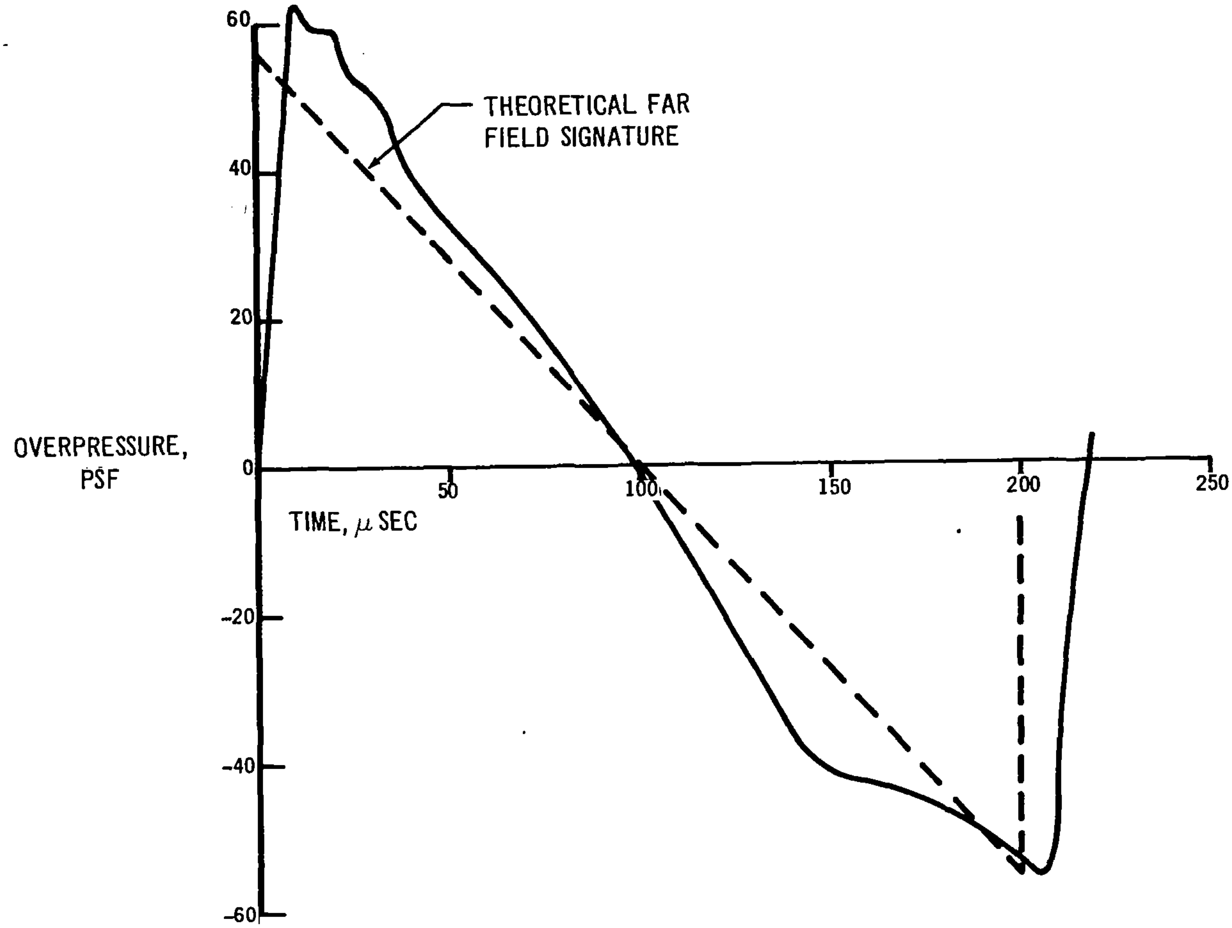

TRANSDUCER SENSITIVITY = 5.61 VOLTS/PSI

1 VOLT/CM

50μ SEC/CM

FIGURE 50 (c). SHOT 28: CONE PRESSURE SIGNATURE; M = 1.83

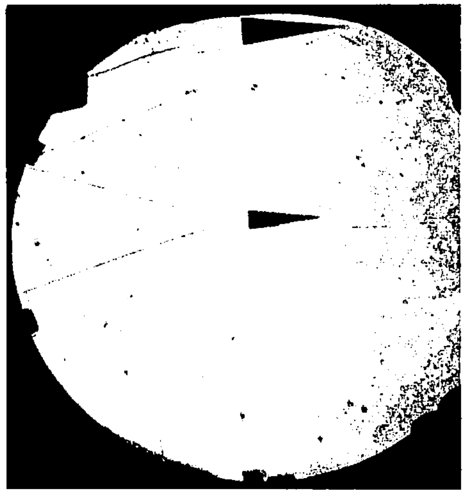

STATION 3

STATION 4

SHADOWGRAPH
NOT AVAILABLE
FOR THIS STATION

STATION 5

FIGURE 51 (a). SHOT 61: HORIZONTAL VIEW SHADOWGRAPHS; M = 3.00

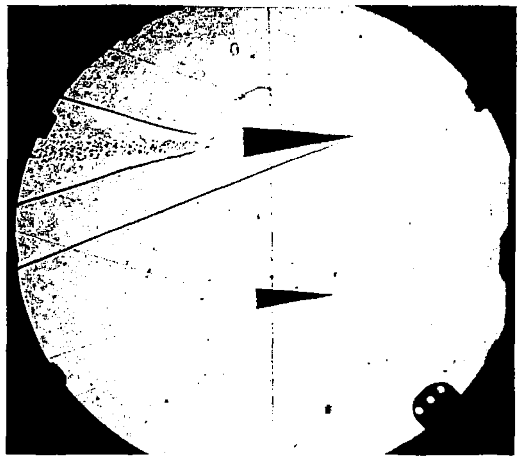

STATION 3

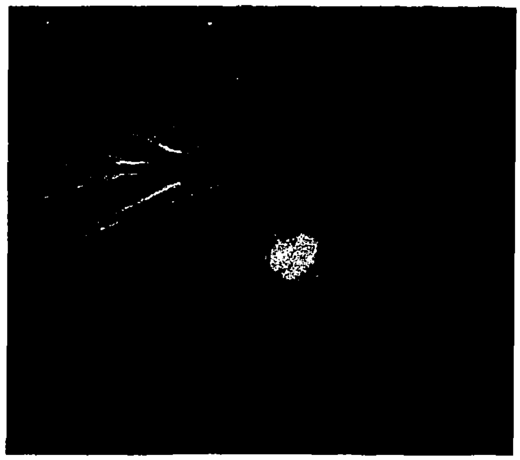

STATION 4

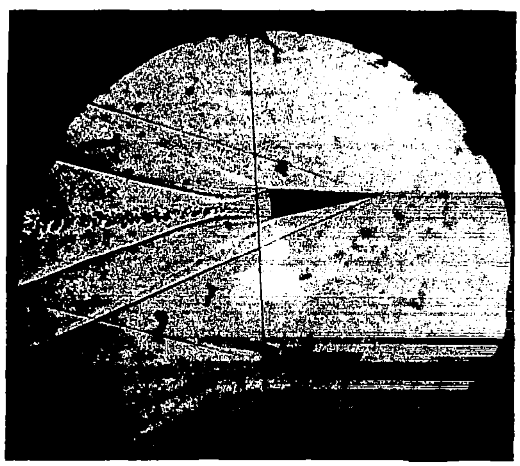

STATION 5

FIGURE 51 (b). SHOT 61: VERTICAL VIEW SHADOWGRAPHS; M = 3.00

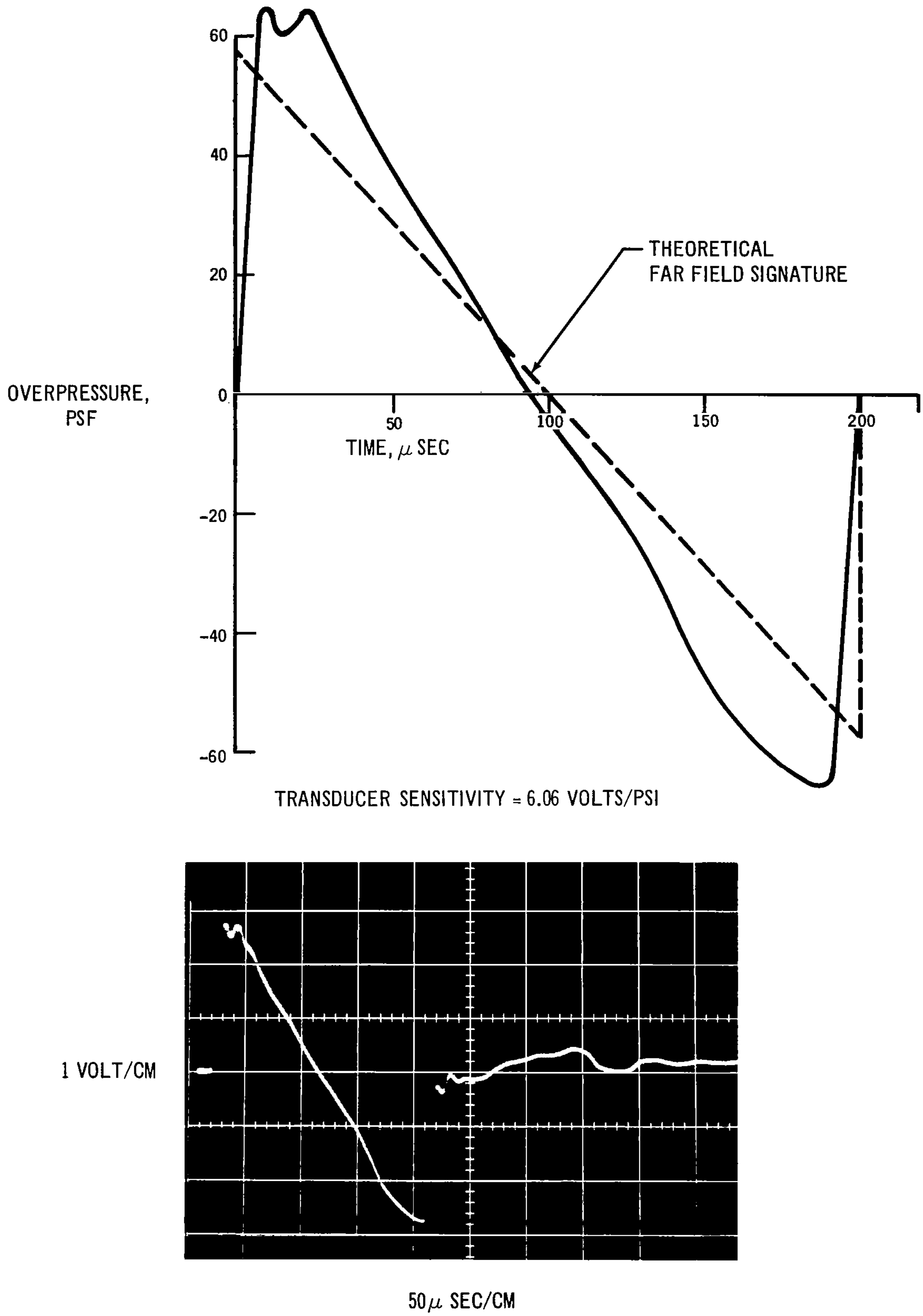

FIGURE 51 (c). SHOT 61: CONE PRESSURE SIGNATURE; M = 3.00

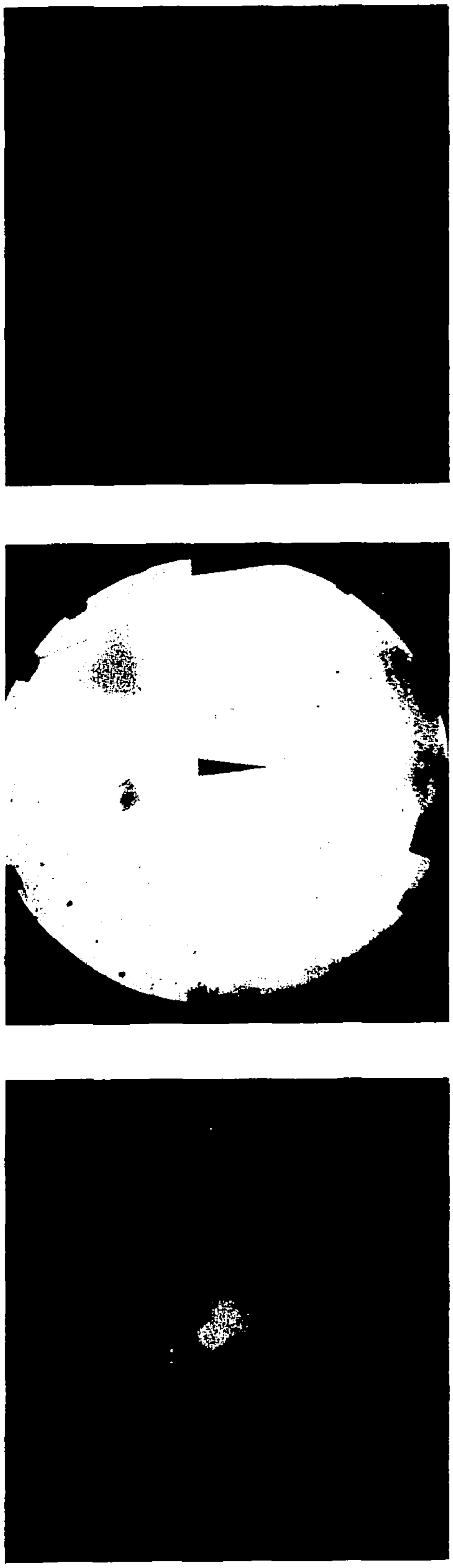

STATION 3

STATION 4

STATION 5

FIGURE 52 (a). SHOT 27: HORIZONTAL VIEW SHADOWGRAPHS; M = 3.20

STATION 3

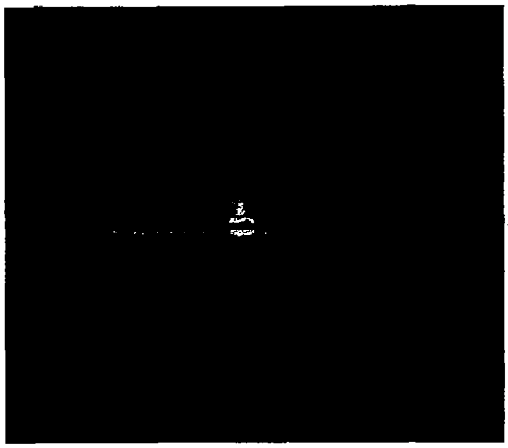

STATION 4

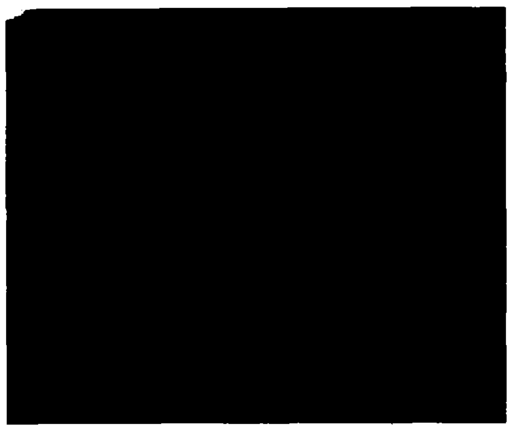

STATION 5

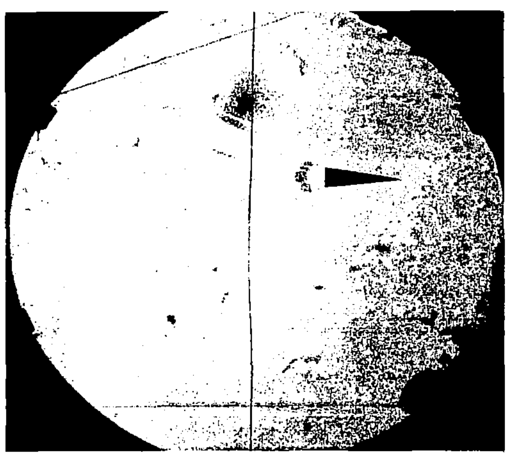

FIGURE 52 (b). SHOT 27: VERTICAL VIEW SHADOWGRAPHS; M = 3.20

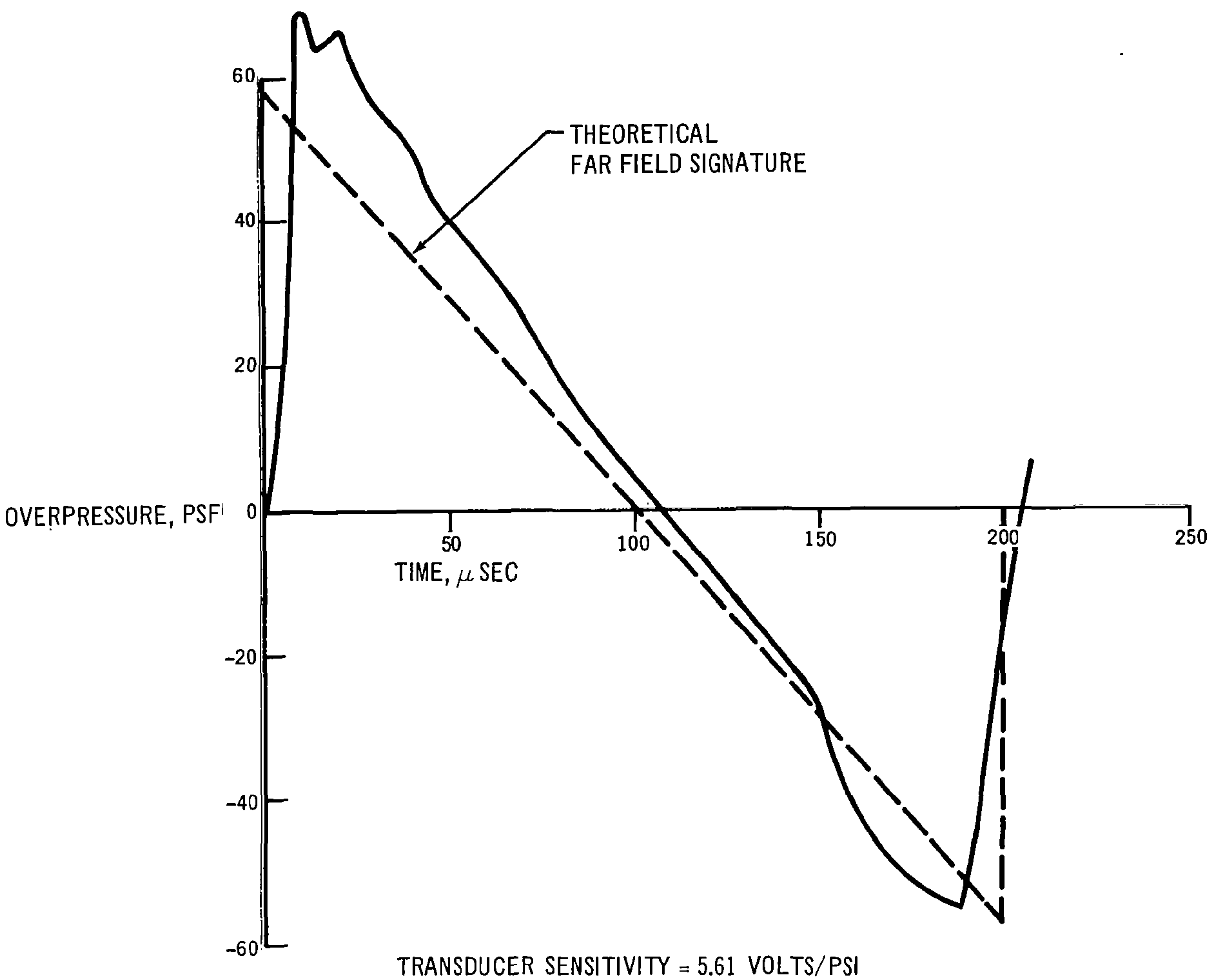

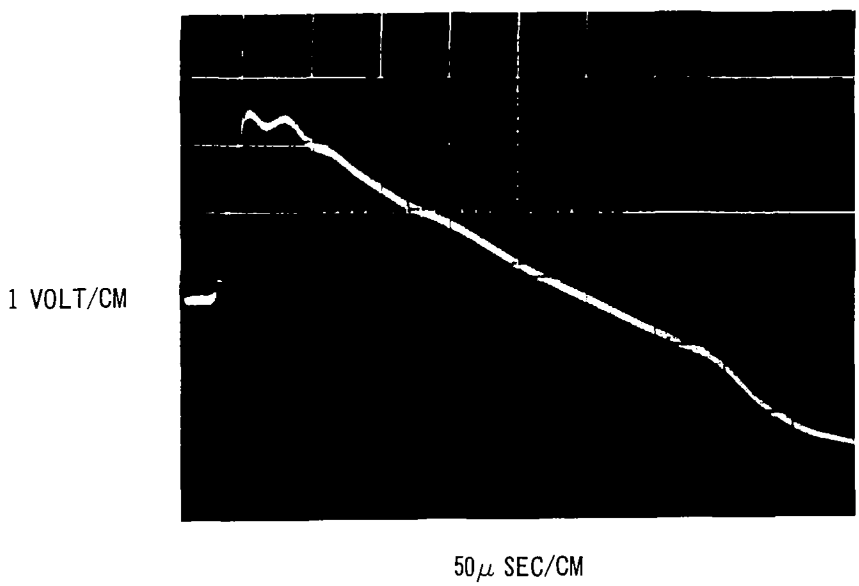

FIGURE 52 (c). SHOT 27: CONE PRESSURE SIGNATURE; M = 3.20

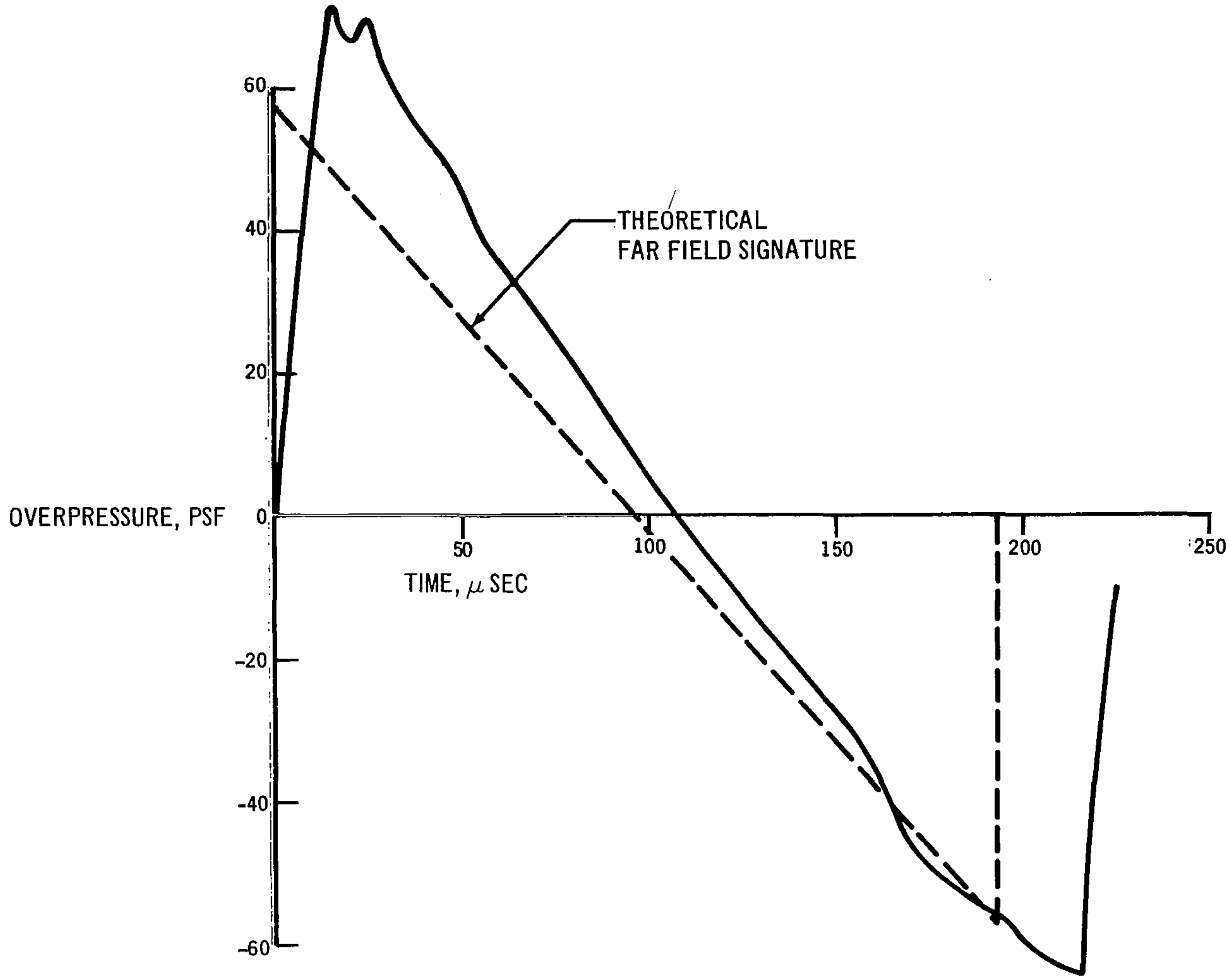

TRANSDUCER SENSITIVITY = 5.61 VOLTS/PSI

1 VOLT/CM

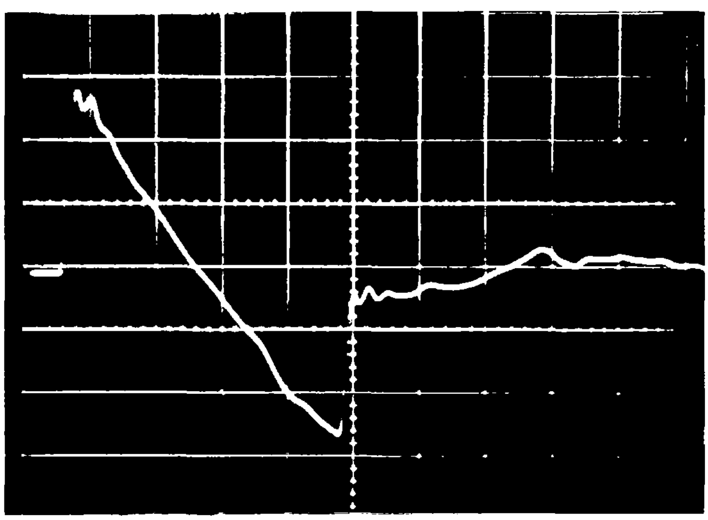

50μ SEC/CM

FIGURE 53. SHOT 51: CONE PRESSURE SIGNATURE; M = 5.14

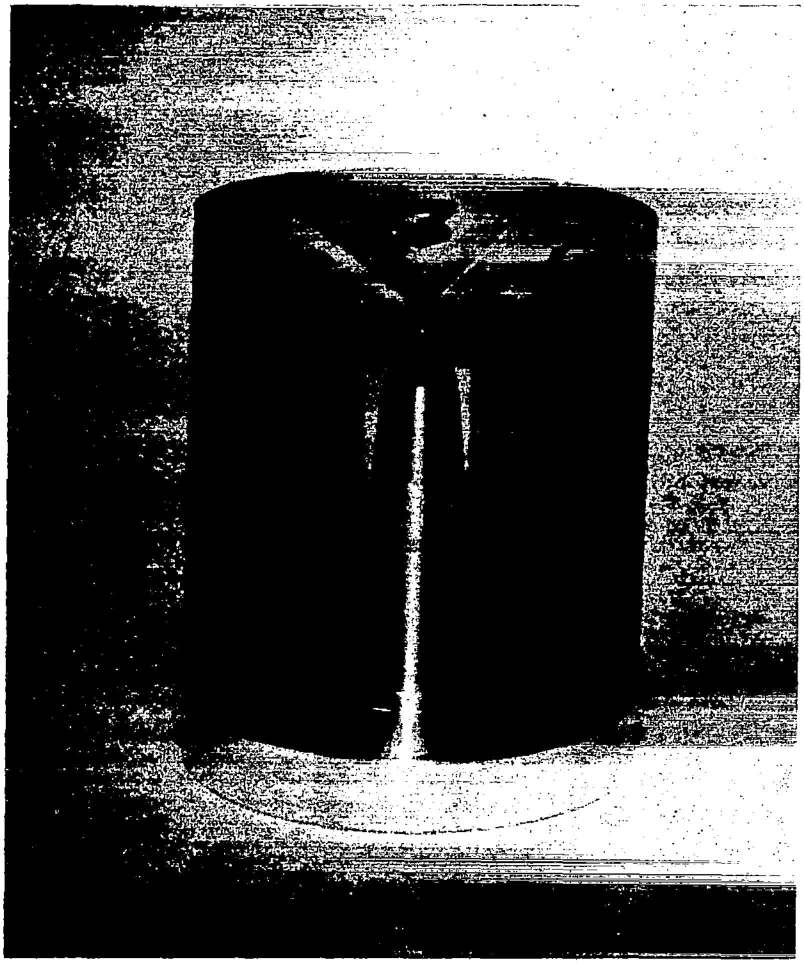

FIGURE 54. FABRICATED .30 CALIBER RIFLE BULLET SHAPE IN SABOT.

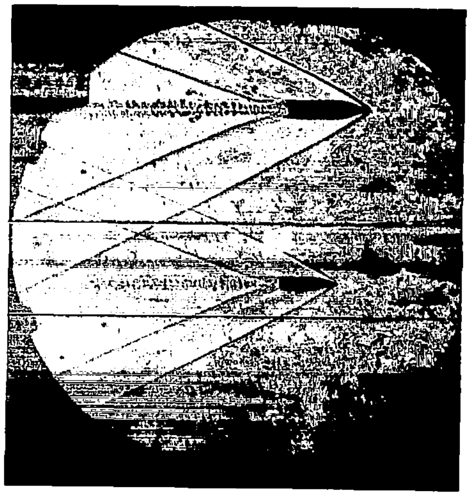

STATION 3

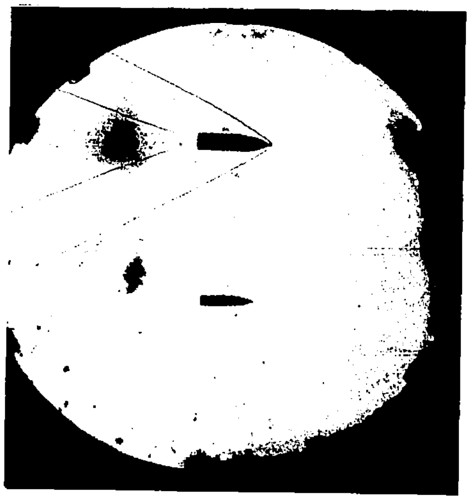

STATION 4

SHADOWGRAPH
NOT AVAILABLE
FOR THIS STATION

STATION 5

FIGURE 55 (a). SHOT 66: HORIZONTAL VIEW SHADOWGRAPH; $M = 2.47$

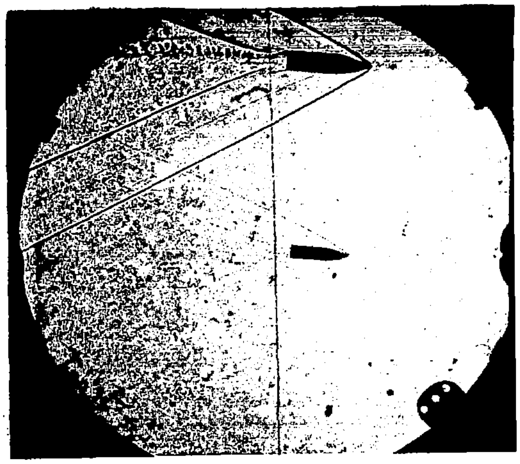

STATION 3

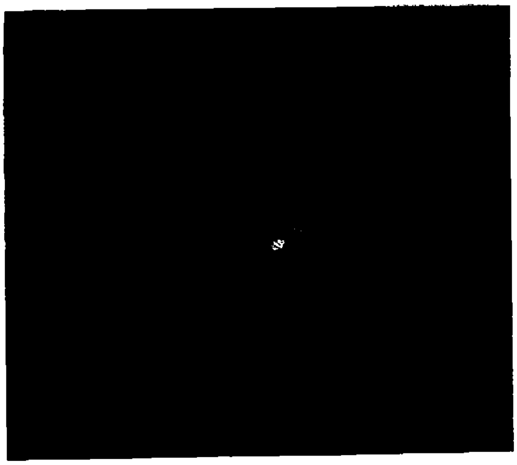

STATION 4

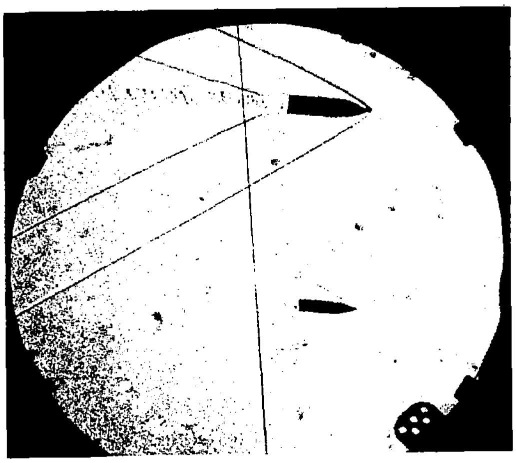

STATION 5

FIGURE 55 (b). SHOT 66: VERTICAL VIEW SHADOWGRAPHS; M = 2.47

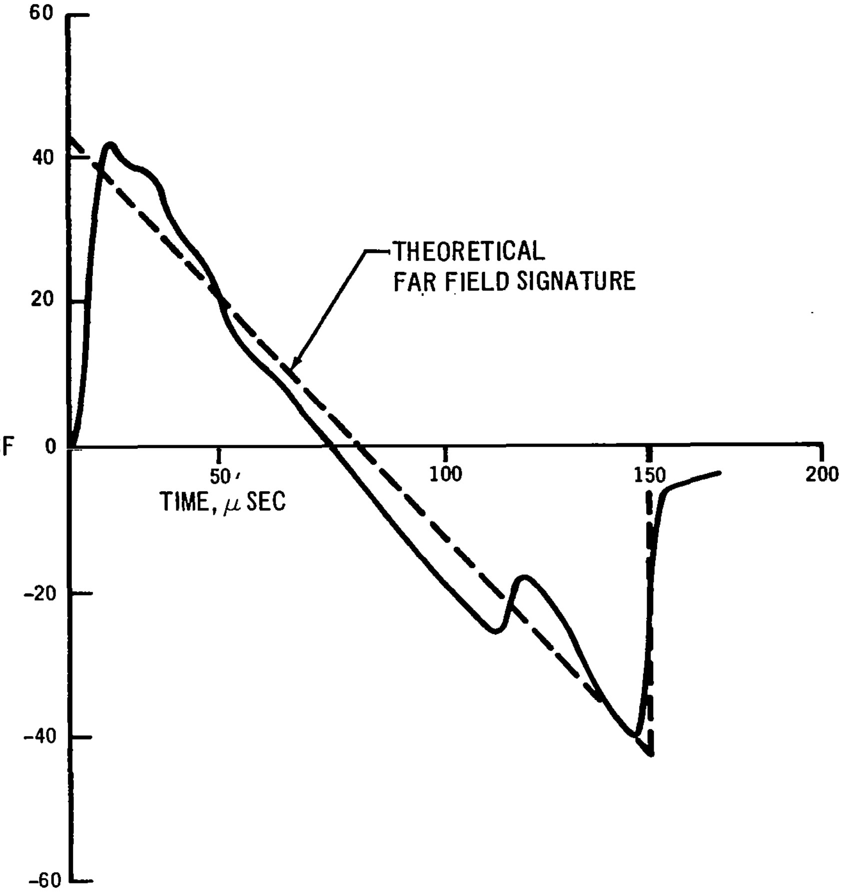

TRANSDUCER SENSITIVITY = 5.61 VOLTS/PSI

1 VOLT/CM

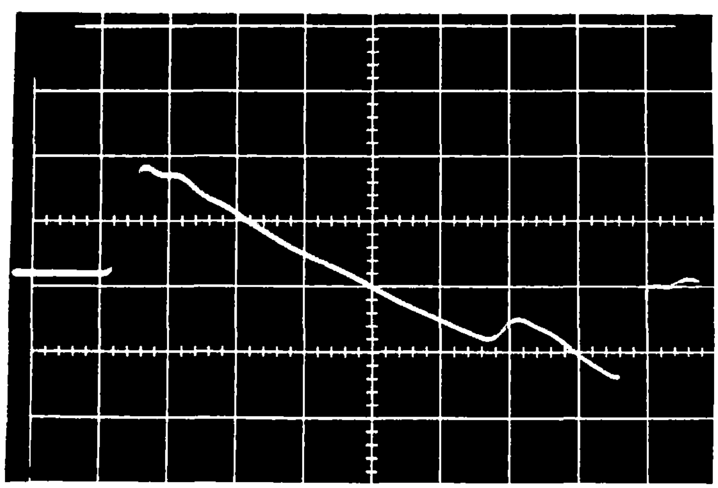

20μ SEC/CM

FIGURE 55 (c). SHOT 66: .30 CALIBER RIFLE BULLET SHAPE PRESSURE SIGNATURE; M = 2.47

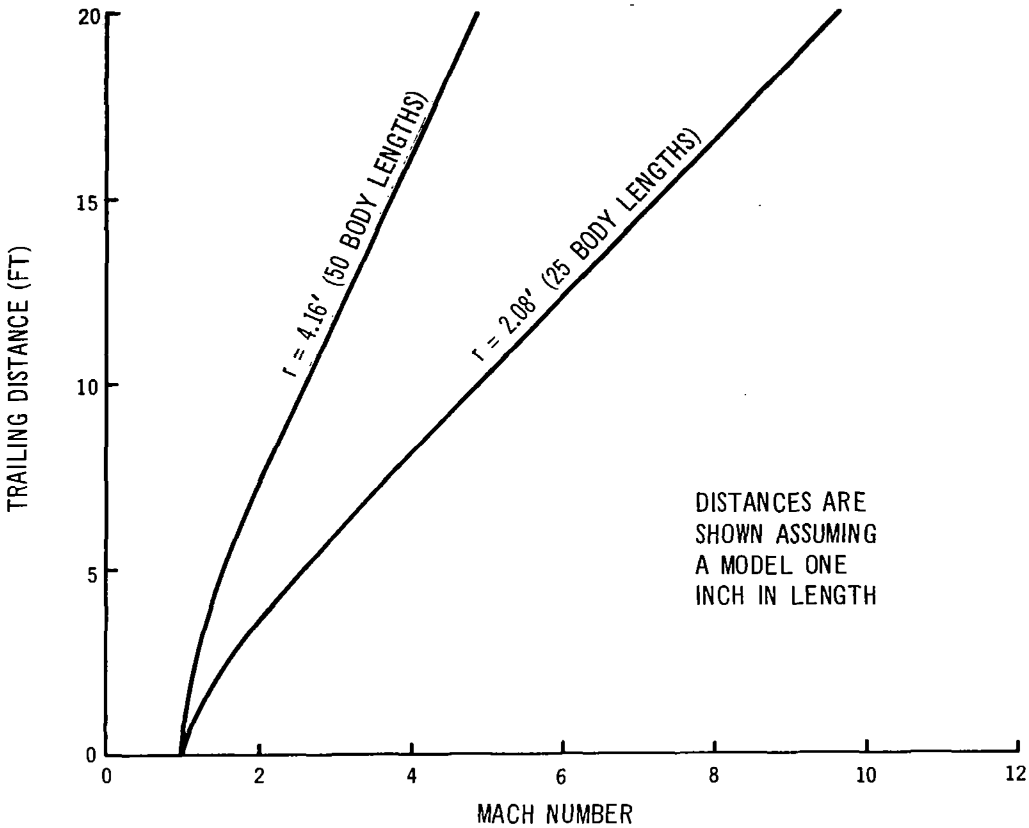

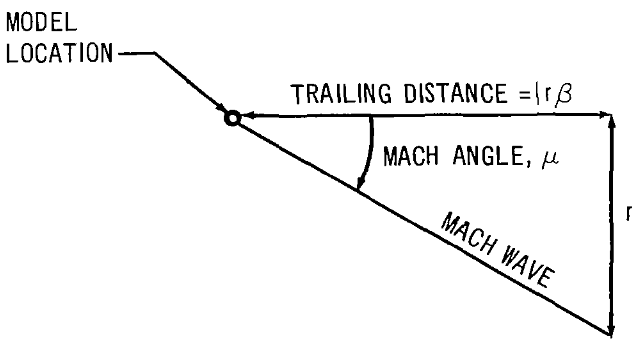

$$\mu = \tan^{-1}\left(\frac{1}{\sqrt{M^2-1}}\right)$$

$$= \tan^{-1}\left(\frac{1}{\beta}\right)$$

r IS HEIGHT CORRESPONDING TO A FIXED NUMBER OF BODY LENGTHS

$r\beta$ IS THE DISTANCE THE TRANSDUCER MUST BE LOCATED BEHIND THE MODEL FOR FIXED r

FIGURE 56. TRANSDUCER LOCATION REQUIREMENT

NASA-Langley, 1966 CR-603